Excitonic Complexes in Natural Quantum Dots Formed in Type II GaAs/AlAs Structures

Barbara Pietka

Thèse

Présentée par

Barbara PIĘTKA
née 22 novembre 1979

Pour obtenir le titre de Docteur
de l'Université Joseph Fourier - Grenoble I
Spécialité : Physique

(Arrêtés ministériels du 7 août 2006 et 6 janvier 2005)

Excitonic Complexes in Natural Quantum Dots Formed in Type II GaAs/AlAs Structures.

Complexes Excitoniques dans des Boîtes Quantiques Naturelles dans des Structures GaAs/AlAs de type II.

Soutenue publiquement le 27 juillet 2007

Composition du jury :			
Marek	Potemski	*LCMI, CNRS*, Grenoble, France	directeur de thèse
Roman	Stępniewski	*UW*, Varsovie, Pologne	directeur de thèse
Michał	Nawrocki	*UW*, Varsovie, Pologne	rapporteur
Paul	Voisin	*LPN, CNRS*, Marcoussis, France	rapporteur
Witold	Bardyszewski	*UW*, Varsovie, Pologne	membre
Henri	Mariette	*CEA, Institut Néel*, Grenoble, France	membre

Thèse préparée au sein du
Laboratoire des Champs Magnétiques Intenses, CNRS, Grenoble, France
et
University of Warsaw, Varsovie, Pologne

Uniwersytet Warszawski

Instytut Fizyki Doświadczalnej
Zakład Fizyki Ciała Stałego

Barbara PIĘTKA
ur. 22 listopada 1979

Praca Doktorska

Excitonic Complexes in Natural Quantum Dots Formed in Type II GaAs/AlAs Structures.

Kompleksy ekscytonowe w naturalnych kropkach kwantowych powstających w strukturach GaAs/AlAs II typu.

Obroniona publicznie 27 lipca 2007

Skład komisji egzaminacyjnej :			
Marek	Potemski	*LCMI, CNRS*, Grenoble, Francja	promotor
Roman	Stępniewski	*UW*, Warszawa, Polska	promotor
Michał	Nawrocki	*UW*, Warszawa, Polska	recenzent
Paul	Voisin	*LPN, CNRS*, Marcoussis, Francja	recenzent
Witold	Bardyszewski	*UW*, Warszawa, Polska	członek komisji
Henri	Mariette	*CEA, Institut Néel*, Grenoble, Francja	członek komisji

Praca została przygotowana w
Zakładzie Fizyki Ciała Stałego Uniwersytetu Warszawskiego, w Polsce
i
Laboratoire des Champs Magnétiques Intenses, CNRS, w Grenoble, we Francji

Acknowledgements

The PhD thesis was performed under the "co-tutelle" convention between the Université Joseph Fourier in Grenoble, France, and the University of Warsaw in Warsaw, Poland. I would like to thank Jacques Derouard and Frank Hekking, the directors of Ecole Doctorale de Physique at Université Joseph Fourier, and Jan Bartelski, the dean of Department of Physics at University of Warsaw, for accepting me as a PhD student.

I am grateful to the University of Warsaw for financial support for all years of my PhD.
I am grateful to the French Ministry of Foreign Affairs for "Eiffel Doctorate Scholarship" for the last year of my studies in Grenoble.

The work presented in this thesis was carried out at the High Magnetic Field Laboratory in Grenoble, in France, and in the Division of Solid State Physics, in University of Warsaw, in Poland. I would like to thank Gerard Martinez and Jean-Louis Tholence, the directors of High Magnetic Field Laboratory, and Michał Baj and Roman Stępniewski, the directors of Division of Solid State Physics, for giving me the opportunity to work in the laboratories and providing financial support for the scientific conferences in which I participated.

This work has been co-supervised by two persons, Marek Potemski and Roman Stępniewski, who were constantly guiding me during the years of my PhD. I would like to thank them for many encouraging words, invaluable support and every-day understanding. Their help cannot be overestimated.

I would like to thank the members of the jury: Henry Mariette and Witold Bardyszewski, and Paul Voisin and Michał Nawrocki, the two referees who agreed to read the manuscript and for their very useful remarks regarding this work.

During the years of my PhD I had a great pleasure to work with Andrzej Wysmołek whose experimental knowledge and abilities are always impressing. I would like to thank Andrzej for teaching me such a lot on the experimental systems and especially for his optimism and always helpful hand.

Special thanks must go to Marcin Sadowski for the task of proofreading the manuscript and the always "good-word" and nice company in morning coffees.

I also greatly enjoyed working together with Adam Babiński and Jaś Suffczyński. Without them the μ-PL and photon correlation experiments wouldn't be possible.

Thanks to Paweł Hawrylak and Arkadiusz Wójs, the theory of carrier interactions in quantum dots are much more understandable. Thank you very much for the discussion and patience in explanations.

The work in the High Magnetic Field Laboratory was very interesting and fruitful due to the many people whom I had a pleasure to meet as a permanent staff and as visitors when they were coming to the lab for measurements and discussions:

Duncan Maude, Clement Faugeras, Zbyszek Wilamowski, Sergei Studenikin, Leszek Bryja, Sasha Tartakovskii.

I would like to thank also all permanent staff and professors at the University of Warsaw whose professional and scientific abilities I could appreciate. I'm grateful for all the discussions during the conferences, "wtorkowe" and "piątkowe" seminars that helped me that much in understanding the physics. The number of physical problems that I met during my studies were always carefully reviewed and all the their offices were open for discussions.
I would like to thank Marian Grynberg, Jan Gaj, Jacek Baranowski, Piotr Kossacki, Andrzej Golnik, Krzysztof Korona, Krzysztof Karpierz, Tomasz Słupinski and Maria Kamińska for their interest in my work and suggestions. Andrzej Witowski and Jurek Łusakowski for many helpful advices. Rafał Bożek and Krzysztof Pakuła for always warm reception at Pasteura, explanation of KFM and MOCVD techniques.

Any experimental system couldn't work without the technical support from the most skilled people: Ivan Breslavetz, Jean Florentin and Krzysztof Głowacki; and any computer and printer without Sebastien Buisson and Thomas Dolmazon. I would like to thank also Eric Mossang and Christiane Warth-Martin for their efficient planning of magnet time.

The "fast actions" in buying plane tickets, after-deadline documents and "papers" are the small-big things that made the every-day life easy thanks to Joanna Konwicka, Magdalena Białkowska and Beata Czajkowska. I would like to thank them for goodwill and kindness. Gislaine Meneroud, Amelie Pic and Kim Pla for all the help they have given in the administration procedures in High Magnetic Field Laboratory and patience in listening to my poor-French explanation of the problems.

There are many PhD students and post-docs that I met during my work at the University of Warsaw and in Grenoble High Magnetic Field Laboratory that I would like to thank for the time we spent together on coffees, lunches, discussions, and in the lab. Of course, it's not possible to mention all, but I would like to thank specially Marcin Byszewski, Kasia Surowiecka, Oleh Fedorych, Aneta Drabińska, Konrad Dziatkowski, Marta Gryglas, Jacek Szczytko, Jacek Kasprzak, Wojtek Pacuski, Kasia Kowalik, Sebastien Moreau for giving some "social" life to my PhD studies, a lot of fun and smile.

There are also my friends that during the years of my PhD, when I was hung up between Grenoble and Warsaw, keep in touch with me and always found a time for a chat when I was arriving to one of the places. I would like to thank them all for their time, mails, phones and just that they simply "are".

Among all I would like to thank my Parents, my Husband, my Brother, and my whole Family for their patience, support and love. This work would never be possible without them.

B.P.

RÉSUMÉ

Des boîtes quantiques à fort confinement tridimensionnel et de très basse densité (10^6 cm^{-2})ont été démontrées dans des structures qui ont été originellement développées comme des double puits quantique de GaAs/AlAs avec des barrieres de GaAlAs. Le fait que ces structures soient de type II permet de détecter les boîtes quantiques très facilement grâce à la très longue durée de vie des excitons indirects (de l'ordre de quelques millisecondes) et à leur capacité à diffuser efficacement (jusqu'à 100 μm) dans les pièges zéro dimensionnels. Cet effet est généralement difficile à obtenir dans les structures directes. Les boîtes quantiques peuvent donc être facilement remplies par des excitons, provoquant la formation, non seulement d'excitons, mais aussi d'excitons chargés et de biexcitons, et également de molécules excitoniques plus complexes montrant un caractère zéro dimensionnel.

Ce travail est consacré à l'étude des complexes excitoniques fortement confinés, à leur nature et aux processus permettant leur formation.

Nous présentons des études spectroscopiques de l'émission d'une boîte quantique unique sous différentes conditions d'excitation et détectée de différentes manières.

La possibilité de contrôler optiquement le nombre d'électrons et de trous qui occupent les niveaux discrets des boîtes quantiques nous a permis d'étudier la formation de complexes multi-excitoniques en fonction de la densités d'excitons. Les effets observés sont décrits par le modèle de la normalisation des bandes d'énergie comprenant les effets multi-corps, les interactions d'échange et les effets de corrélation.

L'influence d'un champ magnétique sur les complexes multi-excitoniques est d'abord discutée. De manière générale, il est montré comment l'application d'un champ magnétique modifie la structure énergétique des transitions observées. Des propriétés typiques de boîtes quantiques telles que l'effet Zeeman, décalage diamagnétique et l'énergie de liaison excitonique sont discutées. Ces études ont permis une analyse de la symétrie et de la taille du potentiel de confinement des boîtes.

Ensuite, les mécanismes de capture d'excitons dans les boîtes sont considérés. Le rôle important des processus de diffusion contribuant au temps de relaxation de l'émission des boîtes quantiques uniques est discuté sur la base d'expériences de spectroscopie résolue en temps.

Le rôle des processus radiatifs et non radiatifs dans l'émission de complexes multi excitoniques est montré dans l'émission thermiquement activée de boîtes quantiques uniques.

Les mesures de corrélation de photon ont permis la classification des différentes lignes d'émission des complexes multi-excitoniques, d'étude du caractere de mécanisme de capture des porteurs photo-créés et la dynamique des fluctuations de charge caractéristiques d'une boîte quantique unique.

L'approche expérimentale à un probleme de boîte quantique unique est largement discutée et des modèles théoriques sont appliqués pour décrire les effets observés.

PODSUMOWANIE

W strukturach wyhodowanych jako układ podwójnych studni kwantowych GaAs/AlAs II typu zaobserwowano nowy typ kropek kwantowych. Te naturalnie powstające kropki kwantowe charakteryzują się bardzo małą gęstością powierzchniową ($10^6 cm^{-2}$) i bardzo silnym potencjałem wiążącym.

Skośny charakter badanych struktur pozwala na osiągnięcie bardzo dużych koncentracji nośników o długich czasach życia (rzędu ms) dyfundujących na odległości nawet do $100\mu m$. Kropki kwantowe tworzą w badanym układzie centra pułapkujące nośniki stanowiąc efektywny kanał rekombinacji promienistej, co jest bardzo trudne do uzyskania w strukturach prostych. Pozwala to na wiązanie w kropkach nie tylko ekscytonów, ale też bardziej skomplikowanych obiektów jak naładowane ekscytony, biekscytony, czy bardziej złożone kompleksy ekscytonowe.

Celem pracy jest zbadanie natury, procesu tworzenia, jak również oddziaływań w układzie kompleksów ekscytonowych.

Dzięki zastosowaniu metody spektroskopii optycznej, a w szczególności mikro-luminescencji, wykonano pomiary emisji z pojedynczej kropki kwantowej przy różnych warunkach pobudzania i detekcji.

Możliwość kontrolowanej zmiany ilości elektronów i dziur zajmujących dyskretne poziomy energetyczne w pojedynczej kropce kwantowej pozwoliła na dyskusję tworzenia się coraz bogatszych struktur ekscytonowych w miarę zwiększania ilości ekscytonów. Obserwowane efekty opisane zostały przy użyciu modelu renormalizacji przerwy energetycznej uwzględniającym oddziaływania wielociałowe, wymiany i korelacji.

W pracy przedstawiono wyniki badań wpływu zewnętrznego pola magnetycznego na obserwowane obiekty. W szczególności pokazano jak modyfikacja poziomów energetycznych pojedynczej kropki kwantowej wpływa na strukturę przejść optycznych kompleksów ekscytonowych.

Przedyskutowano typowe własności pojedynczych ekscytonów jak energia wiązania, rozszczepienie Zeemanowskie, przesunięcie diamagnetyczne. Dają one informacje o rozmiarach i symetrii obserwowanych kropek kwantowych.

W pracy omówiono również mechanizmy transferu nośników do kropki. W pomiarach czasowo rozdzielonych z pojedynczej kropki kwantowej wykazano istotną rolę dyfuzji dwu-wymiarowych ekscytonów w procesach wychwytu nośników przez kropkę.

Rola procesów radiacyjnych i nie-radiacyjnych w emisji z pojedynczej kropki kwantowej została opisana dzięki pomiarom luminescencji z kopki kwantowej w szerokim zakresie temperatur.

Pomiary korelacji fotonów pozwoliły na sklasyfikowanie szeregu linii emisyjnych. Pokazana została różnica w wychwycie przez kropkę ekscytonów i pojedynczych nośników oraz przedyskutowane zostały efekty fluktuacji ładunku charakterystyczne dla pojedynczej kropki.

W pracy szeroko omówione zostały metody eksperymentalne pozwalające na obserwację emisji z pojedynczej kropki kwantowej, jak również podstawy teoretyczne opisywanych zjawisk.

ABSTRACT

Quantum dots with strong three dimensional confinement and low surface density ($10^6 cm^{-2}$) have been identified in a structure which was nominally grown as a type II GaAs/AlAs bilayer surrounded by GaAlAs barriers. The unique type II system makes the dots easy to detect due to characteristic, very long-lived (ms range) indirect two-dimensional excitons. The 2D excitons efficiently diffuse (up to 100μm) into zero-dimensional traps, which is difficult to obtain in conventional, direct type structures. The dots can therefore be effectively filled by excitons, giving rise to the formation of not only excitons, charged excitons and biexcitons, but also more complex excitonic molecules which show a multiple zero-dimensional shell structure.

This work is devoted to investigations of the nature, process of formation and interactions in the strongly confined exciton complexes system.

Spectroscopic studies of single quantum dot emission under different conditions of excitation and detection are presented.

The possibility of optically controlling the number of electrons and holes populating the discrete dot energy levels allows a discussion of the exciton complexes formation depending on exciton densities. The observed effects are described in the band-gap renormalisation model including many-body, exchange, and correlation type interactions.

The influence of a magnetic field on the exciton complexes is discussed. In general, it is shown how the application of a magnetic field modifies the energy structure of the observed transitions. Typical quantum dot properties such as Zeeman splitting, diamagnetic shift, and exciton binding energy are discussed. They allowed an analysis of the symmetry and size of the dots' confining potential.

Moreover, the mechanisms of exciton capture in the dots are considered. The important role of diffusion processes revealed in single dot time resolved experiments is discussed.

The role of radiative and non-radiative processes in the multiexciton emission is shown in temperature activated emission from a single dot.

Photon correlation experiments allowed to classify the number of multiexciton emission lines, to study the character of capture of photo-created carriers, and to investigate the dynamics of charge fluctuations characteristic of a single quantum object.

The experimental approach to a single quantum dot problem is widely discussed, and theoretical models are applied to describe the observed effects.

This work is split into eleven chapters:

Chapter 1 presents a short introduction to the subject of exciton complexes in single quantum dots. It define the term *exciton complexes* and points out the advantages of quantum dots formed in a GaAs/AlAs type II bilayer as compared with other systems.

Chapter 2 shows the general and most important properties of carriers confined in zero dimensional systems - quantum dots - including magnetic field effects.

Chapter 3 describes the energy structure of the investigated materials. The details about the potential distribution in a GaAs/AlAs type II bilayer and the GaAs quantum dots are given.

Chapter 4 goes into details about the experimental techniques used in photoluminescence measurements. The μ- and *macro*- PL setups are described, including the techniques that allowed to work in high magnetic field, low and high temperature, with ns time resolution.

Chapter 5 reviews the properties of a GaAs/AlAs type II double quantum well system. The macro-photoluminescence experiments that led to the discovery of quantum dot formation in the GaAs/AlAs bilayer are described.

Chapter 6 tells about the simplest exciton complexes confined in quantum dot potentials. The single exciton, trion and biexciton properties are discussed, including the effects of magnetic field.

Chapter 7 discusses the effects of high carrier concentration in a single quantum dot. The multi-exciton complex formation with increasing electron-hole pair density and modification of its energy structure by a magnetic field is shown.

Chapter 8 shows the effects of a temperature increase on the observed emission from multiexciton complexes. Typical effects such as energy shift, intensity decrease, emission line broadening, are described.

Chapter 9 presents the time resolved emission spectra from a single quantum dot. The decay of emission is traced in time for different excitation power conditions and temperatures. The very long decay time, in μs range, characteristic for this system, is discussed.

Chapter 10 shows the results of photon-correlation experiments performed on single exciton complexes emission lines. The identification of particular emission lines is given and their "charged" or "neutral" nature is described. The process of exciton creation in the dot and charge state fluctuation is discussed. Evidence for biexciton triplet formation is given.

Chapter 11 contains conclusions. The most important results obtained in the work are pointed out.

Table of Contents

Chapter 1

Introduction

Dans l'introduction, nous présentons les motivations de ce travail. Nous introduisons la notion de "complexe excitonique" et nous décrivons l'utilisation du confinement électronique dans une boîte quantique pour étudier ces complexes excitoniques. Les avantages proposés par le système de double puits quantique GaAs/AlAs de type II sont exposés.

The physics of quantum dots is often likened to that of atoms and molecules because of the discrete nature of their energy levels. Although this analogy has some merits, one difference worth emphasizing is the possibility of creating multiple electron-hole pair excitations in a quantum dot. Such multi-particle complexes quickly relax into a quasiequilibrium state in which they exhibit features of a spatially confined many-particle system such as an atom, with an added advantage that the eventual radiative decay of this state offers a convenient way to probe the complexity of multi-particle correlations.

Experimentally, the excitation of multiple electron - hole pairs in a single quantum dot is relatively easy. The main conditions for achieving it are:

- very low surface densities of quantum dots
- deep confining potential
- special structure of barrier material that would offer an efficient channel for pumping the carriers into the dot

These particular properties, together with developments in single dot spectroscopy, make possible controlled optical studies of many electron - hole pairs in a single dot.

In this work, having met all the above conditions, we study, by means of optical spectroscopy, the exciton complexes confined in single quantum dots formed in GaAs/AlAs type II bilayer.

The term `exciton complexes` is defined in the first section of this chapter. In the second section, the advantages of quantum dots formed in GaAs/AlAs type II bilayer over many other systems in exciton complex studies are given.

1.1 What are exciton complexes?

Single excitons are the quanta of excitation in semiconductors that are composed of an electron excited across the band gap and bound to the hole left behind. The Coulomb forces between negatively (electron) and positively (hole) charged particles determine the binding energy of this composite particle. The ground state of the exciton in a zero dimensional system is formed from the electron and hole confined in the first electronic level, the *s*-shell.

A more complicated structure of two electrons and a single hole forms the charged exciton (trion), negatively charged in this case. The addition of a single hole to this configuration will result in bi-exciton formation, as the bound state of two electrons and two holes. The more carriers are added to the system, the more complicated is the state that is formed, which is a multiple-electron-hole system that is referred in this work as an *exciton complexes*.

The many-particle state is determined by the inter-particle interactions: electron-electron, hole-hole, electron-hole. In a quantum dot, additionally, the multiple carriers are bound due to the quantum confinement, and the shell structure is given by the sub-levels determined for a single carrier. The carrier-carrier correlation results in the renormalisation of the single carrier energy levels.

The recombination from the multi-particle complexes, which is an annihilation of a single electron - hole pair, results in the formation of a new complex with a reduced number of carriers. Thus the effective emission energy is the effect of the possible initial and final configuration of carriers, giving rise to many emission lines in the spectra.

1.2 The advantages of GaAs QDs formed in a type II structure

μ-PL experiments performed on a GaAs/AlAs type II bilayer, described in the following sections, showed that the investigated emission is typical for quantum dots having several unusual properties that distinguish them from all other investigated systems. Among others, the most important are:

- `the surface density of quantum dots is as low as` $10^6 cm^{-2}$.
  This was revealed in μ-PL mapping experiments (6.1), that showed that the dot emission is randomly spread in the sample.

- `very strong three-dimensional confinement`
  In the μ-PL spectra from a single dot, not only the single exciton, biexciton and charged exciton emission is observed but also the recombination from a number of excited states (p, d, f ... shells) is visible (7.1).

- `indirect type barriers that assure an efficient supply of carriers to the dot`

The barriers for the quantum dots are formed of X-type material with very long carrier lifetimes (in the ms range (5.3), that diffuse (5.4) over large distances, what was confirmed in PL-imaging experiments. In time resolved experiments (5.3) it was revealed that the dots are direct-type systems. They thus serve as a very efficient recombination channel for long lived carriers.

In the described system even very high carrier concentrations can be achieved. Confined in the dot potential, the carriers form stable multiexcitonic complexes that are the subject of this work.

The characteristic properties of the dots were all observed in the photoluminescence experiments. Namely:

- The emission from an ensemble of quantum dots spreads over a very broad energy range below the main quantum well transitions (6.1). This indicates that the `potential traps are very deep, up to 150meV`.
- The diamagnetic shift of emission energies (6.3.2) and the excitation power dependent spectra (7.1) allowed to estimate the `lateral diameter of dots to be of tens of` nm.
- The possibility to observe a number of excited state emission lines, with typical Fock - Darwin type evolution in a magnetic field (7.3), shows that the confining in-plane potential can be approximately described by a `harmonic shape`.
- Time resolved experiments performed under below- and above- band gap excitation confirmed that the investigated emission from the dot is very fast, in the order of ns. Thus `the symmetry of the bands inside the dot is of` Γ `type`. This observation was confirmed in photon correlation experiments (10.2.2).

The process of formation of the quantum dots in the type II GaAs/AlAs double quantum well structure is not well understood yet. However, it's important to stress that all the optical properties indicate that the origin of the investigated objects is not simple well width fluctuations, as already reported elsewhere [1, 2, 3, 4, 5, 6, 7], but rather the natural formation of dots, typically of tens nm in lateral diameter, and very deep potential traps.

The most similar emission spectra to those presented in this work is given by GaAs/GaAlAs quantum dots that are grown in so-called "gallium droplet epitaxy" [8] and by combining solid-source molecular beam epitaxy and atomic-layer precise in situ etching [9, 10, 11].

Bibliography

[1] H. F. Hess, E. Betzig, T. D. Harris, L. N. Pfeiffer, and K. W. West, "Near-field spectroscopy of the quantum constituents of a luminescent system," *Science*, vol. 264, p. 1740, 1994.

[2] D. Gammon, E. S. Snow, B. V. Shanabrook, D. S. Katzer, and D. Park, "Homogenous linewidths in the optical spectrum of a single gallium arsenide quantum dot," *Science*, vol. 273, p. 87, 1996.

[3] Q. Wu, R. D. Grober, D. Gammon, and D. S. Katzer, "Excitons, biexcitons, and electron-hole plasma in a narrow 2.8nm GaAs/$Al_xGa_{1-x}As$ quantum well," *Phys. Rev. B*, vol. 62, p. 13022, 2000.

[4] K. Brunner, G. Abstreiter, G. Böhm, G. Tränkle, and G. Weimann, "Sharp-line photoluminescence and two-photon absorption of zero-dimensional biexcitons in a GaAs/AlGaAs structure," *Phys. Rev. Lett.*, vol. 73, p. 1138, 1994.

[5] K. Leosson, J. R. Jensen, W. Langbein, and J. M. Hvam, "Exciton localization and interface roughness in growth-interrupted GaAs/AlAs quantum wells," *Phys. Rev. B*, vol. 61, p. 10322, 2000.

[6] A. G. Steffan and R. Phillips, "Two different types of natural quantum dots in narrow GaAs/AlGaAs QWs," *Physica E*, vol. 17, p. 15, 2003.

[7] K. Matsuda, T. Saiki, S. Nomura, M. Mihara, Y. Aoyagi, S. Nair, and T. Takagahara, "Near-field optical mapping of exciton wave functions in a gaas quantum dot," *Phys. Rev. Lett.*, vol. 91, p. 177401, 2003.

[8] V. Mantovani, S. Sanguinetti, M. Guzzi, E. Grilli, M. Gurioli, K. Watanabe, and N. Koguchi, "Low density GaAs/AlGaAs quantum dots grown by modified droplet epitaxy," *J. Appl. Phys.*, vol. 96, p. 4416, 2004.

[9] A. Rastelli, R. Songmuang, and O. Schmidt, "Self-assembled GaAs/AlGaAs quantum dots by molecular beam epitaxy and in situ $AsBr_3$ etching," *Physica E*, vol. 23, p. 384, 2004.

[10] A. Rastelli, S. Kiravittaya, L. Wang, C. Bauer, and O. Schmidt, "Microphotoluminescence spectroscopy of hierarchically self-assembled quantum dots," *Physica E*, vol. 32, p. 29, 2006.

[11] A. Rastelli, S. Stufler, A. Schliwa, R. Songmuang, C. Manzano, G. Costantini, K. Kern, A. Zrenner, D. Bimberg, and O. Schmidt, "Hierarchical self-assembly of GaAs/AlGaAs quantum dots," *Phys. Rev. Lett.*, vol. 92, p. 166104, 2004.

Chapter 2

Quantum Dot - Three Dimensional Confinement

Dans ce chapitre, nous introduisons les notions nécessaires à la compréhension des propriétés optiques des boîtes quantiques. Nous discutons les propriétés typiques des systèmes de zéro dimension et les comparons aux systèmes tridimensionnels.

In the following section the general properties of carriers confined in all three dimensions are reviewed. This section addresses only the most important points in this broad subject. It is focused on the quantum dot properties that are necessary to understand and describe the results presented in this work. For more details, the reader is referred to reviews published in popular magazines: [1, 2, 3, 4, 5, 6, 7, 8, 9] and books: [10, 11] or many others.

In first part of the following chapter the type of confining potential and the problem of the density of states are discussed.

In the second part the effects of the application of a magnetic field on the discrete quantum dot energy levels are considered. The model that describes the single exciton energy shift is discussed in terms of interplay of electron - hole Coulomb interaction and magnetic field induced confinement. Further on, the Fock - Darwin model of the excited state energy shift in a quantum dot of parabolic confinement is described.

2.1 Zero dimensional systems

Quantum dots are formed by constructing a lateral confinement V(x,y) that additionally squeezes the electron and hole motion, already confined in the narrow quantum well, in the perpendicular direction $V_{QW}(z)$. Usually, the shapes of quantum dots are thus of disks or lenses with lateral dimensions wider than their height. This is schematically illustrated in Fig.2.1. The energy of single particle excitations across the quantum dot is much higher than other characteristic energies in the system. The lateral confining potential does not have any peculiarities, such as for

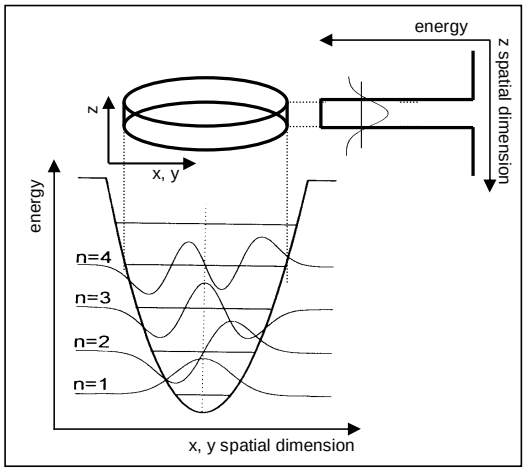

Figure 2.1: *Illustration of a quantum dot as an object formed from a quantum well system in the z spatial direction, due to a harmonic type confining potential in the x and y directions. The wave functions, corresponding to different energy levels, in both systems are schematically marked.*

example the Coulomb potential that binds the electrons in an atom. Depending on the quantum dot type, this lateral potential can be approximated by different model potentials. In general, if the quantum dots are small (i.e. the quantum dot radius is comparable to the bending of potential at the dot edges) the best are the most smooth potentials: harmonic, Gaussian or Pöschl-Teller potentials.

There have been many different theoretical attempts to find the best models of confining potential for different quantum dots [4, 12, 13, 14, 15]; in the experiments it is very often shown [6, 10] that the harmonic type is one of the most accurate ones. However, it has to be stressed that this is a very simplified model. Especially when "optical" dots are considered, which bind simultaneously electrons and holes. In comparison to electrons, the hole band structure is often very complicated and involves a number of subbands that very often interact and mix. The quantum dot properties have been studied by a number of methods: exact digitalization techniques, Hartree-Fock approximations and density functional approaches, or were treated as a crystal field perturbation of the surrounding semiconductor in the effective mass approximation. The models has been successfully confronted with experiments and the reader is referred to the relevant literature [4, 11, 12, 16, 17, 18], with references therein, for more details.

2.1.1 Harmonic confining potential

In the investigated system, as shown in experiments, the best approximation of the lateral potential is given by the anisotropic harmonic-oscillator (compare with Fig.2.1 that illustrates the potential shape in one spatial direction):

$$V(x,y) = V_0 + \frac{1}{2}m * \omega^2(\delta x^2 + \frac{1}{\delta}y^2) \tag{2.1}$$

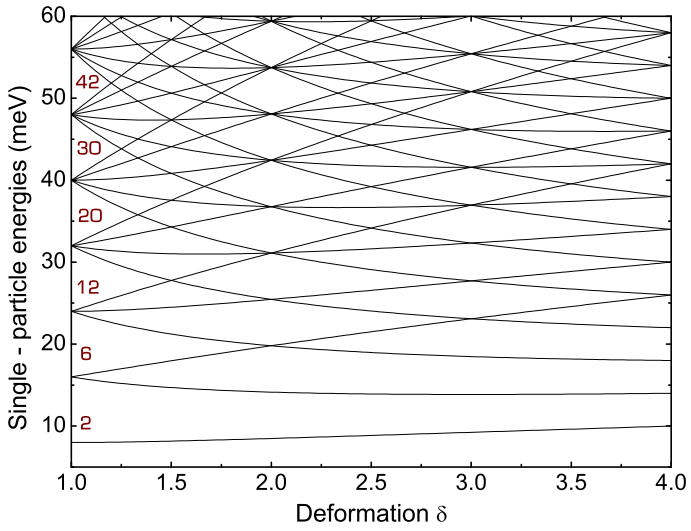

Figure 2.2: *Single particle states of a two-dimensional anisotropic harmonic oscillator as a function of deformation $\delta > 1$. Degeneracies in the isotropic case δ=1 lead to closed shells for quantum dot occupations N=2,6,12,20,... including spin degeneracy. The spectrum is illustrated for $\hbar\omega_0$=8meV.*

It can be treated as a mean-field potential in which N carriers with an effective mass $m*$ are assumed to move independently. The ratio $\delta = \frac{\omega_x}{\omega_y}$ with frequencies $\omega_x = \omega\sqrt{\delta}$ and $\omega_x = \omega/\sqrt{\delta}$ defines the ratio of semi-axes of the ellipse equipotentials. The constraint $\omega_0^2 = \omega_x\omega_y$ conserves the area with deformation.

The corresponding single particle energy spectrum:

$$\epsilon_{n_x,n_y}(\delta) = \hbar\omega[(n_x + \frac{1}{2})\sqrt{\delta} + (n_y + \frac{1}{2})/\sqrt{\delta}] \tag{2.2}$$

is shown in Fig.2.2 as a function of the deformation δ. n_x and n_y are integers that total $n = n_x + n_y$=0,1,2,3,....

The isotropic case corresponds to δ=1 and the single particle energy spectrum is composed of equidistant energy levels with a characteristic energy determined by:

$$\epsilon_n(\delta) = \hbar\omega_0(n + 1) \tag{2.3}$$

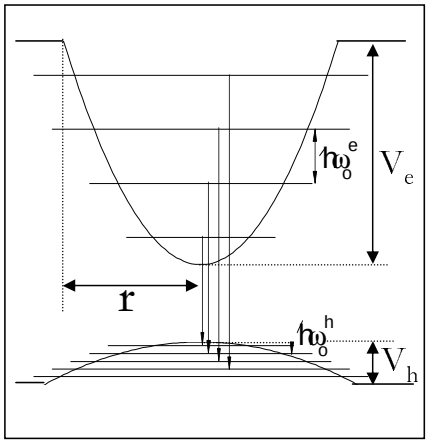

Figure 2.3: *Illustration of general notations for quantum dot potential shape description used in this work.*

The depth of the electron and hole harmonic potential, $V_{e,h}$, and the characteristic electron and hole energies, $\hbar\omega_e$ and $\hbar\omega_h$, respectively, are the most general properties of the investigated quantum dots. The notation used in this work is illustrated in Fig.2.3, where r represents the spatial dimensions of the dots, x and y, and, in the case of isotropic dots, determines their radius. In general, if not otherwise stated, it is assumed that the quantum dots are isotropic in shape.

The example of dimensions and width of the lateral potential for a typical dot is shown in Fig.2.4. The main allowed transitions from ground and excited levels, which follow the momentum conservation rule, are marked by vertical arrows. The E_0 transition is the ground state transition and E_1, E_2 correspond to the recombination of an electron and a hole from the first and second excited shells, respectively. Since no emission from the third excited state is visible with increasing excitation

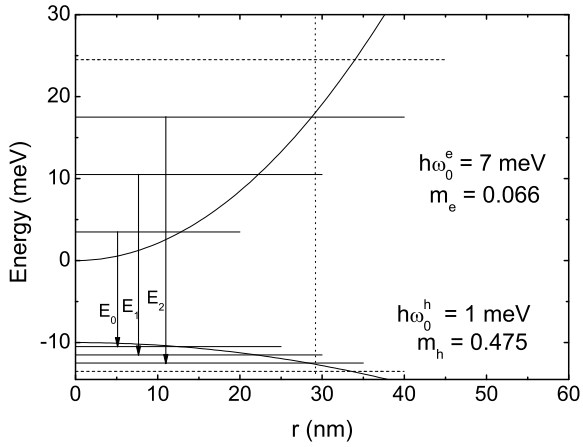

Figure 2.4: *Evaluated dimensions and width of electron and hole potential in harmonic oscillator model for typical quantum dot. The dots' emission spectrum is illustrated in Fig.7.10 and Fig.7.9.*

power (see Fig.7.10), it is assumed that there is not third excited bound state that can be populated by carriers. The vertical dashed line illustrates the limit of the quantum dot dimension that can be deduced from the experiment. Thus the radius of the dot can be estimated as being slightly bigger than the second excited electronic level, approx. 30nm in this particular case.

2.1.2 Shell degeneracy

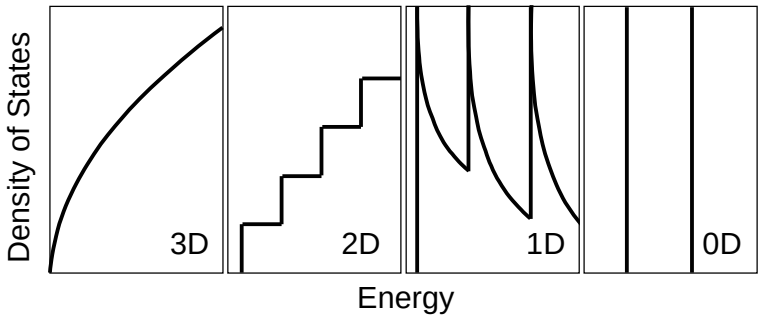

Figure 2.5: *The density of states versus energy in systems of different dimensions 3D- bulk material; 2D - quantum well; 1D - quantum wire; 0D - quantum dot.*

As it was discussed in the previous section, the energy of carriers confined in

all three dimensions in a quantum dot is strongly quantized with the spectrum composed of discrete energy levels. In general, the reduced dimensionality strictly influence both the energy and the density of states. Fig.2.5 illustrates this effect when increasing the confinement from 3D system (bulk) materials to 0D systems (quantum dots). In the quantum dot the density of states becomes discrete and is similar to set of δ-functions. For this reason, the quantum dots are often described as *artificial atoms*.

Filling the discrete energy levels with noninteracting fermions (electrons or holes) in the case of a cylindrically symmetric, harmonic potential leads to the closed shell structure for a sequence of N=2,6,12,20,... particles (as marked in Fig.2.2). This includes the spin degeneracy with the factor of 2 and the Pauli principle has to be respected. For these configurations, a particular stability of the system is reached, therefore they are often referred to as *magic numbers*. The shells are then populated according to Hund's rule: due to the Pauli exclusion principle and the repulsive Coulomb interaction, the spin is maximized for half filled orbitals.

This particular shell degeneracy leads to a number of properties that are significantly different from other systems. For example, Coulomb blockade oscillations or state blocking effects (due to the Pauli exclusion principle) play an important role in the carrier properties in quantum dots.

2.2 Exciton in a quantum dot

Excitons are the bound states of electrons and holes. The Coulomb forces act attractively between the two particles: negatively and positively charged, respectively, and a stable state can be formed.

Two factors are responsible for the exciton properties in a quantum dot. The first is the Coulomb interaction between the electron and hole. The second is the confinement by the quantum dot three-dimensional potential. The Coulomb interaction is controlled by the static dielectric constant of the quantum dot semiconductor material and imposes exciton binding. The confinement is ruled by the size and shape of the dot as well as by the dot and barrier material to produce various bands offsets. In the quantum dots the confinement also influences binding energy. Therefore, both factors influence the energy and oscillator strength of exciton in a complex way.

The effect of quantum confinement on excitons in semiconductors of low dimensions have been intensively investigated for many years [19, 20, 21]. As the size of the quantum dots approaches the Bohr radius of bulk exciton, quantum confinement effects become apparent.

There are two limiting cases depending upon the ratio between the radius of the quantum dot r and the effective Bohr radius of the bulk exciton $a*_B$:

$$a*_B = \frac{\varepsilon\hbar^2}{m*e^2} = 0.0529\frac{\varepsilon}{m*/m_0} \tag{2.4}$$

where $m*$ is the effective reduced mass of the exciton $1/m* = 1/m_e + 1/m_h$, with m_e and m_h being the electron and hole effective masses,respectively.

For $r/a*_B \gg 1$ the exciton can be treated as a quasiparticle moving around inside the quantum dot with only little energy increment due to the confinement.

In the opposite limit, $r/a*_B \ll 1$, confinement effects dominate, and the individual particles predominantly in their respective single - particle ground states with only little spatial correlation between them. This regime is called the strong-confinement regime.

In the case of pure GaAs, with $m*=0.058m_0$ and $\varepsilon=12.85$, the exciton Bohr radius according to eq.2.4 is $\simeq$10nm. The sizes of the investigated quantum dots can be estimated at tens of nm (see 2.1.1). Thus the both dimensions are comparable and the problem of an exciton in a confining potential is complex in this case.

2.2.1 Exciton binding energy

The exciton binding energy is the difference in energy between an electron-hole pair bound by the Coulomb forces and an uncorrelated electron - hole pair. The exciton binding energies in confined systems are found to be substantially increased with respect to the bulk value, and the effect of confinement was found to begin with sizes as large as ten times the Bohr radius [22].

The strong confinement of excitons in the quantum dots enhances the electron and hole interaction due to increased overlap of electron and hole wave functions in two ways. First, the overlap is enhanced because of reduced dimensionality in 0D dots. Second, the electron and hole overlap is determined by the size and shape of the quantum dot, and the barrier height. Both effects significantly affect the exciton binding energy.

In general, different methods have been applied to evaluate the exciton binding energy in a quantum dot of defined size. The most common is to calculate the value from the diamagnetic coefficient (compare with 2.3.1) by comparing the measured diamagnetic shifts with those for a bulk system having anisotropic masses [22, 23, 24]. In the method the effect of geometric confinement potential is represented approximately by the anisotropic deformation of the exciton wave function in the bulk model. The exciton binding energy is given in this case by the effective Rydberg $R*_0$ [22]:

$$E_B \simeq R*_0 \simeq \frac{e^4\mu}{2\hbar^2\varepsilon^2} \simeq 13.6\frac{\mu/m_0}{\varepsilon^2}eV \tag{2.5}$$

where

$$\frac{1}{\mu} = \frac{1}{3}\left(\frac{1}{\mu_x} + \frac{1}{\mu_y} + \frac{1}{\mu_z}\right) \tag{2.6}$$

$$\mu_x \approx \mu_y \tag{2.7}$$

for quantum dots. The values of E_B are of ∼5meV in bulk GaAs and ∼10meV in GaAs quantum wells.

In the case of the investigated quantum dot the exciton binding energy is evaluated at about a dozen meV. The experiments that allowed to estimate the value are described in 6.3.5 and 7.2.1.

2.3 Modification of energy levels in a magnetic field

The problem of excitons confined in a quantum dot exposed to a magnetic field is not trivial. The three energies: Coulomb binding energy of the electron and hole pair, spatial confinement and cyclotron energy interplay. For strongly spatially confined particles, where the confinement is smaller than the magnetic length, the magnetic field can be treated as a perturbation of the energy structure of carriers induced by confinement. However, for strong magnetic field the cyclotron energy is much larger than the typical Coulomb energy, so that the properties of atoms, molecules or finally quantum dots with carriers are qualitatively changed by magnetic field.

In the following sections the effect of a magnetic field on excitons in quantum dots is discussed within two approaches:

- In the case when single excitons in the quantum dot are discussed, the exciton is treated as a Coulomb-bound quasiparticle exposed to a magnetic field. This approach is justified in the sense that, for single exciton formation, the electrons and holes are confined in the smallest s shells and the Coulomb forces are considered to be strong with comparison to the confinement effect.

- In a highly populated quantum dot carriers occupy orbits of large diameter and thus electron and hole wave functions are more delocalized and carriers can be treated as two separate systems, in the first approximation. They are described in the model of a single particle in a harmonic confining potential in a magnetic field, which is a Fock - Darwin approach to the problem.

Both described models are justified by the experimental results.

2.3.1 Quantum dot exciton in a magnetic field

The application of an external magnetic field on an exciton in a quantum dot has two effects on the energy structure. The first is spin splitting of the levels, which is linear in magnetic field. The second is the sub-linear increase in energy of both spin-split energy levels.

There are two limits in magnetic field behaviour depending on the strength of the field. The magnetic length scale given by:

$$l^2 = \frac{\hbar}{eB} \tag{2.8}$$

determines the crossover from low to high field regime. As long as $l \ll a_B$ it is the low-field regime.

Equivalently, the parameter:

$$\gamma = \frac{\hbar\omega_c}{2E_B} \tag{2.9}$$

describes the magnitude of the two energy scales. If the cyclotron energy $\hbar\omega_c = \hbar eB/\mu$ is much smaller than the exciton binding energy E_B, the low field regime is considered. In the opposite case it is the high-field regime.

In the case of a `weak magnetic field`, the energy increases quadratically with the applied field. The energy shift is expected to vary quadratically as long as the shifts are small compared to the exciton binding energy. This quadratic shift in energy with magnetic field gives the information about effects of confinement and the Coulomb interaction in quantum dot. In this case the exciton energy in a magnetic field can be written as:

$$E(B) = E_0 \pm \frac{1}{2} g * \mu_B B + dB^2 \tag{2.10}$$

where $g*$ is the effective g-factor of a confined exciton, $\mu_B = e\hbar/2m$ is the Bohr magneton and d is the diamagnetic coefficient, which describes the low-field limit of the diamagnetic shift.

The diamagnetic shift magnitude is determined by the spatial dimensions of the exciton wave function in the direction perpendicular to the magnetic field. In the Faraday configuration the magnetic field confines the carriers in the $x - y$ plane. Therefore the diamagnetic coefficient represents the wave function along the lateral direction (x and y). Due to the flat shape of the quantum dots, the confinement along the z direction is much stronger than that along the x and y directions, thus the exciton wave function is significantly shrunk along the z direction even at 0T. The application of a magnetic field, even of small magnitude in the Faraday configuration, causes additional confinement with significant effect.

Exciton diamagnetic shifts have come to be of considerable interest in semiconductor nanostructures because, apart from being taken to be a measure of exciton confinement, are also used to estimate the exciton binding energy. The quantitative connections between the diamagnetic coefficient and the effect of confinement has been discussed in the number of theoretical and experimental papers [22, 23, 24, 25, 26].

The diamagnetic coefficient can be approximated [25] by:

$$d = \frac{e^2}{8}\left(\frac{< r_e^2 >}{m*_e} + \frac{< r_h^2 >}{m*_h}\right) \tag{2.11}$$

where $< r_{e,h}^2 >$ are the mean square lateral extensions of the electron and hole wave functions in the plane of the dot.

However, confinement influences both the effective exciton radius and the exciton reduced mass [27]. As it is shown in paper [27]: stronger confinement decreases the exciton radius and increases the exciton reduced mass. Both factors decrease the diamagnetic coefficient. Therefore, the reduction of the exciton diamagnetic shift is consistently interpreted as a confinement effect.

In general, the diamagnetic shift is quadratic in the field up to a few tesla before reaching a mostly linear asymptotic limit at very high field strengths. If the Coulomb interaction between the electron and hole forming the exciton is taken into account, the total diamagnetic shift of the exciton is effectively smaller than that given by eq.2.11, due to additional confinement of the exciton wave function in the dot.

This effect can be included, if a different approach to the quantum dot exciton in a magnetic field is applied. If the exciton confined in the quantum dot is considered as a hydrogen atom in potential barriers, the description of the exciton energy levels can give better results, especially in high magnetic field regime.

The problem of a two-dimensional hydrogen atom at arbitrary magnetic field is discussed in Ref.[28]. The weak-field regime is treated by considering the magnetic field as a perturbation while in the strong-field regime the coulomb potential is treated as a perturbation. The interpolation between these two limiting situations is given by a two-point Padé approximant $\xi_{k,m}^{s,t}$, where k and m are the principal and azimuth quantum number of the hydrogen-like state, respectively, and s and t denote the order of interpolation. This gives the analytic expression for the magnetic field dependent spectrum at arbitrary magnetic field strength for the ground and excited states.

The $1s$ state energy of an exciton in such an approach is described by:

$$E_{1s} = E_0 \pm \frac{1}{2} g * \mu_B B + \xi_{1s}^{s,t}(z) \tag{2.12}$$

where

$$\xi_{1s}^{s,t}(z) = \frac{P_{1s}^s}{Q_{1s}^t} \tag{2.13}$$

$$P_{1s}^s = p_0 + p_1 z + \ldots + p_s z^s \tag{2.14}$$

$$Q_{1s}^t = q_0 + q_1 z + \ldots + q_t z^t \tag{2.15}$$

$$z = \sqrt{\gamma} \tag{2.16}$$

and γ is given by eq.2.9. The exact values for p_s and q_t are given in Ref.[28] in Table V.

2.3.2 Carriers in a harmonic potential in a high magnetic field

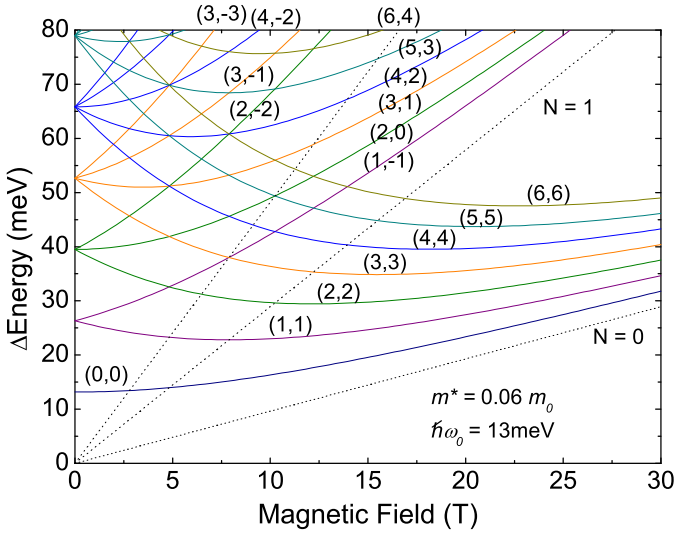

Figure 2.6: *Fock - Darwin energy levels at magnetic field. Dotted lines correspond to the first three Landau levels.*

The application of magnetic field to a zero - dimensional quantum object imposes the change of its discrete energy levels. The single particle motion confined in a two dimensional quantum well potential of parabolic shape exposed to a magnetic field can be described by the Hamiltonian (in the effective mass approximation):

$$H = \frac{1}{2m*}(\mathbf{p} - \frac{e}{c}\mathbf{A})^2 + \frac{1}{2}m*\omega_0^2 r^2 = \frac{p^2}{2m*} + \frac{1}{2}m*(\omega_0^2 + \frac{1}{4}\omega_c^2)r^2 - \frac{1}{2}\omega_c l_z \quad (2.17)$$

where $m*$ is the electron effective mass, r is the distance, p - momentum, with $l_z = xp_x - yp_y$ being the z component of the angular momentum operator, $\mathbf{A} = \frac{1}{2}\mathbf{B} \times \mathbf{r}$ is the magnetic field $\mathbf{B}$ vector potential (in the symmetrical gauge) and $\omega_c = \frac{eB}{m*}$ is the cyclotron frequency.

The eigen states of such a Hamiltonian and thus the corresponding eigen energies were found analytically by Fock [29] and Darwin [30] and at given field are given by:

$$\epsilon(n, m) = \hbar\Omega(n + 1) - \frac{1}{2}\hbar\omega_c m \quad (2.18)$$

$$\Omega^2 = \omega_0^2 + \frac{1}{4}\omega_c^2 \quad (2.19)$$

The quantum numbers (n, m) follows: n=0,1,2,3,... as the radial quantum numbers, and the azimuthal momentum quantum number $m = -n, -n+2, \ldots, n-2, n$.

The evolution of the energy spectrum in the increasing magnetic field is illustrated in Fig.2.6. In the picture the spin Zeeman splitting was neglected. The photoluminescence from the excited states of the investigated quantum dots is very broad and the effect of Zeeman splitting is not visible in the experiment. Thus, the Fock - Darwin orbital states are here twice degenerate.

The pairs of values indicated in Fig.2.6 correspond to the (n, m) quantum numbers and the dotted, straight lines illustrate the subsequent, first three Landau levels. The Landau level fan-chart, in this case, corresponds to the situation when there is no parabolic confinement potential in the dot plane. The clustering of the discrete energies of the quantum dot in the high magnetic field regime into bands with the limit at the Landau levels is a characteristic feature of the system. At high magnetic field, i. e. when $\omega_c \gg \omega_0$, the localization of the carriers at the cyclotron orbits is so strong that the carriers do not feel the confining parabolic potential any more, thus behave like free carriers in a magnetic field and form *Landau level bands*.

From the spectrum it is observed that at high magnetic fields it is energetically favourable to populate only the lowest states sequentially with single-particle angular momentum m=1,2,3,4,..., and the energy increases monotonically with magnetic field.

Bibliography

[1] M. Reed, "Quantum dots," *Scientific American*, vol. 268, p. 118, 1993.

[2] R. C. Ashoori, H. L. Stormer, J. S. Weiner, L. N. Pfeiffer, K. W. Baldwin, and K. W. West, "N-electron ground state energies of a quantum dot in magnetic field," *Phys. Rev. Lett*, vol. 71, p. 613, 1993.

[3] M. A. Kastner, "Artificial atoms," *Phys. Today*, vol. 46, p. 24, 1993.

[4] S. M. Reimann and M. Manninen, "Electronic structure of quantum dots," *Rev. of Modern Physics*, vol. 74, p. 1283, 2002.

[5] L. Kouwenhoven and C. Marcus, "Quantum dots," *Phys. World*, vol. 6, p. 35, 1998.

[6] L. Kouwenhoven, D. Austing, and S. Tarucha, "Few-electron quantum dots," *Reports on Progress in Physics*, vol. 64, p. 701, 2001.

[7] K. Harmans, "Next electron, please. . . ," *Phys. World*, vol. 5, p. 50, 1992.

[8] R. C. Ashori, "Electrons in artificial atoms," *Nature*, vol. 379, p. 413, 1996.

[9] A. Zunger, "Electronic-structure theory of semiconductor quantum dots," *MRS Bulletin*, p. 35, 1998.

[10] L. Jacak, P. Hawrylak, and A. Wòjs, "Kropki kwantowe," *Oficyna Wydawnicza Politechniki Wrocławskiej, Wrocław*, 1996.

[11] P. Michler(Ed.), "Single quantum dots. Fundamentals, applications and new concepts," *Topics in Applied Physics, Springer*, vol. 60, 2003.

[12] K. Varga, P. Navratil, J. Usukura, and Y.Suzuki, "Properties of few-electron artificial atoms," *arXiv:cond-mat/0010398v1 [cond-mat.mes-hall]*, 2000.

[13] W. Jaskólski, "Confined many-electron systems," *Physics Reports*, vol. 271, p. 1, 1996.

[14] S. J. Lee, N. H. Shin, J. J. Ko, M. J. Park, and R. Kummel, "Density of states of quantum dots and crossover from 3D to 0D electron gas," *Semicond. Sci. Technol.*, vol. 7, p. 1072, 1992.

[15] G. W. Bryant, "Electronic structure of ultrasmall quantum-well boxes," *Phys. Rev. Lett.*, vol. 59, p. 1140, 1987.

[16] P. Hawrylak, A. Wójs, and J. A. Brum, "Magneto-excitons and correlated electrons in quantum dots in a magnetic field," *Phys. Rev. B*, vol. 54, p. 11397, 1996.

[17] P. Hawrylak, A. Wójs, and J. A. Brum, "Magneto-excitons in droplets of a chiral luttinger liquid formed in quantum dots in a magnetic field," *Solid State Communications*, vol. 98, p. 847, 1995.

[18] A. Wójs, P. Hawrylak, S. Fafard, and L. Jacak, "Electronic structure and magneto-optics of self-assembled quantum dots," *Phys. Rev. B*, vol. 54, p. 5604, 1996.

[19] G. T. Einevoll, "Confinement of excitons in quantum dots," *Phys. Rev. B*, vol. 45, p. 3410, 1992.

[20] L. E. Brus, "Electron - electron and electron - hole interactions in small semiconductor crystalities: The size dependence of the lowest excited electronic state," *J. Chem. Phys.*, vol. 80, p. 4403, 1984.

[21] Y. Kayanuma and H. Momiji, "Incomplete confinement of electrons and holes in microcrystals," *Phys. Rev. B*, vol. 41, p. 10261, 1990.

[22] M. Bayer, S. N. Walck, T. L. Reinecke, and A. Forchel, "Exciton binding energies and diamagnetic shifts in semiconductor quantum wires and quantum dots," *Phys. Rev. B*, vol. 57, p. 6584, 1998.

[23] Y. Nagamune, Y. Arakawa, S. Tsukamoto, M. Nishioka, S. Sasaki, and N. Miura, "Photoluminescence spectra and anisotropic energy shift of GaAs quantum wires in high magnetic fields," *Phys. Rev. Lett.*, vol. 69, p. 2963, 1994.

[24] R. Rinaldi, R. Cingolani, M. Lepore, M. Ferrara, I. M. Catalano, F. Rossi, L. Rota, E. Molinari, P. Lugli, U. Marti, D. Martin, F. Morier-Gemoud, P. Ruterana, and F. K. Reinhart, "Exciton binding energy in GaAs V-shaped quantum wires," *Phys. Rev. Lett.*, vol. 73, p. 2899, 1994.

[25] S. N. Walck and T. L. Reinecke, "Exciton diamagnetic shift in semiconductor nanostructures," *Phys. Rev. B*, vol. 57, p. 9088, 1997.

[26] A. Kuther, M. Bayer, A. Forchel, A. Gorbunov, V. B. Timofeev, F. Schäfer, and J. P. Reithmaier, "Zeeman splitting of excitons and biexcitons in single $In_{0.60}Ga_{0.40}As$/GaAs self-assembled quantum dots," *Phys. Rev. B*, vol. 58, 1998.

[27] N. Schildermans, M. Hayne, V. V. Moshchalkov, A. Rastelli, and O. G. Schmidt, "Nonparabolic band effects in GaAs/$Al_xGa_{1-x}As$ quantum dots and ultrathin quantum wells," *Phys. Rev. B*, vol. 72, p. 115312, 2005.

[28] A. H. MacDonald and D. S. Ritchie, "Hydrogenic energy levels in two dimensions at arbitrary magnetic fields," *Phys. Rev. B*, vol. 33, p. 8336, 1986.

[29] V. Fock, "Bemerkung zur quantelung des harmonischen oszillators in magnetfeld," *Z. Phys.*, vol. 47, p. 446, 1928.

[30] C. G. Darwin *Proc. Cambridge Philos. Soc.*, vol. 27, p. 86, 1930.

Chapter 3

The Investigated System

Dans ce chapitre, nous présentons les détails des échantillons étudiés. Ils sont constitués de doubles puits quantiques GaAs/AlAs de type II. Deux types de structures sont présentés : les structures de type "indirect" et celles de type "pseudo-direct".
Nous démontrons ensuite l'existence de ces boîtes quantiques dans les structures étudiées et nous proposons un modèle de distribution de potentiel expliquant leur formation.

The following chapter contains the general descriptions of the samples that were used in this work.

Most of the experiments were performed on samples containing `GaAs quantum dots`. The detailed description of the potential distribution and symmetry of the bands in quantum dots can be found in section 3.2.

However, the quantum dots were not grown intentionally. In a number of experiments described in chapter 5 it was discovered that they can be formed naturally in `the GaAs/AlAs type II double quantum well` structures. Thus the first part of the chapter, 3.1, describes the GaAs/AlAs double quantum well system, the position of the energy levels and the symmetry of the bands.

All studied samples were grown at the Laboratoire de Microstructures et de Microélectronique, CNRS, in Bagneux, France by R. Planel and V. Thierry - Mieg by the MBE method.

3.1 GaAs/AlAs type II double quantum wells

Two types of GaAs/AlAs double quantum well structures, with different values of quantum well width and therefore with different respective alignment of the X_{XY} and X_Z subbands in the AlAs layer, were studied. In the so-called `indirect` structure X_{XY} is located below the X_Z subband. This alignment is inverted in the so-called `pseudo-direct` structure. (See 3.1.1 for details). The nominal, main parts of the pseudo-direct, sample J709, and indirect, sample J707, structures are

presented in Tab.3.1 and Tab.3.2, respectively.

Moreover, an additional sample, M26L12, was studied. Its main part was similar to the structure of sample J709 (see Tab.3.3), thus it was pseudo-direct in structure. However, the sample was made without substrate rotation to increase the lateral alloy inhomogeneities. In comparison to sample J709 it consists additionally of two quantum wells (see Tab.3.4).

During the growth procedure in all samples the process was interrupted to assure the smoothness at the interfaces.

Sample	J709
substrate	
undoped GaAs buffer	$\sim 0.9\mu$m
$Ga_{0.67}Al_{0.33}As$	90nm
AlAs	5nm
GaAs	2.4nm
$Ga_{0.67}Al_{0.33}As$	90nm
GaAs	10nm

Table 3.1: *The nominal structure of the main part of the* pseudo-direct*-type, J709, sample.*

Sample	J707
substrate	
undoped GaAs buffer	$\sim 0.9\mu$m
$Ga_{0.67}Al_{0.33}As$	90nm
GaAs	2.4nm
AlAs	10nm
$Ga_{0.67}Al_{0.33}As$	90nm
GaAs	10nm

Table 3.2: *The nominal structure of the main part of the* indirect*-type, J707, sample.*

3.1.1 Energy structure

The effect of type II alignment in GaAs/AlAs double layer structures was achieved by the appropriate choice of the GaAs and AlAs layers' width [1, 2]. The energies of the X and Γ conduction bands in GaAlAs vary strongly depending on the Al composition [3]. The lowest energy band is of X-type for GaAs and of Γ-type for pure AlAs. In the GaAs/AlAs double quantum well system, due to the confinement, the Γ band eigenstate in the conduction band of GaAs can be pushed up in energy by

Sample	M26L12
$Ga_{0.60}Al_{0.40}As$	100nm
GaAs	3nm
AlAs	5nm
$Ga_{0.60}Al_{0.40}As$	100nm
GaAs	50nm

Table 3.3: *The nominal structure of main part of the* pseudo-direct-*type, M26L12, sample.*

Sample	M26L12
substrate	
undoped GaAs buffer	$\sim 0.9\mu$m
AlAs	5nm
GaAs	10nm
AlAs	5nm
GaAs	50nm
AlAs	5nm
GaAs	5nm
$Ga_{0.60}Al_{0.40}As$	1 monolayer
GaAs	5nm
AlAs	5nm
GaAs	50nm

Table 3.4: *The nominal structure of additional two quantum wells in the M26L12 sample.*

reducing the width of GaAs layer. It is therefore higher in energy than the X-band eigenstate in the AlAs layer. The lowest energy level of the valence band is always in the GaAs layer and is of Γ symmetry. As a result, a spatially separated electron and hole system is achieved.

An additional effect that gives the splitting of the X-band eigenstate in the AlAs layer into X_{XY} and X_Z symmetry eigenstates is the strain that is induced by the lattice mismatch [4]. GaAs and AlAs crystallize in the same lattice structure (zinc blende) and have almost the same lattice constants (a_0(GaAs)=5.6531$\mathring{A}$ and a_0(AlAs)=5.6622$\mathring{A}$ [5]). Even if the lattice mismatch is of 0.16%, the AlAs layer deposited on GaAs feels a small stress, leading to compression along the axis perpendicular to the growth direction and to dilatation along the growth direction. The resulting splitting of the X-symmetry eigenstate is not negligible. In consequence the X_{XY} eigenstate is lower in energy by approx. 15-20meV than the X_Z eigenstate. Further on, due to the different effective masses of carriers on both X_{XY} and X_Z levels, the confinement effect pushes the X_{XY} level up in energy more strongly than the X_Z level.

Whenever X_Z is the lowest energy level, the structure is called `pseudo-direct`; whenever X_{XY} is the lowest energy level, the structure is called `indirect`.

The reason for this classification is given by the optical properties of the respective transitions. Pseudo-direct transitions (X_Z - Γ) can appear in the spectrum without any phonon assistance although they are indirect in k-space. The k selection rule for this transition is weakened because of a broken translationary invariance of the Hamiltonian operator due to the interface between two layers. On the contrary, for the indirect transitions (X_{XY} - Γ), the translationary invariance is normally not broken and therefore only phonon-assisted transitions are allowed. The PL spectra obtained on both structures are presented in chapter 5 in section 5.1.

The evolution of the energy bands in the main part of the pseudo-direct and indirect structure are illustrated in Fig.3.1 a) and b), respectively.

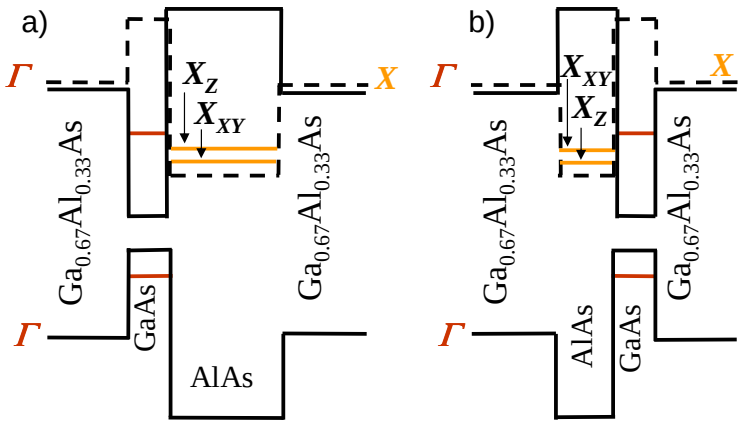

Figure 3.1: *Distribution of the energy bands and the position of the eigenstates in the GaAs/AlAs DQW in the main part of the a) indirect and b) pseudo-direct structures. Solid line - Γ-symmetry band; dashed line - X-symmetry band; the position of Γ- and X- symmetry levels in the quantum well are marked in red and yellow colours, respectively.)*

3.1.2 TEM images

Transmission Electron Microscopy (TEM) images allowed the determination of the alloy composition across the structure, thus the nominal structure can be compared with the real one. Moreover it showed the quantum well thickness fluctuations in the investigated structures.

TEM measurements, illustrated in Fig.3.2, of indirect (J707) and pseudo-direct (J709) structures were done at the Laboratoire de Photonique et de Nanostructures, CNRS in Marcoussis, France by G. Pattriache. All the images are made in dark

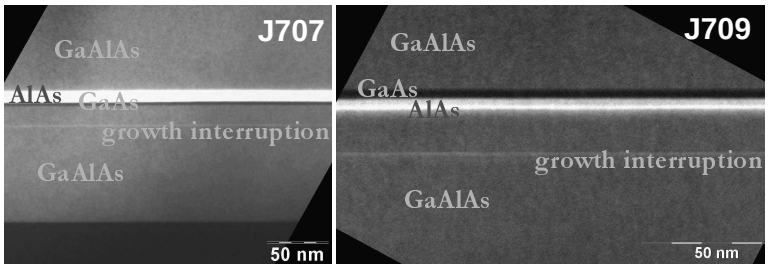

Figure 3.2: *TEM images of the J707 (left panel) and J709 (right panel) samples.* By G. Patriache, Laboratoire de Photonique et de Nanostructures, CNRS, Marcoussis, France. *The gray intensity scale in both images is different.*

field obtained on 002 reflection. This method is known as "chemically sensitive" because it is based on the difference of the diffusion factors of the atoms occupying the two III and V sublattices. The replacement of Ga atoms by Al atoms will increase the structure factor and thus the contrast. The more the (AlGa)As alloy is rich in Al, the more the layer will appear "clear" (in comparison with GaAs).

The images show that in sample J709, contrary to sample J707, the order of GaAs/AlAs stacking is reversed. I. e. in sample J707 the GaAs layer is made before the AlAs layer, in sample J709 the AlAs layer is made before the GaAs layer, in agrement with the nominal structure that has been described (compare with chapter 3.1).

The defects of width and composition variation observed in samples J707 and J709 for AlAs and GaAs layers are very weak. There are fluctuations in the order of one monolayer especially at the GaAs/AlAs interface.

3.2 GaAs quantum dots

3.2.1 Energy structure

The shape of the potential distribution in the quantum dot that can be deduced from the optical experiments (compare with section 1.2) is illustrated in Fig.3.3. In the right panel, on the scheme of the potential distribution of indirect GaAs/AlAs double quantum well (sample J707), compare with Fig.3.1a), the evolution of the quantum dot bands is marked with green, dotted lines.

It is believed that the quantum dots result from imperfections in the growth process, presumably the formation of gallium droplets (compare with Fig.3.4 and discussion in chapter 1.2). This leads to a formation of gallium-rich "islands" in which the nominal GaAs/AlAs structure is replaced by a GaAs/$Ga_{1-x}Al_xAs$ sequence, where x<0.33. This assures that the emission from the dots is observed below the main quantum well transitions. The sizes of the dots and the Ga content in the barriers cause the emission to be spread over a broad energy range, up to

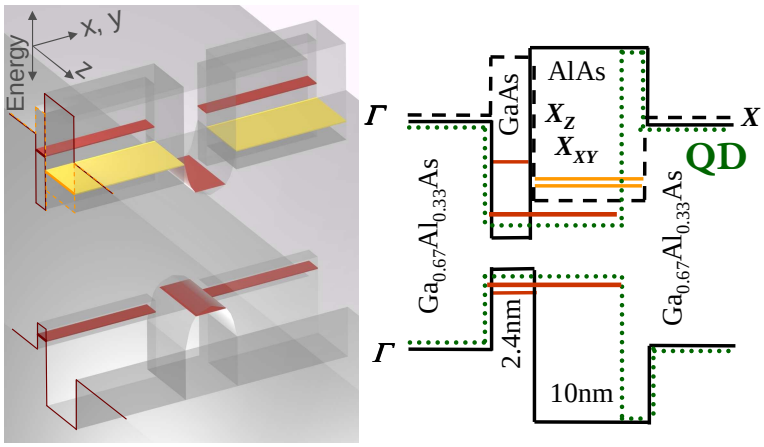

Figure 3.3: *Potential distribution through the quantum dot formed in the GaAs/AlAs type II double quantum well structure is marked schematically on the potential distribution of double quantum well structure (compare with Fig.3.1 a); solid line - Γ-symmetry band; dashed line - X-symmetry band; and green dotted line - distribution of the potential through the dot in the growth direction. The three dimensional picture illustrates the symmetry and shape of the dot potential (harmonic type) in the plane of the quantum well layers. The x and y coordinates are the plane and z is the growth direction. The positions of the first electronic levels in the quantum well and dot are marked as the colored layers. The levels of Γ-symmetry and of X-symmetry are illustrated with red and yellow colour, respectively.*

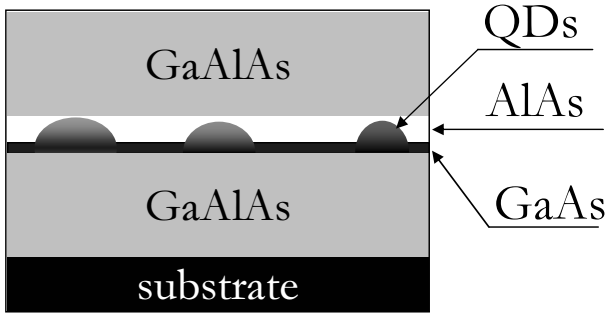

Figure 3.4: *General scheme of the sample structure containing quantum dots.*

150meV. However, the characteristic cut-off of the photoluminescence at approx. 1.56eV in Fig.5.2 is assigned to the situation when a pure GaAs dot is formed in the whole AlAs layer and thus has a height of 12.4nm.

The three dimensional image of the sample structure in the left panel in Fig.3.3 illustrates the potential evolution in the quantum dot in comparison to the energy position of surrounding barriers. The harmonic shape potential confines the quantum dot in the quantum well plane. The electronic level in the dot is of Γ symmetry (marked in red) and the surrounding barrier is of X symmetry (marked in yellow).

3.2.2 KFM images

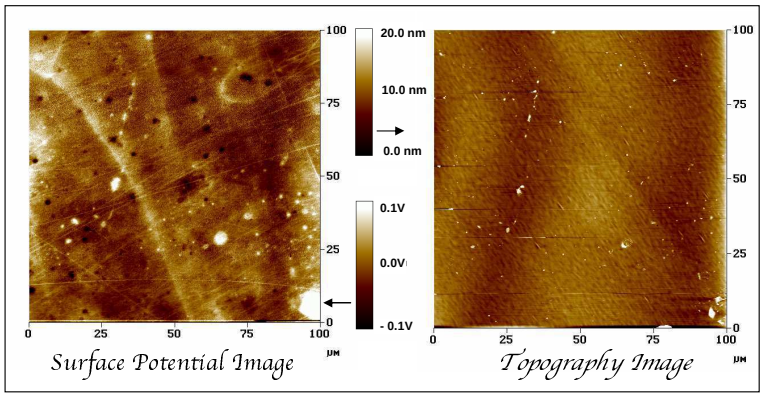

Figure 3.5: *KFM images of the 100µm x 100µm sample region. Left panel: potential distribution for electrons. Right panel: topography image.* By R. Bożek, University of Warsaw, Warsaw, Poland.

One of the indications about the surface distribution of the quantum dots and their potential structure came from the topography image of the sample and surface potential distribution obtained by Kelvin Force Microscopy (KFM). The experimental setup, available at the *Institute of Solid State Physics* at *University of Warsaw* in Poland, consisted of Nanoscope IIIa equipped with an extender electronics module [6, 7].

In this technique the topology of the sample surface and potential distribution inside (equivalent to the work function for electrons) are measured.

The obtained images are illustrated in Fig.3.5. Although the sample has a flat morphology, pits in the form of black dots in the potential distribution are visible, not correlated with any features at the surface. They correspond to the minimum of the potential for electrons. Such an image would be obtained if, for example, islands of lower band gap, Ga-rich in this case, were formed. This suggests that the segregation of Ga into AlAs well is responsible for the investigated dots.

Bibliography

[1] G. Danan, B. Etienne, F. Mollot, R. Planel, A. Jean-Louis, F. Alexandre, B. Jusserand, G. L. Roux, J. Marzin, H. Savary, and B. Sermage, "Optical evidence of the direct-to-indirect-gap transition in GaAs-AlAs short-period superlattices," *Phys. Rev. B*, vol. 35, p. 6207, 1987.

[2] H. van Kesteren, E. Cosman, P. Dawson, K. Moore, and C. Foxon, "Order of the x conduction-band valleys in type-II GaAs/AlAs quantum wells," *Phys. Rev. B*, vol. 39, p. 13426, 1989.

[3] M. R. Teisser, "Effects electro-optiques dans les hétérostructures GaAs/AlAs de type II," *PhD, Université Paris VI*, 1992.

[4] P. Lefebvre, B. Gil, M. Mathieu, and R. Planel, "Piezospectroscopy of GaAs-AlAs superlattices," *Phys. Rev. B*, vol. 40, p. 7802, 1985.

[5] B. L. Sharma and R. K. Purhoit, "Semiconductor heterojunctions," *Pergamon Press, Oxford*, 1974.

[6] M. Nonnenmacher, M. P. O. Boyle, and H. K. Wickramasinghe, "Kelvin probe foce microscopy," *Appl. Phys. Lett.*, vol. 58, p. 2921, 1991.

[7] R. Bozek, "Application of kelvin probe microscopy for nitride heterostructures," *Acta Physica Polonica A*, vol. 108, p. 541, 2005.

Chapter 4

Experimental Techniques

Dans ce chapitre, nous discutons comment il est possible, grâce à la technique de micro-photoluminescence, d'étudier les transitions optiques d'une boîte quantique unique. Nous détaillons les différentes méthodes expérimentales que nous avons utilisées pour l'étude des complexes excitoniques : la cartographie de la micro-photoluminescence, la micro-photoluminescence résolue en temps, résolue en température, la magnéto-photoluminescence et les expériences de corrélation de photons.
De manière générale, tous les dispositifs expérimentaux de micro-photoluminescence utilisent un objectif de microscope pour focaliser un faisceau laser de manière extrême, à la limite de la diffraction, et permettre d'adresser optiquement une boîte quantique unique. Les expériences optiques ont été effectuées avec un laser Argon pour les excitations au-dessus de la barrière des boîtes ou avec un laser Ti : Saphir de longueur d'onde ajustable pour les excitations quasi-résonantes. La détection de la lumière émise est réalisée par un spectromètre optique.
Le dispositif expérimental permettant la mesure de la magnéto-photoluminescence est adapté pour être utilisé dans une bobine de 50 mm de diamètre interne. Des fibres optiques sont utilisées pour véhiculer l'excitation optique jusqu'à la boîte quantique et pour collecter l'émission. La fibre d'excitation est une fibre monomode de 5 μm de diamètre qui, placée devant deux micro-lentilles adaptées aux basses températures, permet de focaliser sur une zone de l'ordre de 5 μm. L'échantillon est placé sur un module piezo-électrique de la société Attocube qui permet de choisir une boîte quantique particulière. Le champ magnétique est produit soit par une bobine supraconductrice jusqu'à 14 T soit par une bobine résistive pour les champs plus intenses.

Several experimental techniques have been used to determine the properties of the excitonic complexes that were formed in quantum dots. They all consist of the detection of the photoluminescence (PL) signal. The experiments were performed under different detection and excitation conditions. The approach was to detect the emission from a single, well isolated quantum dot. Therefore all the micro-photoluminescence (μ-PL) experimental setups were equipped with microscope objectives, of different types, as it is shown below. The spectroscopic studies of single quantum dots include μ-PL mapping, time resolved experiments and photon correlations.

The studies of type II GaAs/AlAs quantum wells to investigate the properties of the indirect system of quantum dot barriers were performed in macro-photoluminescence (macro-PL) setups.

The experimental conditions were changed in a wide range of parameters. These include excitation power variation, temperature changes from 1.7K up to 200K, application of magnetic field up to 23T.

Those various experimental methods involves different setups. The following sections describe the experimental techniques employed during the study.

4.1 Common characteristics

All the optical setups consisted of an excitation source and a spectrometer.

4.1.1 Excitation sources

Above band gap excitation was performed by a continuous wave Ar^+ laser. The emission line at λ=514.5nm was selected by an interference filter placed in the laser beam.

Below band gap excitation was performed by a continuous wave Ti:Sapphire laser tuned to the desired wavelength. It was mainly used in the photon correlation experiments.

4.1.2 Detection

The collected light was analyzed in either a single-grating (1m long, available gratings: 1800 and 3600 lines/mm) or a double-grating (2m long, available gratings: 300 and 1800 lines/mm) optical spectrometer. Both spectrometers were equipped with a 1024x512 CCD camera. The double-grating spectrometer offers a better resolution at the cost of reduced luminosity.

A 1800 lines/mm grating was used in the single-grating spectrometer in the 800nm wavelength range and the available resolution was 0.02nm per pixel in a 20nm window.

Two sets of gratings of 300 and 1800 lines/mm for the double-grating spectrometer allow measurements in the wavelength range of interest. The high density grating allowed a resolution of 0.005nm per pixel in a 2.5nm window while the 300lines/mm grating resolution was 0.05nm in a 25nm window.

In all experiments a low-pass filter was placed in front of the spectrometer to eliminate the laser and the scattered light.

4.2 Macro-photoluminescence

In the macro-PL experiments the excitation laser spot dimension was approx. 0.5mm. It was achieved by simple focusing of the laser beam on the sample surface by a standard macroscopic lens placed in front of the spectrometer (see 4.2.1 for details). Alternatively, a set of optical fibers was used. The fiber transmitting the exciting beam was placed in the proximity of the sample surface (see 4.2.2 for details).

4.2.1 Standard PL setup

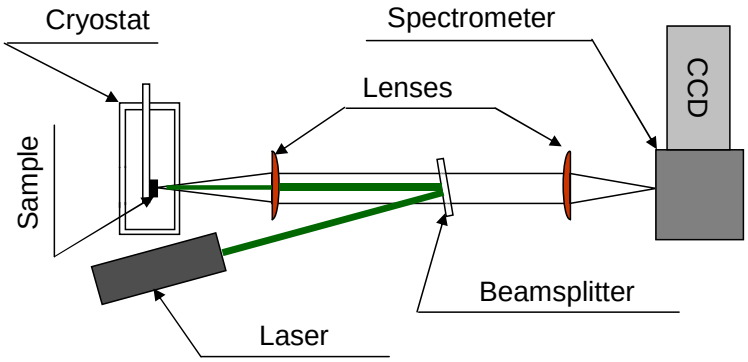

Figure 4.1: *The experimental setup for macro-photoluminescence experiments.*

The scheme of the standard photoluminescence setup is illustrated in Fig.4.1. In this system the same lens, placed in front of the spectrometer, is used to focus the exciting laser beam and to collect the photoluminescence. The PL-signal is further on focused on the slit of the spectrometer by a second lens. A set of plano-convex lenses was used to minimize spherical aberrations as they are applied in infinite conjugate geometry.

The experimental setup was available in the *Institute of Solid State Physics* at the *University of Warsaw*, in Poland.

4.2.2 Optical fiber system

The approach was to use the optical fiber system in macro-PL experiments performed in a magnetic field. Due to the small dimensions of the magnet bore and large total dimensions of the magnets it is difficult to reach the center of the magnetic field and align the beams with respect to the sample surface by placing macroscopic optical equipment outside the magnet. Thus the sample was placed in the center of the magnetic field and the light was transmitted through a set of two optical fibers, usually of 200μm core.

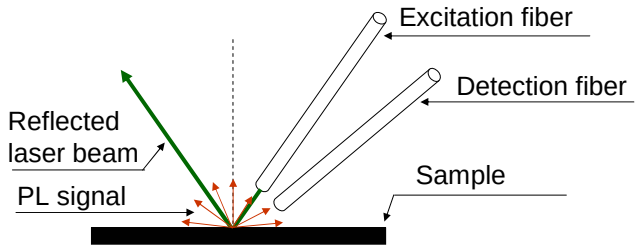

Figure 4.2: *Geometry of a two-fiber system to minimize the gathered laser light. Reflected laser light is rejected from the system.*

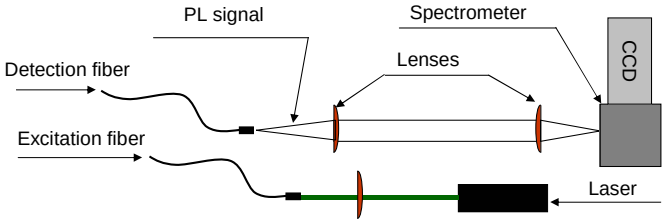

Figure 4.3: *Scheme of the connections of the output parts of the fibers with spectrometer and laser.*

The optical fibers were placed in the geometry illustrated in Fig.4.2. This assures that most of the laser light is reflected from the sample surface away from the collecting fiber. The only laser light that can enter the fiber is the one scattered from the surface imperfections. The presented geometry is almost a Faraday configuration as the magnetic field (upwards on the picture) is not completely parallel to the k-vector of the incident light and luminescence. Nevertheless, due to the large value of the GaAs refraction coefficient (n = 3.3) the incident light enters the sample almost parallel to the magnetic field direction.

The connection of the laser and the spectrometer with the outputs of the optical fibers is illustrated in Fig.4.3. The laser beam is focused by an optical lens to the entrance of the exciting fiber. The emitted light from the detection fiber is transmitted to the spectrometer by two plano-convex optical lenses placed in the *f-f* geometry.

The experimental setup was available at the *High Magnetic Field Laboratory, CNRS* in Grenoble, in France.

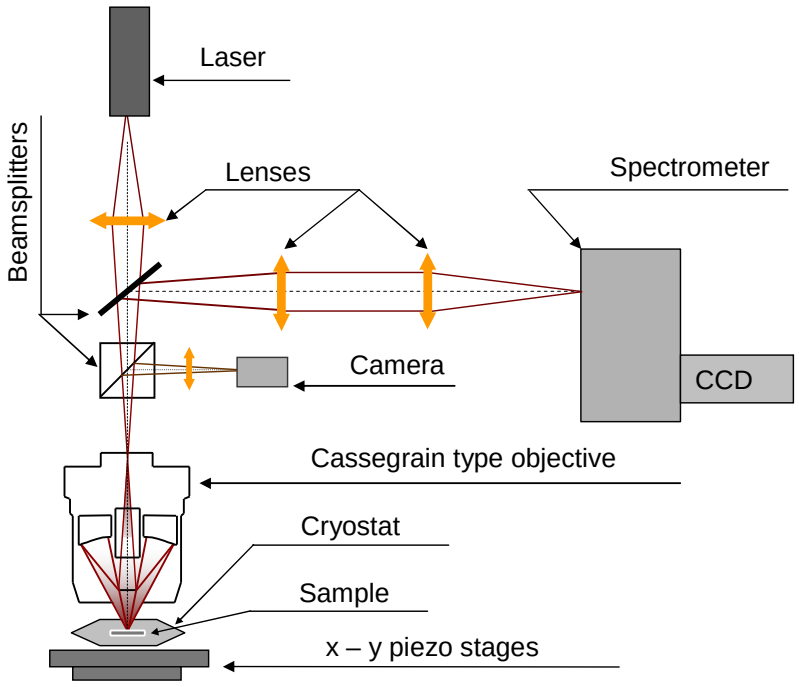

Figure 4.4: *Scheme of the micro-photoluminescence setup.*

4.3 Micro-photoluminescence

The purpose of the micro-PL experiments is to detect the emission light from the smallest possible sample region. In this work, it was used to investigate the emission from a single quantum dot. To achieve this it was necessary to reduce the exciting laser beam diameter down to several μm. This was done by passing the laser light through a microscope objective. The diameter of the focused laser beam depends on the objective and the geometry of the experimental setup. The smallest spot diameter reached in the presented systems was approx. 1μm, very close to the diffraction limit of the laser light.

The most general experimental setup used for μ-PL experiments is illustrated in Fig.4.4. The sample is placed in a He-continuous flow cryostat. All the optical parts are of macroscopic sizes and are mounted outside the cryostat. The exciting laser beam is focused on the sample surface by a microscope objective of the Cassegrain type. The objective consists of a set of mirrors instead of lenses. This assures the same focusing point for all wavelengths of the light used in the experiment. This is very useful as the exciting laser beam and the detected signal, which have different energies, are passing through the same objective. The PL signal reflected by the beamsplitter is then focused on the spectrometer slit by an optical lens. A collimated beam is formed out of the collected light to simplify the alignment of the optical parts and to place the necessary optical filters in the parallel beam.

The cryostat is mounted on x-y piezostages. This assures easy scanning of the sample and best choice of the desired place for measurement.

The experimental setup was available at the *High Magnetic Field Laboratory, CNRS* in Grenoble, in France and *Institute of Solid State Physics* at the *University of Warsaw*, in Poland.

4.3.1 Variable temperature experiments

The temperature of the sample was controlled directly in the cryostat. A small size cryostat, cooled by the constant flow of helium, was used. The temperature was controlled either by the helium flux or by the use of a small heater mounted below the sample inside the cryostat. In the experiments the temperature was varied from 4.2K up to 200K with a best precision of 0.1K.

4.3.2 Micro-PL mapping

The scanning of the defined sample region is a very useful technique to precisely define the position of the investigated object (i.e. the quantum dot) and to determine its surroundings (i.e. the vicinity of other quantum dots or impurities).

In the experimental configuration illustrated in Fig.4.4 the exciting laser beam and the collected signal are not independent. Both beams passing through the microscope objective are focused on the same sample region. A movement of the

exciting laser beam involves at the same time a change of the region of collection.

The scan of the sample surface was done by placing a thick parallel plate in front of the microscope objective. The position of the laser beam on the sample surface was changed by rotation of the plate. The movement was synchronized with a motor and a computer. The selected region of the sample was scanned with a precision of approx. 1μm.

The other possible method of scanning of the sample surface was to move the entire cryostat, with the sample mounted inside, by piezostages. The minimal step of the piezostages used was appox. 1μm.

Both techniques were successfully applied and gave similar results.

The experimental setups were available at the *High Magnetic Field Laboratory, CNRS* in Grenoble, in France, in the *Institute of Solid State Physics* at the *University of Warsaw*, in Poland, and at the *Institute for Microstructural Science, NRC* in Ottawa, in Canada in A. Sachrajda group with collaboration of S. Raymond.

4.3.3 PL imaging

The spatially and spectrally resolved photoluminescence signal may be observed directly on the CCD camera in the system illustrated in Fig.4.4. The PL signal from the sample, projected on the matrix of CCD camera, is spectrally resolved by monochromator gratings along the horizontal axis, and reflects the spatial dimensions of the sample in the vertical direction. The PL-images illustrate the distribution of PL from the observed sample region (in only one spatial direction) versus the emission energy.

4.3.4 High magnetic field setup

The experimental setup for micro-PL in a high magnetic field was specially designed to enter the 50mm magnet bore with all micro-optical parts working in liquid helium. The sample was mounted on the sample holder as illustrated in Fig.4.5. The two optical fibers were used to transmit the laser beam and the emission signal to/from the center of the magnetic field, where the sample was placed.

The small excitation spot of the exciting laser beam, of approx. 10μm, was achieved by using a monomode fiber, of 5.4μm core diameter. The laser was focused by two micro lenses on the sample surface.

The PL signal was detected by a thick 600μm fiber. The use of a large bore fiber ensures that more light is detected, at the cost of reduced resolution. Resolution is, therefore, in this system, determined only by the size of the excitation spot.

The sample was mounted on an x-y-z piezostage provided by Atto-cube. The minimum displacement of the stage was 0.1μm.

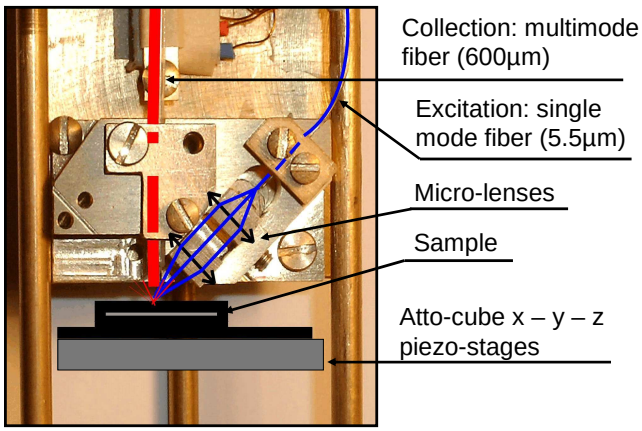

Figure 4.5: *Scheme of the sample holder for micro-photoluminescence experiments in high magnetic field.*

The connection of the laser and the spectrometer with the outputs of the optical fibers are similar as illustrated in Fig.4.3.

All the experiments were performed in a magnetic field perpendicular to the quantum well plane.

The experimental setup was available at the *High Magnetic Field Laboratory, CNRS* in Grenoble, in France.

4.4 Generation of magnetic fields

The low and moderate magnetic field experiments were performed using an Oxford superconducting coil magnet with a maximum achievable magnetic field of 14T. The coil has a 50mm warm bore inside which a liquid helium (LH2) cryostat was inserted. The experiments were performed in a temperature range of 4.2K to 1.7K.

Higher fields were achieved by the resistive magnets. The maximum magnetic field produced by the 10MW resistive magnets is 23T. A liquid helium cryostat was inserted inside the 50mm bore of the magnet for the experiments performed at helium temperatures (4.2K). The 50mm magnet bore had to accommodate the cryostat and the sample holder so the effective diameter available for the experimental setup was ∼33mm in a LH2 cryostat.

The magnets were available in *High Magnetic Field Laboratory, CNRS* in Grenoble, in France.

4.5 Time resolved experiments

Time resolved experiments were performed in the setup illustrated in Fig.4.4.

The exciting laser beam was chopped by an acoustooptic modulator. The laser light was formed into a rectangular pulse train with a 50% duty cycle. The minimum time period possible in the system was T=1ns.

In general, the first period was chosen to be long enough to achieve a steady state of the system. Then, the exciting light was switched off and the photoluminescence transients were observed.

The photoluminescence signal was detected by a fast Acton CCD camera. The highest time resolution of the camera was of 1ns.

The experimental setup was available at the *High Magnetic Field Laboratory, CNRS* in Grenoble, in France.

4.6 Photon correlation

The photon correlation experiment was performed in a Hanbury-Brown and Twiss setup [1] as illustrated in Fig.4.6.

The sample was excited with a continuous wave laser. The laser beam was focused on the sample surface by an immersion mirror objective [2] placed directly in the liquid helium inside the magnet bore. The system allows to focus the laser beam to a spot of approx. 1μm in diameter. The highest magnetic fields available in the system were of 8T.

The photoluminescence was sent through a beam splitter to two grating monochromators (spectral resolution of 100μeV each) set to pass a desired wavelength of light. The filtered light was then detected on two avalanche photodiodes (APD's). The electric output of the diodes was fed to the start and stop inputs of the correlation counting card Time Harp 200. Overall temporal setup resolution was determined as 1.5ns. Depending of the chosen wavelengths (equal or different) the auto- or cross- correlation between the same or different excitonic emission lines was measured. The single correlation event is constituted by the detection of such a photon pair that one photon is detected on the 'start' and the second one on the 'stop' diode. The correlation measurement yields as the result a histogram plotting the number of correlated counts as a function of time separating the detection of the first and the second photon in the pair. The negative values on the time axis of the histogram refer to the events where the first photon in pair was detected on the 'stop' and the second one on the 'start' diode.

The experimental setup was available at the *Institute of Solid State Physics* at *University of Warsaw*, in Poland, in J.A.Gaj group with the collaboration of J.Suffczyński, A.Golnik and P.Kossacki.

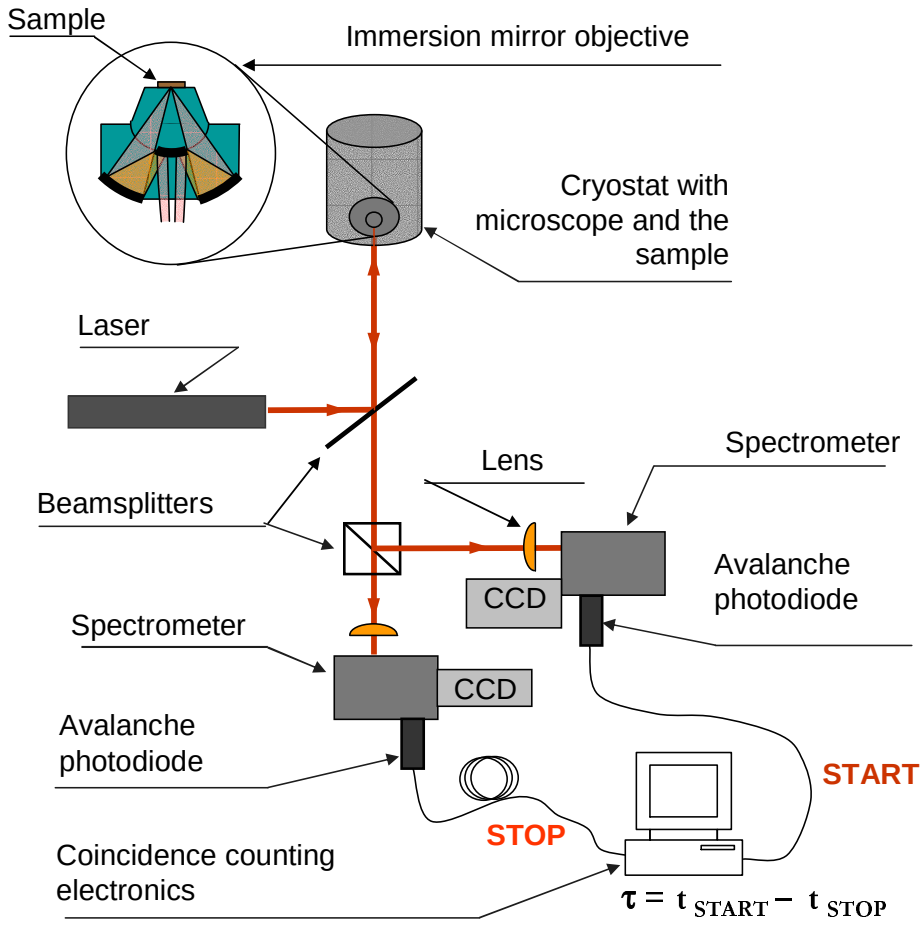

Figure 4.6: *Scheme of the photon correlation experimental setup.*

Bibliography

[1] R. Hanbury-Brown and R. Q. Twiss, "The question of correlation between photons in coherent light rays.," *Nature (London)*, vol. 178, p. 1447, 1956.

[2] J. Jasny and K. Sepioł, "Single molecules observed by immersion mirror objective. a novel method of finding the orientation of a radiating dipole.," *Chem. Phys. Lett.*, vol. 273, p. 439, 1997.

Chapter 5

Review of the Optical Properties of an Indirect GaAs/AlAs DQW : Towards QD Emission

Dans ce chapitre, nous décrivons les principales caractéristiques des systèmes à double puits quantique GaAs/AlAs de type II en insistant sur les propriétés spécifiques qui confèrent à ces matériaux un intéret particulier pour les études optiques. Le but de cette discussion est de clarifier le comportement surprenant de la macro-luminescence dans ces systèmes, qui apparaît sous forme de raies très fines ce qui prouve qu'elle est due à la formation de boîtes quantiques.
Nous discutons dans un premier temps les propriétés typiques des excitons indirects en deux dimensions, c'est-à-dire leur temps de vie radiatif très important (1 ms) et leur forte diffusion (jusqu'à 100 μm). Dans un deuxieme temps, nous décrivons grâce à des expériences de macro-photoluminescence, les propriétés optiques d'ensembles de boîtes quantiques.

Investigations of a double quantum well system such as, for example, a GaAs/AlAs bilayer with a built-in type-II interface, started with the quest for the possibility of optical generation of cold, tunable-density, two-dimensional electron-hole gas. Luminescence spectra of such systems were known to exhibit a number of intriguing properties which were interpreted as the observation of a precursor of an exciton condensate [1]. Alternatively, they were assigned to effects of trapping of photoexcited carriers in built-in quantum-dot like objects formed by potential fluctuations caused by interface roughness [2, 3].

The structures studied in this work show conventional spectra characteristic of their (intentional) 2D character, but unexpectedly also a number of sharp emission lines. The latter lines, their origin and properties, are the main object of this thesis. As shown in this work, these lines can be attributed to quantum dots formed in the GaAs/AlAs type II bilayer. However, in contrast to previous studies on similar systems, the dots are not due to interface roughness but exhibit a strong 3D con-

finement.

In this chapter, the optical properties of the investigated structures, mostly as seen from macro-PL measurements, are discussed. The characteristic spectra related to the 2D character, the appearance of sharp emission lines from ensembles of quantum dots and the diffusion process of photocreated carriers are presented [4, 5].

5.1 Indirect and pseudo - direct transitions

The intentional 2D character of the investigated structure is best recognized in macro-PL spectra measured under very low excitation power. Such spectra obtained for two different characteristic structures: indirect and pseudo-direct, are shown in Fig.5.1 a) and b), respectively. (See chapter 3.1 for layer sequences of those samples).

The spectrum of the `indirect structure` (Fig.5.1a) consists of a weak emission peak which corresponds to the direct Γ^{GaAs}-Γ^{GaAs} recombination and four, more pronounced lines, associated with indirect X_{XY}^{AlAs}-Γ^{GaAs} transitions: a zero-phonon line and its $TA(X)_{GaAs}$, $LO(X)_{GaAs}$, and $LO(X)_{AlAs}$ phonon replicas [3, 6, 7]. Such a spectrum is characteristic of type-II GaAs/AlAs indirect systems for which the lowest electronic state in the AlAs well is of X_{XY} symmetry and the X_Z state is located a few meV higher.

This is in contrast to the type-II GaAs/AlAs `pseudo-direct structure` for which the lowest electronic state in the AlAs well is of X_Z symmetry and the X_{XY} state is located a few meV higher. The dominant transition is therefore associated with the indirect X_Z^{AlAs}-Γ^{GaAs} transition (Fig.5.1b). A weak emission peak which corresponds to the direct Γ^{GaAs}-Γ^{GaAs} recombination is also visible in the spectra. Less pronounced phonon replicas of zero-phonon lines correspond to $LA(X)_{AlAs}$ and $LO(X)_{AlAs}$ phonons.

The main difference in both spectra is the relative strength of the X_{XY}^{AlAs}-Γ^{GaAs} and X_Z^{AlAs}-Γ^{GaAs} emission lines, in Fig.5.1a) and b), respectively. In both cases they correspond to the ground state emission. The selection rules which strictly forbid the X^{AlAs}-Γ^{GaAs} transitions, in the ideal case, are relaxed due to interface roughness. This relaxation of the selection rules is more efficient for the X_Z^{AlAs}-Γ^{GaAs} transition as compared to X_{XY}^{AlAs}-Γ^{GaAs} [7].

The indirect-type spectrum changes considerably under higher excitation intensities. As can be seen in Fig.5.2, for an excitation density of a few mW/cm^2, the spectrum shows an ensemble of numerous sharp emission lines, with typical half-widths less than 0.1meV. These lines are observed over a very broad spectral range (1.56eV - 1.72eV). As it is proved in the following chapter, they correspond to ensembles of quantum dot emission. The very characteristic onset of photoluminescence at 1.56meV is assigned to the situation when the dot is formed out of both GaAs and AlAs layers in the growth direction.

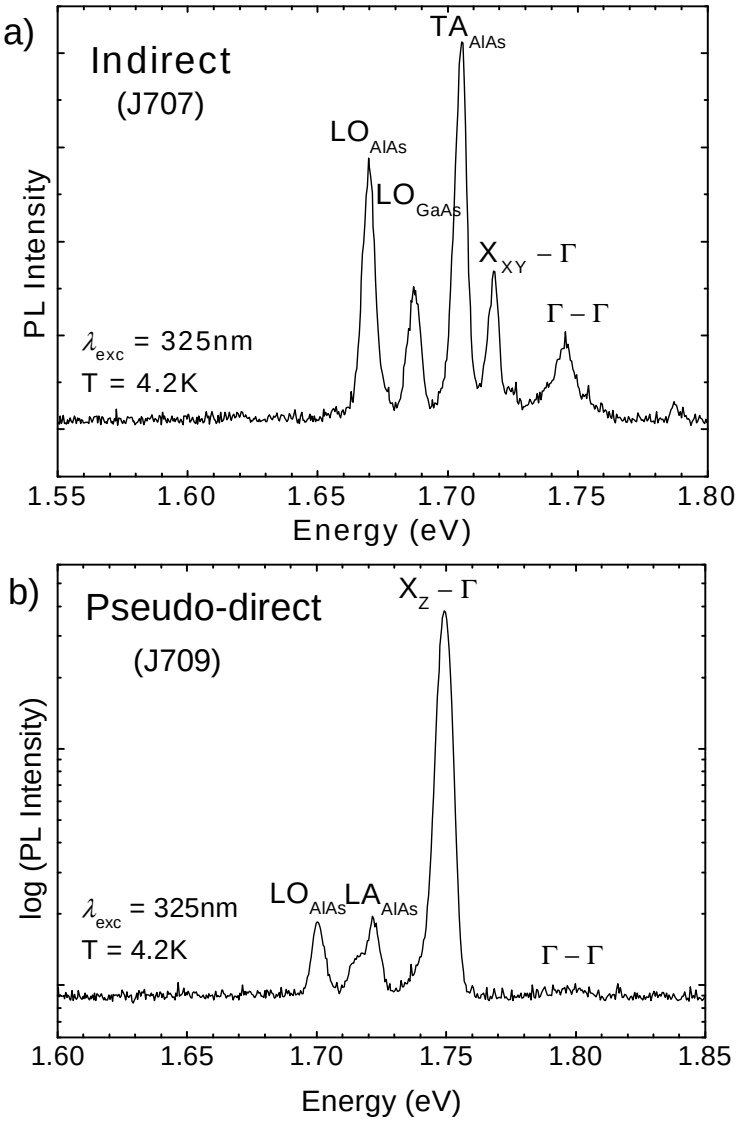

Figure 5.1: *A representative macro-PL spectra of a) indirect (J707) and b) pseudo-direct (J709) structures taken with an excitation power of* $\sim 0.1 mW/cm^2$.

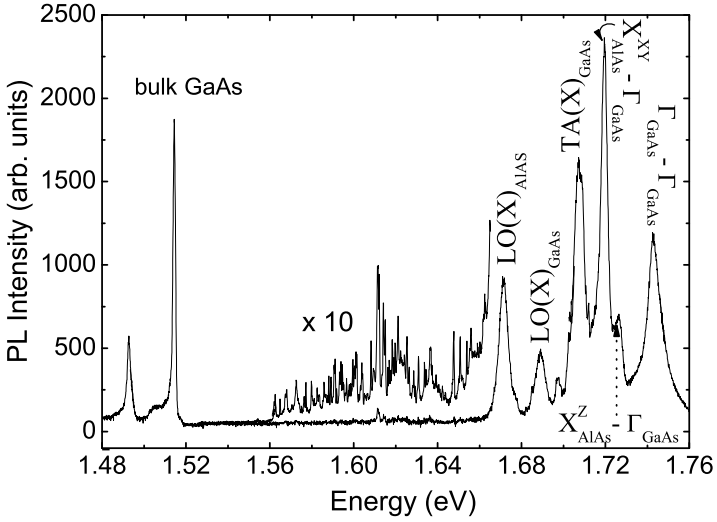

Figure 5.2: *Photoluminescence spectrum of a 1mm size area of the indirect sample (J707) measured at T=4.2K with high power density.*

The macro-photoluminescence spectra from the GaAs/AlAs type II bilayer are of two types, depending on whether the structure has an indirect or pseudo-direct band alignment. The indirect transitions are mostly associated with strong phonon replicas. Under high excitation power the number of sharp emission lines is visible in the energy region below the main quantum well transitions and spread over a very broad spectral range.

5.2 Quantum-dot-like luminescence

Interestingly, the sharp emission lines in the emission spectra observed from indirect-type structure are very stable when the temperature of the sample is increased, which allowed to draw first conclusions about their origin.

Photoluminescence spectra of the indirect-type structure measured at temperatures between 4.7K and 104K are shown in Fig.5.3.

The emission lines attributed to the recombination of indirect excitons disappear from the photoluminescence spectrum with increasing temperature and above 30K they are not present in the spectra any more. This result suggests that the emission identified as due to indirect excitons involves mostly indirect excitons localized at fluctuations of the GaAs/AlAs interface.

It is clear that temperature is not a critical parameter for the observation of the

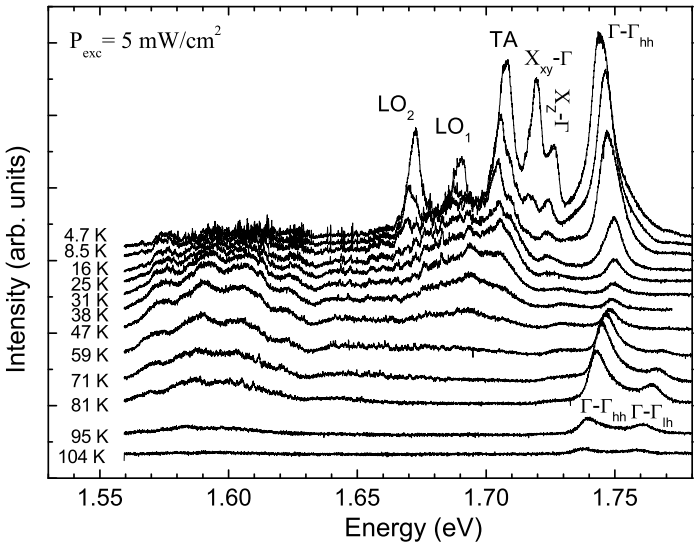

Figure 5.3: *Photoluminescence spectra measured for different temperatures between 4.7K and 104K on indirect type sample [4].*

sharp lines. Some of them even gain in intensity with temperature in the low temperature range. Certain sharp lines can be followed up to temperatures as high as 60K in this particular experiment. The absolute intensity of the QDs-band increases with increasing temperature, reaches a maximum around 40K then decreases, and finally disappears from the spectrum at temperatures as high as ∼110K.

The appearance of sharp lines is therefore clearly not a low temperature phenomenon* and also it can hardly be explained in terms of localization effects at the GaAs/AlAs interface, simply induced by GaAs/AlAs well-width fluctuations [2].

Very probably, there exists another type of "localization trap" in the active part of the sample which leads to the emergence of the observed sharp emission lines. The density of these traps must be quite low, as resolved sharp lines are easily observed in macro-luminescence experiments. On the other hand, the characteristic localization energy associated with the "traps" must be quite large, since the sharp emission lines spread over a wide spectral range and the lines are visible at rather high temperatures. To account for the appearance of such "deep traps" in the investigated sample, the possibility of effective Ga diffusion into the AlAs layer during the MBE growth of the structure is noted. This diffusion, if

*Early works [1] on similar structures claim the appearance of "spikes" in PL spectra, which were attributed to the "spectral noise" as a precursor of Bose-Einstein condensation of excitons.

laterally inhomogeneous, could lead to the formation of islands where the perfect double GaAs/AlAs layer is replaced by a kind of GaAs-GaAlAs quantum well layer embedded in between regular GaAlAs barriers. Such islands could serve as efficient type-I recombination centers for nearby long lived carriers (confined in the X-conduction band minimum of the AlAs layer and Γ-valence band maximum in the GaAs layer). The proposed scenario implies that the diffusion process of the long-lived carriers is an important element in understanding the observed phenomena and should be reflected in the kinetics of the emission. This picture should also be confirmed in micro-PL measurements. The results of such experiments are reported in the following sections.

The temperature dependent macro-photoluminescence experiment allowed to conclude that the origin of the sharp emission lines is due to very localized states present in the structure, most probably quantum dots.

5.3 Characteristic lifetimes in the system

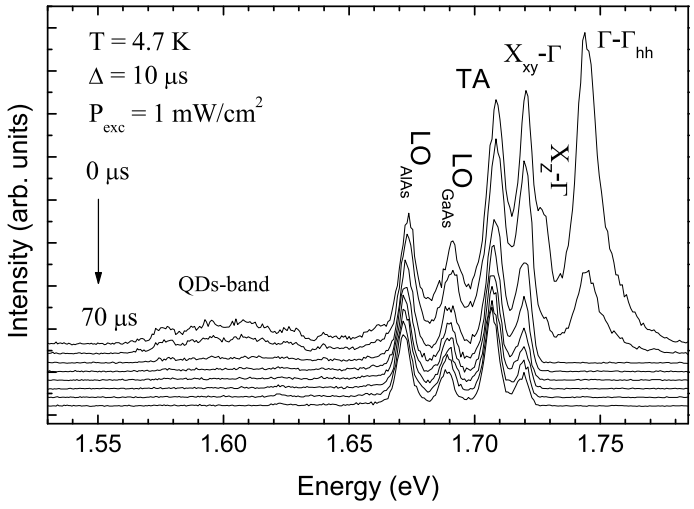

Figure 5.4: *Photoluminescence spectra of the indirect sample (J707) measured for different delay times after the excitation pulse [4].*

The experimental setup for time resolved experiments is described in chapter 4.5.

Fig.5.4 illustrates spectrally resolved photoluminescence from the sample taken at different delays following the excitation laser pulse.

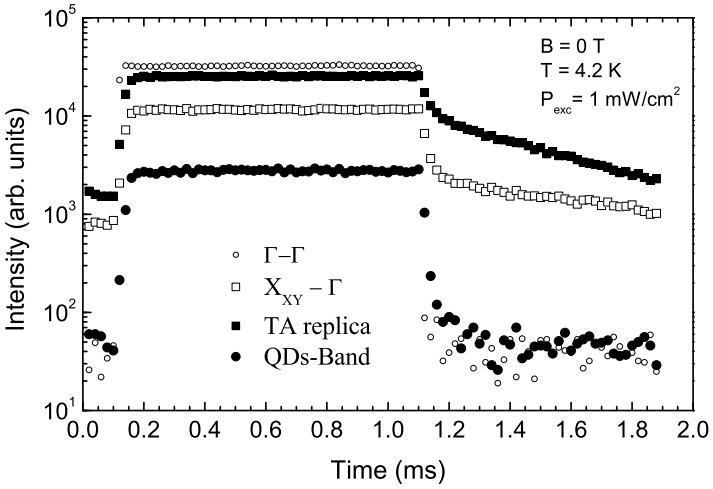

Figure 5.5: *Time-resolved decay measured for different transitions with a time window of $\Delta t = 20\mu s$. Fast raise time of the signal is visible in the times ∼0.2ms, then stability of the emission during the laser pulse is achieved up to 1.1ms and a decay of the emission is observed [4].*

The fastest decay times observed in the emission are associated with direct Γ-Γ recombination in the GaAs quantum well and X_Z-Γ transitions involving electrons from the AlAs quantum well and holes from the GaAs quantum well. They are shorter than 10ns, which is the limit of the experimental setup in this case.

As can be seen in Fig.5.5, the transients observed for the X_{XY} emission and its phonon replicas cannot be described by a mono-exponential dependence. Just after switching off the excitation pulse, the emission intensity decays fast (microsecond scale) but later a much slower decay is observed (millisecond range). The longest decay time, of about 1ms, is seen for the X_{XY} transition, for times sufficiently long after the excitation pulse. The fast decay process is more pronounced when the excitation intensity is increased. On the other hand, a few microseconds after switching off the laser the photoluminescence intensity is independent of the excitation power (see Fig.5.5).

The observed behavior is qualitatively reproduced using a simplified model taking into account the interplay between diffusion and localization of carriers and/or indirect excitons. This is described in detail in Ref.[4].

In short, it is assumed that in the case of low excitation the photo-generated carriers are effectively trapped at interface fluctuations and recombine with a long decay time, in the ms range. This long decay time results from the small overlap of the electron and hole wave-functions as well as from k-selection rules. The number

of such traps is limited, hence by increasing excitation power one can achieve a certain critical concentration for which this recombination channel is not sufficient and the excess excitons (carriers) begin to diffuse "searching" for other "recombination possibilities". This "escape" process can be described by a characteristic time in the μs range.

In general, it was found that the diffusion of indirect excitons (carriers) is a crucial element determining the time characteristics of both the indirect transitions and the ensemble of quantum dot emission lines, what is shown in the next section and discussed in more details in section 9.2.

The lifetimes observed for X_{XY}-type excitons are very long, of the order of ms, in comparison to the very fast recombination of direct type excitons, with a timescale below 10ns. The decay time of the quantum dot luminescence is found to be in the μs range.
Kinetics of the spectra is determined by a combination of the effects of diffusion and slow relaxation rates of 2D carriers. The quantum dots are a direct-type recombination centers for diffusing long lived X-type carriers.

5.4 Diffusion

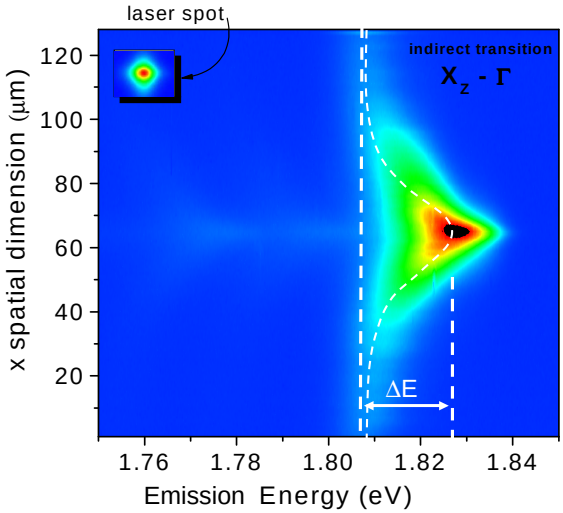

Figure 5.6: *Spectrally resolved μ-photoluminescence images of the pseudo-direct transition. The vertical axis represents the spatial position on the sample in the quantum well plane, while the horizontal axis - the photon energy. ΔE corresponds to the emission energy shift. Inset shows corresponding dimensions of the exciting laser spot. [5]*

In the previous section it was shown that the carriers confined in a type II bilayer at X-symmetry energy levels have very long lifetimes, in the ms range. If a

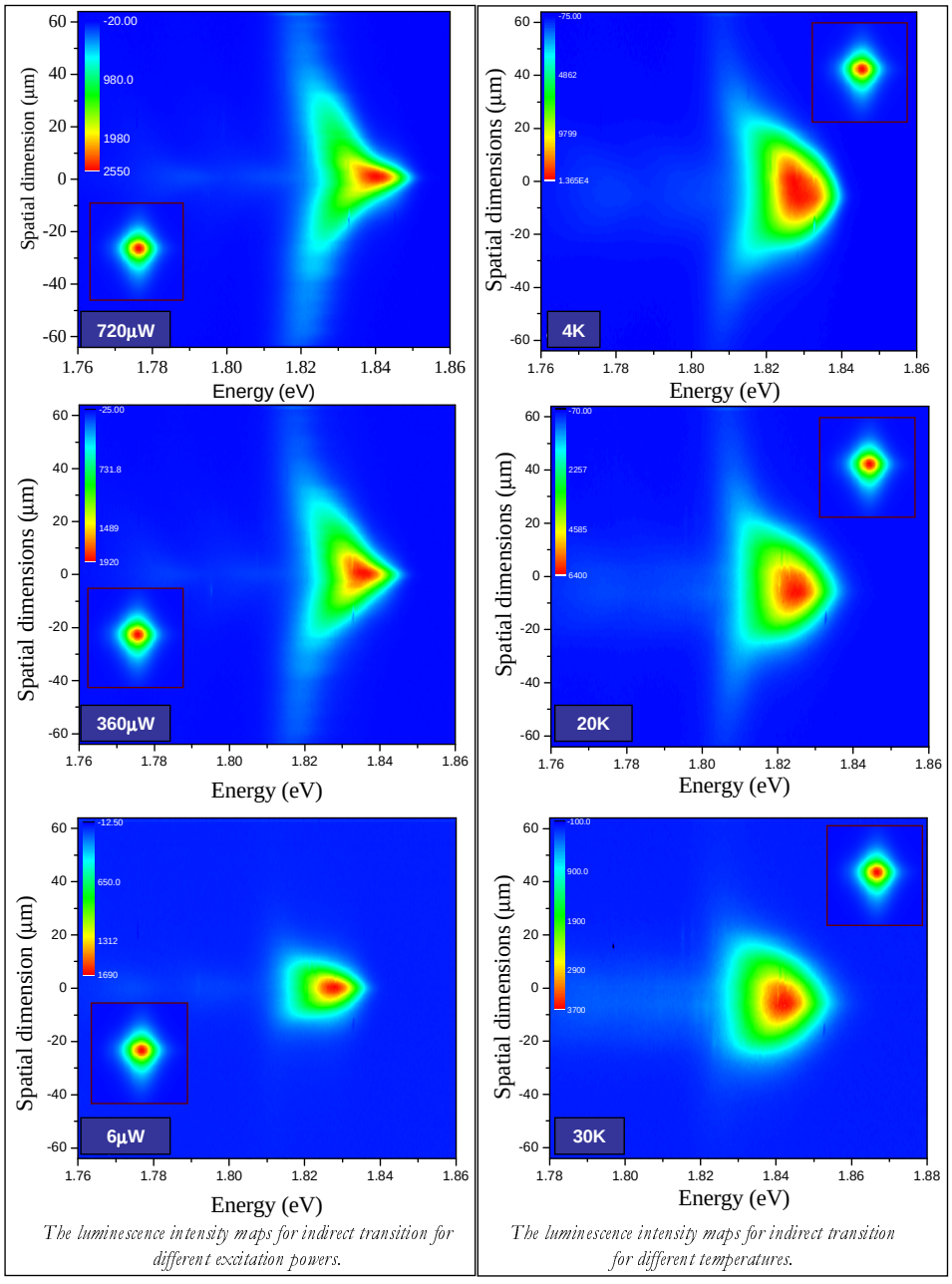

Figure 5.7: *Spectrally resolved μ-PL images taken for pseudo-direct transition. Left panel: for excitation powers of 720μW, 360μW and 6μW, respectively; Right panel: for temperatures of 4K, 20K, 30K, respectively. [5]*

high carrier concentration on these energy levels is reached by the excitation power, the carriers start to diffuse over large distances from the excitation spot. The diffusion effects can be easily observed via intensity and spatial distribution of the pseudo-direct, X_Z-Γ, transition.

The experimental setup for photoluminescence imaging is described in section 4.3.3. The experiment was performed on the type II GaAs/AlAs bilayer with pseudo-direct alignment of the bands (sample M26L12, see table 3.4 for structure details).

Fig.5.6 illustrates a spectrally resolved μ-photoluminescence image, which represents the spatial distribution of the energy and intensity of a pseudo-direct X_Z-Γ transition.

It is clearly seen that the spatial dimensions of the region from which pseudo-direct emission is observed are much larger than the laser spot.

The sizes of the laser spot are estimated by the observation of the spatial dimensions of one of the direct transitions in the structure. As for direct-type recombination no (significant) diffusion is expected, it is assumed that direct transitions directly reflect the laser spot dimensions. The results illustrated in this section are from sample M26L12 (see 3.1 for structure details), where additionally two GaAs/GaAlAs quantum wells of direct type were intentionally grown. Therefore the presented images of laser spot dimensions (insets) are in fact the emission from a type I quantum well.

The diffusion of carriers is observed at distances from the excitation spot up to 100μm. This is due to the low recombination probability resulting from spatial and k-space separation of electrons and holes and consequently very long lifetimes. Carriers move apart from the excitation spot and recombine only at a certain distance.

The observed emission energy gradually decreases with the distance from the excitation spot (marked by ΔE in Fig.5.6). The observed effects can be explained taking into account potential modifications caused by an additional electric field that appears and drives the carriers to spread out from the illuminated area. More details can be found in Ref.[5].

Low temperature spectrally resolved μ-PL images taken for different excitation powers and at different temperatures are shown in Fig.5.7. Two effects are observed:

- the effective diffusion length increases for high excitation powers and it decreases upon raising the temperature;
- "positive band gap renormalisation" with increasing excitation power, revealed as a "blue" shift of the maximum of the emission

It can be expected that the more carriers are photo - created in the illuminated area with increasing excitation power, the higher the electric field that is the driving force for spreading carriers and the higher the effective diffusion length. The effect of the temperature change is more complex. The evolution of the measured

images with temperature may be affected by different factors. Very likely, both the diffusion constant and carrier lifetime are temperature dependent. Time resolved images could be an appropriate experiment for further studies of this phenomenon.

The effective diffusion of indirect excitons has also been observed by other groups [8, 9, 10, 11]. It was mainly investigated in the quest for observing the condensation of a Bose-Einstain type of long lived excitons in semiconductors and/or superfluidity. However, to achieve Bose-Einstein condensation, the main goal was to additionally trap the spreading carriers in order to locally create high densities of cold electron-hole plasma. Different attempts to solve this problem have been made. They consisted of the formation of additional potentials created by external stress on the sample [9] or by local minima in the disordered well and/or electrostatic traps [12, 13, 14].

It is interesting to note that our preliminary results point to the possibility of forming an additional squeezing potential by the application of a strong magnetic field. In the structures investigated in this work, it was discovered that the magnetic field modifies the spatial extension of the pseudo-direct emission. This effect is illustrated in Fig.5.8. In a magnetic field the extent of the pseudo-direct emission is smaller. A detailed analysis is needed for quantitative values of this effect, nevertheless this observation is an important factor in studies of indirect excitons.

All the spectral images of diffusion effects presented up to now were illustrated by pseudo-direct, X_Z-Γ, transitions. However, the highest lifetimes in the system were observed for indirect, X_{XY}-Γ, transitions, thus it should be expected that in the case of indirect structures the observed diffusion length should be even bigger. This is however not possible to observe directly in the PL image. The μ-PL image of the indirect structure in the region of indirect transitions is illustrated in Fig.5.9 and the diffusion is not observed at the X-Γ transition. In this case the quantum dots serve as direct recombination centers for diffusing long lived carriers that relax almost uniquely in the dots. Thus the diffusion extension is only visible through the quantum dot emission. The dots act as probes for diffusing carriers and the dots are supplied by carriers even from large distances from the excitation spot, revealing that the diffusion is very efficient.

This property of the system is a unique advantage for the investigation of exciton complexes in quantum dots, as high concentrations of carriers in the dots can be easily achieved.

The indirect GaAs/AlAs type II bilayer is found to exhibit strong diffusion properties of indirect excitons. Long lived carriers spread up to 100μm from the excitation spot before they recombine. The diffusion length was found to be dependent on the excitation power, temperature and magnetic field.
The indirect-type barriers are ideal systems for direct-type quantum dots, as the dots are very efficiently supplied by carriers even from large distances from the excitation spot.

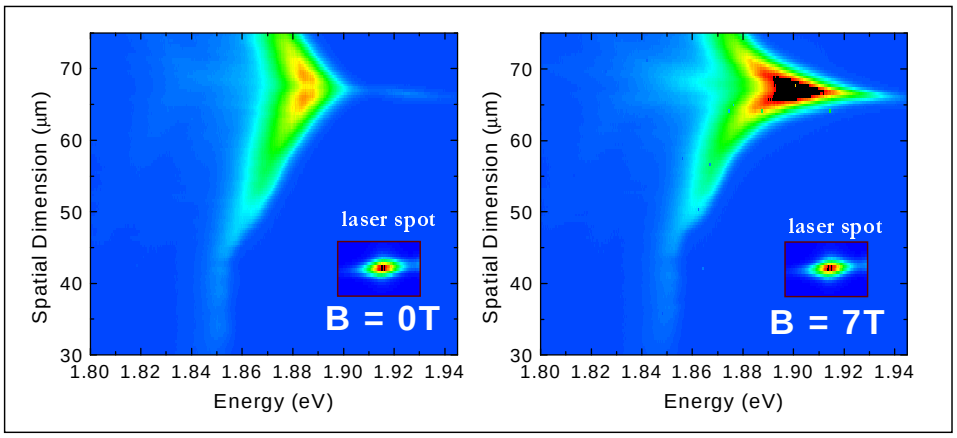

Figure 5.8: *Spectrally resolved μ-PL images of pseudo-direct transition, $X_Z - \Gamma$, at 0T and 7T (M26L12 sample).*

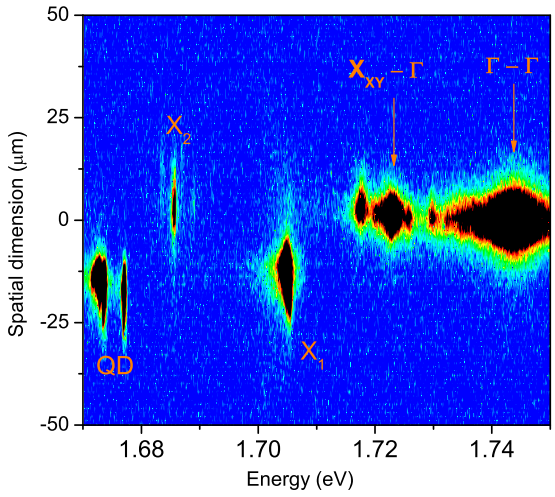

Figure 5.9: *Spectrally resolved μ-PL images in the region of the indirect transition in sample J707 containing quantum dots. The observed extensions of direct $(\Gamma - \Gamma)$ and indirect $(\Gamma_{XY} - \Gamma)$ transitions are very similar in this case. The emission denoted by X_i and QD is due to localized excitons on interface fluctuations and in the quantum dot, respectively.*

Bibliography

[1] L. Butov, A. Zrenner, G. Abstreiter, G. Böhm, and G. Weimann, "Condensation of indirect excitons in coupled AlAs/GaAs quantum wells," *Phys. Rev. Lett.*, vol. 73, p. 304, 1994.

[2] A. Zrenner, L. V. Butov, M. Hagn, G. Abstreiter, G. Böhm, and G. Weimann, "Quantum dots formed by interface fluctuations in AlAs/GaAs coupled quantum well structures," *Phys. Rev. Lett*, vol. 72, p. 3382, 1994.

[3] A. Trüby, M. Potemski, and R. Planel, "Magnetic field effects in the luminescence spectra of type II GaAs/AlAs double layer structures," *Solid State Electronics*, vol. 40, p. 139, 1996.

[4] A. Wysmolek, B. Chwalisz, M. Potemski, R. Stepniewski, A. Babinski, S. Raymond, and V. Thierry-Mieg, "Emission from mesoscopic-size islands formed in a GaAs/AlAs double layer structure," *Acta Physica Polonica A*, vol. 106, p. 367, 2004.

[5] A. Lesiak, B. Chwalisz, A. Wysmolek, M. Potemski, R. Stepniewski, and V. Thierry-Mieg, "Carriers diffusion in GaAs/AlAs type II quantum well," *Acta Physica Polonica A*, vol. 108, p. 755, 2005.

[6] A. Wysmolek, M. Potemski, and V. Thierry-Mieg, "Single-dot-like emission induced by high magnetic fields," *Physica E*, vol. 12, p. 876, 2002.

[7] G. Danan, B. Etienne, F. Mollot, R. Planel, A. Jean-Louis, F. Alexandre, B. Jusserand, G. L. Roux, J. Marzin, H. Savary, and B. Sermage, "Optical evidence of the direct-to-indirect-gap transition in GaAs-AlAs short-period superlattices," *Phys. Rev. B*, vol. 35, p. 6207, 1987.

[8] R. Rapaport, G. Chen, D. Snoke, S. H. Simon, L. Pfeiffer, K. West, Y. Liu, and S. Denev, "Charge separation of dense two-dimensional electron-hole gases: Mechanism for exciton ring pattern formation," *Phys. Rev. Lett.*, vol. 92, p. 117405, 2004.

[9] D. W. Snoke, Y. Liu, Z. Vöröst, L. Pfeiffer, and K. West, "Trapping long-lifetime excitons in a two-dimmensional harmonic potential," *Solid State Communications*, vol. 134, p. 37, 2005.

[10] S. Denev, S. Simon, and D. Snoke, "Luminescence ring formation in quantum wells, a model with Coulomb interaction," *Solid State Communications*, vol. 134, p. 59, 2005.

[11] Z. Vörös, R. Balili, D. W. Snoke, L. Pfeiffer, and K. West, "Long-distance diffusion of excitons in double quantum well structures," *Phys. Rev. Lett.*, vol. 94, p. 226401, 2005.

[12] A. A. Dremin, V. B. Timofeev, A. V. Larionov, J. Hvam, and K. Soerensen, "Phase diagram of the bose condensation of interwell excitons in GaAs/AlGaAs double quantum wells," *JETP Lett.*, vol. 76, p. 450, 2002.

[13] R. Zimmermann, "Probing exciton condensation by speckled emission," *Solid State Communications*, vol. 134, p. 43, 2005.

[14] O. L. Berman, Y. E. Lozovik, D. W. Snoke, and R. D. Coalson, "Phase transitions in a system of indirect magnetoexcitons in coupled quantum wells at high magnetic field: the role of disorder," *arXiv:cond-mat/0408581v1*, 2005.

Chapter 6

Single Excitons in a Quantum Dot

Ce chapitre est consacré à l'étude de propriétés physiques spécifiques des boîtes quantiques sous faible excitation optique. La luminescence d'une boîte quantique unique est tout d'abord mise en évidence par une cartographie de microphotoluminescence de l'échantillon. Les détails les plus simples de l'émission d'une boîte quantique sont observés et expliqués, c'est-à-dire les émissions de l'exciton, de l'exciton chargé et du bi-exciton. Puis, sur la base d'expériences, nous discutons les effets du potentiel de confinement et de l'application d'un champ magnétique intense. Nous nous intéressons de plus à la différence entre les boîtes initialement "chargées" ou initialement "neutres". Les propriétés d'un exciton unique confiné dans des boîtes quantiques différentes, donc dans des profils de potentiel différent, sont étudiées. Nous montrons que le facteur g excitonique dépend de la composition chimique de la boîte. Par contre, la levée de dégénérescence diamagnétique, qui est corrélée avec la séparation énergétique entre les niveaux s et p, est déterminée par les dimensions de la boîte quantique. L'étendue spatiale du niveau s est évaluée expérimentalement à 5 nm, valeur en accord avec des résultats obtenus dans une expérience indépendante (en fonction de la puissance).

The following chapter discusses the general properties of most simplest excitonic states, the single exciton (X), charged exciton (X*) and biexciton (XX) in a single quantum dot.

First, it is illustrated that, indeed, the observed X, X* and XX emission comes from a single, isolated quantum dot. The results of the μ-PL at very low excitation power and μ-PL-mapping experiments are presented.

Second, the general properties of X, X* and XX are discussed. The differences between various quantum dots, i.e. different three dimensional confinements, are pointed out.

Then, the effects of the application of a magnetic field on the characteristic energies of X, X* and XX states are considered. The effective g-factors of the subsequent states, Zeeman splitting and diamagnetic shift that give information about

the symmetry of states and confinement potential are analyzed.

6.1 Spatially resolved emission

In the previous chapter, it was shown that the broad, indirect macro-luminescence of a GaAs/AlAs type - II double quantum well structure can also reveal sharp emission lines spreading up to 150meV below the direct Γ - Γ transition (see section 5.1). The appearance of these sharp emission lines was not well understood until it was possible to resolve single emission lines. This was achieved by the reduction of size of the excitation spot in the μ-PL technique.

The experimental setup used for μ-PL experiment is described in chapter 4.3.

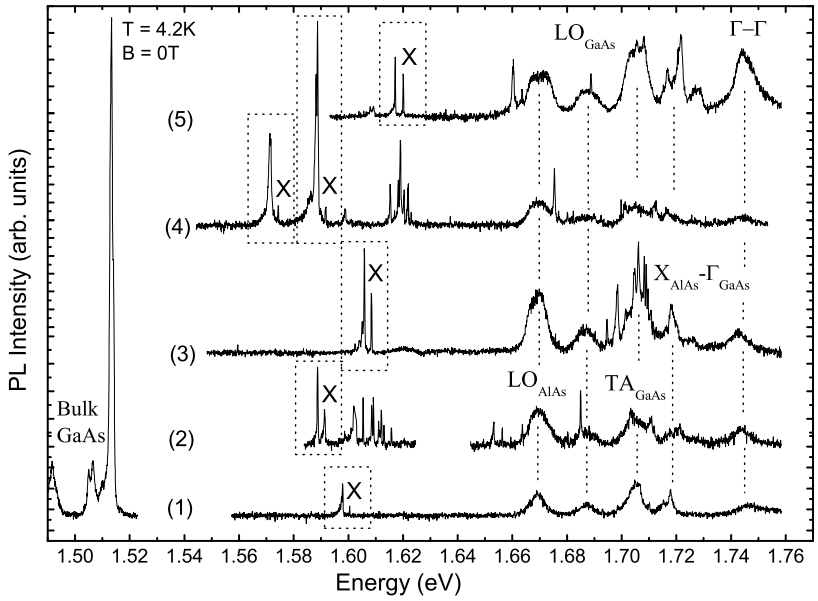

Figure 6.1: *Micro-photoluminescence spectra of different places at the sample. The emission lines that can be attributed to the same quantum dot are marked by dotted squares.*

Fig.6.1 illustrates typical μ-PL spectra in a broad energy range, taken at low excitation power from different places on the sample.

On the high energy part of the spectra, a broad emission characteristic of a 2D system is visible, with a corresponding phonon replica as it was discussed in chapter 5.1. On top of these broad lines, a few sharp transitions are visible. These sharp

peaks are likely due to the emission of carriers trapped at "shallow" quantum dots formed due to potential fluctuations.

The strong emission below 1.52eV originates from the bulk GaAs substrate.

The emission observed in the energy region from 1.56eV to 1.65eV is now composed of well isolated lines, in contrast to the macro-PL spectrum (Fig.5.2). The energy positions of these "isolated" lines clearly depend on the position of the laser spot on the sample. This indicates that they come from well isolated objects, the quantum dots.

At this moment it is assumed, but will be subsequently shown in this thesis, that the emission line denoted by X is due to the recombination of a single neutral exciton. In a similar manner, other strong lines visible in these spectra are attributed to the recombination of charged excitons and biexcitons.

The precise mapping of μ-PL in the vicinity of a single quantum dot allowed to determine the emission lines that are related to that dot.

The μ-PL mapping experiment was performed in the setup described in chapter 4.3.2.

μ-PL scans of a 60μm x 60μm sample region including one quantum dot, taken at an excitation power of $\sim$0.16μW, are shown in Fig.6.2(a) - (d). The spectra illustrate the cross sections in x- and y- spatial directions,(a) and (b) respectively, through the quantum dot. The maps represent the changes of the PL intensity at energies of 1.5838eV (X emission), Fig.6.2(c), and 1.5806eV (X* emission), Fig.6.2(d).

It is remarkable that both emissions, X and X*, are observed only from a very precise place of the sample.

The maximum of the luminescence intensity is in the center of the quantum dot and it gradually decreases as the excitation spot is moved away. The spectra observed from a certain distance from the center of the dot are similar to those observed under reduced excitation power (compare with Fig.6.7). The further the laser spot is from the dot center, the smaller the carrier population in the dot. The spectrum is composed of a single exciton line, X, at the largest distances, therefore at lowest effective excitation power. This indicates that the single exciton emission is the simplest possible excitation in the very low excitation power regime.

The fact that the emission from the quantum dot is still observed even if the excitation spot is several tens micrometers from the dot is due to the very strong diffusion of indirect photo-created carriers to the dots (discussed in 5.1 and 5.4). The dot is therefore populated even from large distances of the excitation spot to the dot. The poor resolution in the detection system results in the observation of the emission from the dot even if the laser spot is far apart. Therefore the μ-size dimensions of the luminescence at the μ-PL map cannot be directly related to the real dimensions of the dot. As it is discussed in chapter 2.1.1, the real diameter of the dots can be estimated to tens of nm.

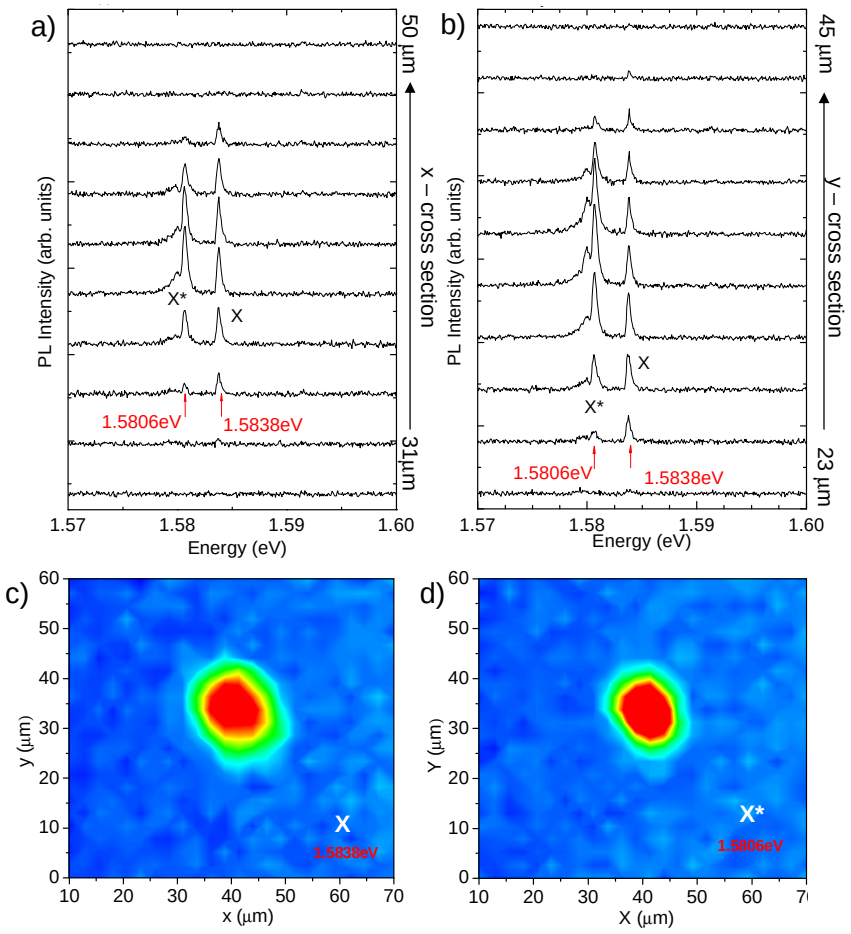

Figure 6.2: *µ-PL spectra of a single quantum dot scanned in the a) x- and b)y-directions. µ-PL intensity maps for the (c) X and (d) X* emission lines. Both µ-PL are presented with the same colour intensity scale.*

The spectra presented in Fig.6.2 do not reveal any emission lines away from the quantum dot in the whole spectral range. This indicates that the other objects are separated from the investigated one by at least 25μm.

It can be noticed in Fig.6.2c) and d), that the X emission extends further than that of X*. (The same effect is visible in the cross sections, where for large distances from the center of the dot, the spectrum is composed of a single X line.) This is not a general rule for the emission from investigated quantum dots. Very often the situation is reversed and the X* emission is observed to appear in the spectra first at very low excitations. This is possible when an impurity is present in the vicinity of the dot(or other source of possible charge fluctuation). This situation is described in section 6.2.3.

The μ-PL mapping experiment illustrates that the PL from a single quantum dot is well isolated from surrounding objects and X and X* emission emerges from the same, precisely defined sample region. The surface density of the dots is observed to be as low as 10^6cm^{-2}. This explains the possibility of observing sharp emission lines even in macro-PL experiments.

6.2 Zero and first order excitonic complexes - X, X* and XX

Fig.6.3 illustrates in details a typical μ-PL spectrum of a single, isolated dot taken at relatively low excitation power (similar to that used to obtain the spectra presented in the previous section, $\sim$0.6 μW), in the center of the dot. The excitation power is set thus in order to observe several emission lines*. The spectrum shows sharp emission lines attributed to the annihilation of single electron - hole pairs, exciton, X, as well as the charged exciton, X*, i.e. electron - hole pair with an extra charge attached.

The X - X* doublet structure is similar to that observed in the micro-luminescence of other GaAs quantum dots formed at the interface fluctuations and InAs quantum dots [1, 2, 3, 4, 5, 6, 7]. There, it was assigned to neutral and charged excitons and/or biexcitons. In this case, the identification of the lines is based on photon correlation experiments and is discussed in detail in chapter 10.

We identify the emission line denoted by XX1 as most probably being due to the biexciton recombination, as its intensity rises very fast with increasing excitation power (see Fig.6.7 and Fig.6.8).

Apart from the main, X, X* and XX1 transitions, several low energy components appear several meV below the X* and XX1 transitions. They are related to

*At lowest excitation power the spectrum of all investigated dots was composed only of a single emission line. The effect of excitation power on the spectra is discussed in detail in chapter 6.2.2.

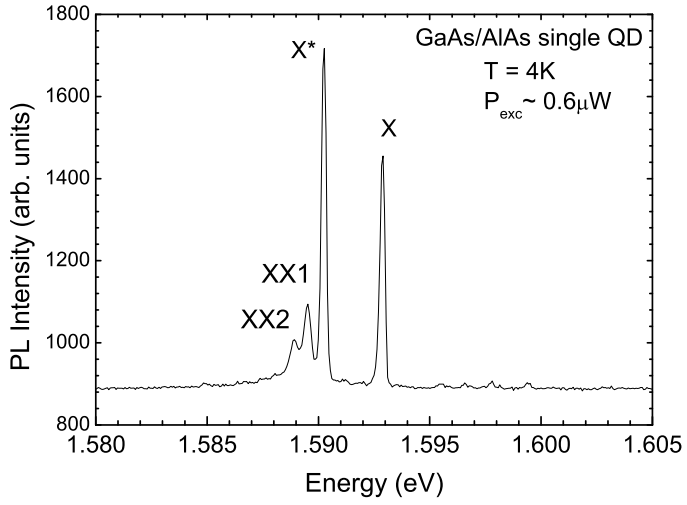

Figure 6.3: *Typical μ-PL spectra of the single quantum dot excited with relatively low excitation power (∼0.6μW).*

emission from more complicated excitonic complexes, as charged biexciton, triexciton or different triplet states. They can also correspond to so-called configuration crossing transitions [8], for example biexciton decay, leaving behind excited states. Similarly to the corresponding phenomenon in bulk semiconductors, known as the inverse exciton series [9], these transitions reveal the mixing of excited configurations in the biexciton ground state ([8, 10, 11, 12]. At this excitation power also a slight occupation of *p*-shell can not be excluded, what could give emission lines in this spectral range.

In general, at this pump intensity, the measured PL spectrum represents the average over a number of photons emitted from the dot in different states (population, charge fluctuation, spin configuration of carriers), so the emission spectrum is composed of several emission lines. A more detailed analysis of this low energy tail is presented in chapter 10, where photon-correlation experiments allowed to precisely determine the origin of most of the emission lines.

As it emerges from Fig.6.4, where the emission from different quantum dots is compared, the relative positions of the exciton complexes emission lines change and often they are not possible to resolve within the limit of the experiment. As is shown in the next section, with the increase of the excitation intensity the excitonic complexes emissions gain rapidly in intensity and finally, in this energy range, become dominant in the spectrum.

A typical single quantum dot spectrum at moderate excitation power is composed of neutral exciton, X, and charged exciton, X*, lines. Sev-

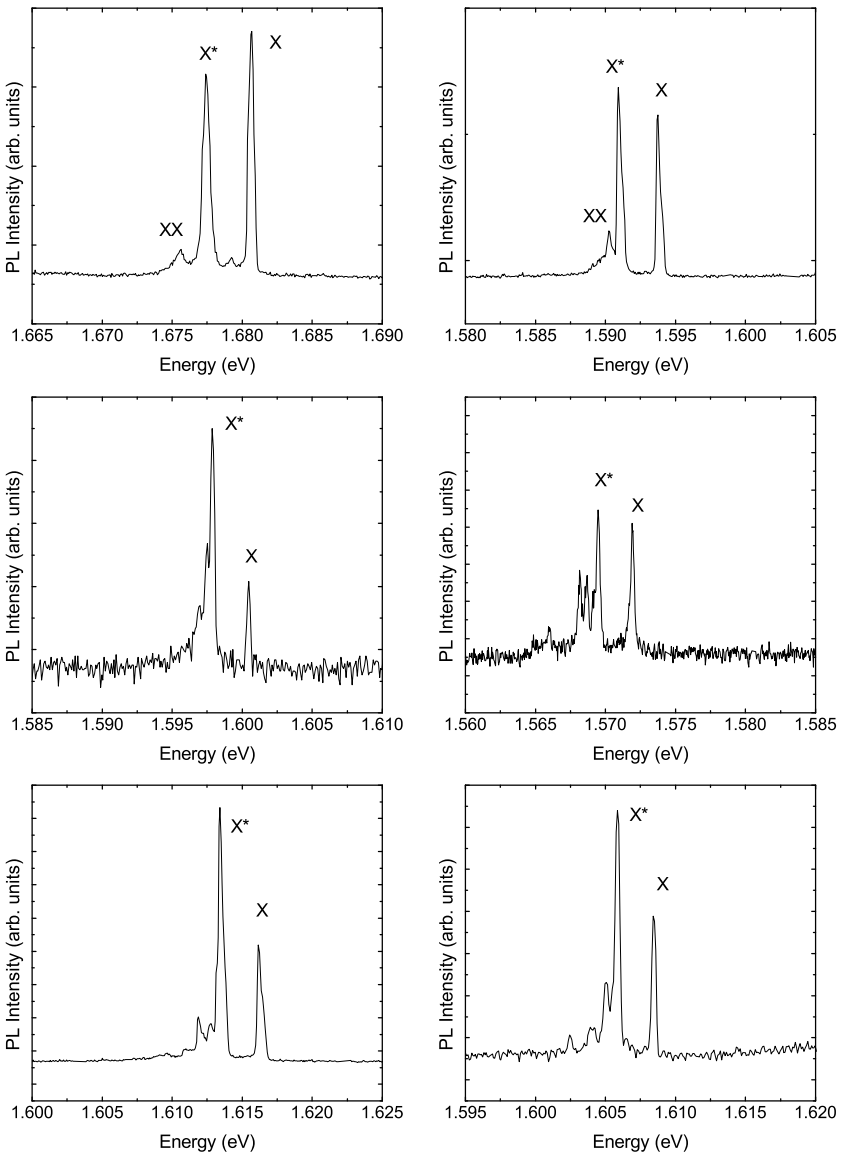

Figure 6.4: *μ-PL spectra of different quantum dots excited with relatively low excitation power. The excitation power in the presented figure is set to observe the strongest emission from X.*

eral low energy components that are visible in the spectra are related to biexcitons, more complex excitonic states and mixed configuration crossing transitions.

6.2.1 Effects of the confining potential and quantum dot composition

The exciton emission energy for different quantum dots is observed in a very broad energy range from 1.56eV up to 1.70eV (compare with Fig.6.1 and Fig.5.2), which is up to 150meV below the main quantum well transitions.

The energy of single exciton recombination is affected by several factors that can cause different emission energy variation, namely:

- alloy composition ∼100meV
- confinement in z - direction ∼50meV
- size of lateral confinement ∼10meV
- binding energy ∼1meV

Among them, the most important are the changes in composition of the dot and barrier material, mostly the Al content, and the height of the dots.

It is observed that the X* binding energy varies slightly, depending on the X emission energy. Fig.6.5 illustrates the energy difference between X and X* for various quantum dots with respect to the X emission energy. The smallest X* binding energy, of approx. 2.1meV is observed for the quantum dots emitting at the lowest energies. The observed X* binding energy is a few times larger than that of the bulk, indicating that the multi-exciton states are stabilized because of the spatial confinement.

The strength of the lateral confining potential determines mostly the distance between excited energy levels, $\hbar\omega_0$. In the investigated quantum dots no dependence between the X emission energy and characteristic s, p, d ...- shells energy was found, what is illustrated in Fig.6.6, where the energy difference between X and p-shell emission is plotted. This observation suggests that the lateral sizes of the dots are not correlated with alloy composition or confinement in the z - direction.

The X* binding energy is very similar for different quantum dots (of different size and alloy composition), and is of approx. 2.7meV. However, it increases slightly for quantum dots emitting in the high energy range. No dependence between X emission energy and the size of the lateral confining potential was found.

6.2.2 X, X* and XX dynamics

A typical excitation power evolution of single quantum dot μ-PL spectra is illustrated in Fig.6.7.

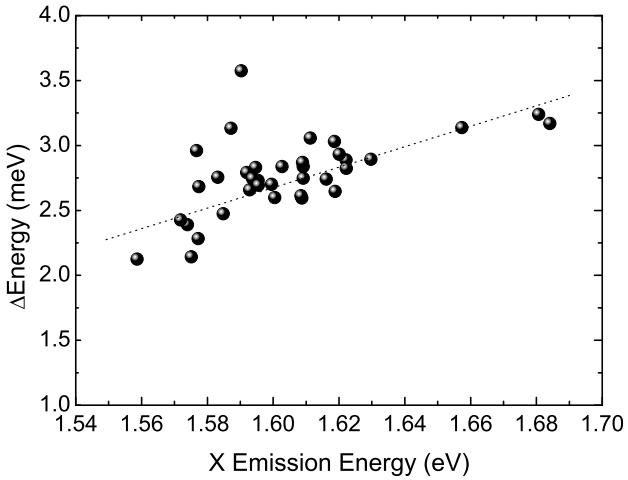

Figure 6.5: *X* binding energy for different quantum dots: the energy difference between X and X* emission versus X emission energy.*

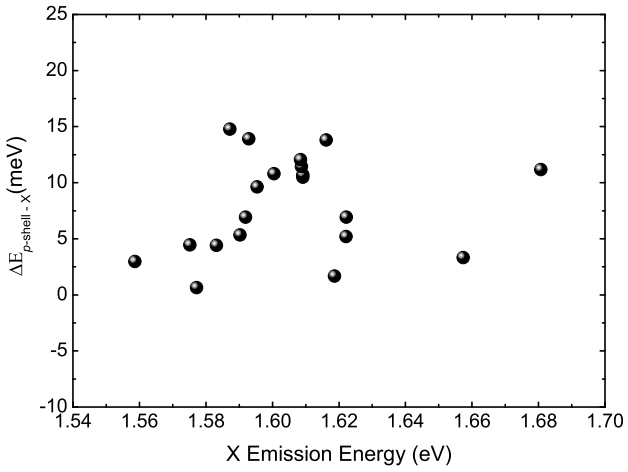

Figure 6.6: *Energy difference between X and p-shell emission with respect to X emission energy for different quantum dots.*

In the limit of low excitation power, below $0.3\mu W^{\dagger}$, only a single exciton, X, emission line is observed. The X* emission appears with increasing excitation power. Further increase of the excitation power leads to the subsequent appearance of additional low energy lines which are attributed to the formation of biexciton (probably the XX1 line) and more complex excitonic molecules.

At sufficiently high excitation intensity the excitonic emission vanishes, the X* emission saturates and the excitonic complex emission dominates the spectra, gradually broadening into a band, a few tens of meV in width.

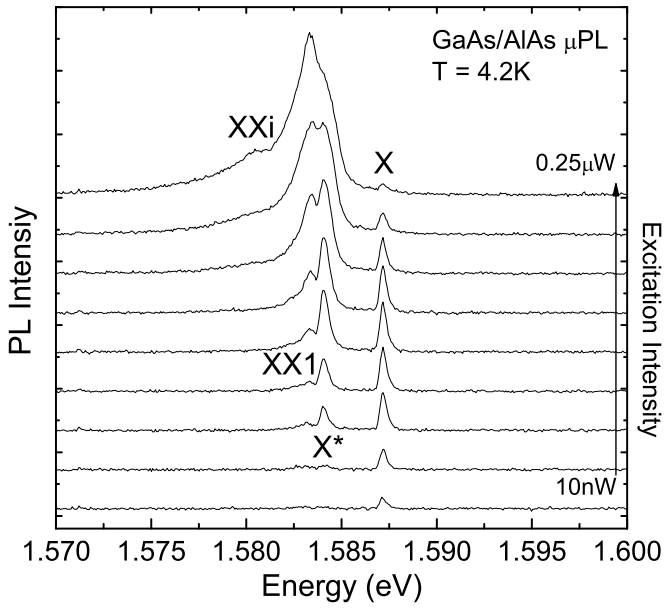

Figure 6.7: *μ-PL spectra of single quantum dot for different excitation powers in low excitation regime.*

In the limit of low excitation (below the observed intensity saturation) the X line intensity varies almost linearly with increasing excitation power, while superlinear growth is observed for X*, XX1 and XX2 emission lines, what is illustrated in Fig.6.8. Such behavior was already observed for a GaAs quantum dot formed at the interface fluctuations [2, 7, 13] and was widely discussed together with the theoretical description consisting of different types of rate equations.

The energy position of the X line as well as the X* line stays unchanged in

[†]The values of the excitation power indicated in the picture are approximate and give only the estimated value of the real exciting laser power.

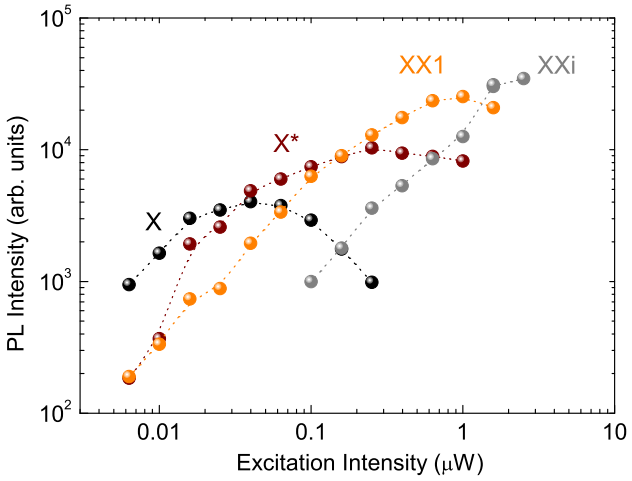

Figure 6.8: *The excitation power evolution of the X, X*, XX1 and XXi emission lines intensity. (The dotted lines are eye-guides.)*

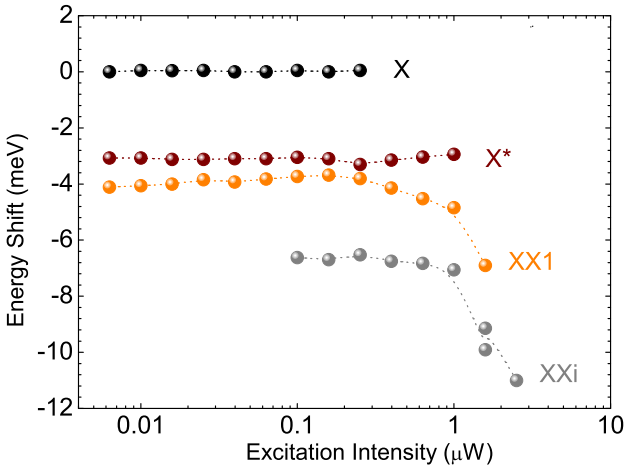

Figure 6.9: *The energy position of the emission lines vs. excitation power. The scale was shifted with respect to the X - excitonic emission line.*

the whole range of the excitation powers, where this emission is observed. Fig.6.9 illustrates the emission energy shift, with respect to the excitonic emission, in the whole range of excitation powers up to the limit where the X emission vanishes.

In the case of XX1 and XXi emissions a significant red shift is observed, starting from the excitation power at which the X line vanishes from the spectra and the X* emission is saturated. This excitation power correspond to the situation where already the first excited state (p-shell) is occupied by carriers, what is shown in detail in section 7.1. The energy shift is discussed in terms of a band gap renormalisation effect in section 7.2.1.

The appearance of the emission lines: X, then X* and XX1 in the PL spectra is observed with increasing excitation power. The subsequent emissions saturate when the emission of a more complex structure gains in intensity. Linear growth of the X emission, and super linear for more complicated structures, is observed with increasing excitation power.

6.2.3 Charged and empty quantum dots

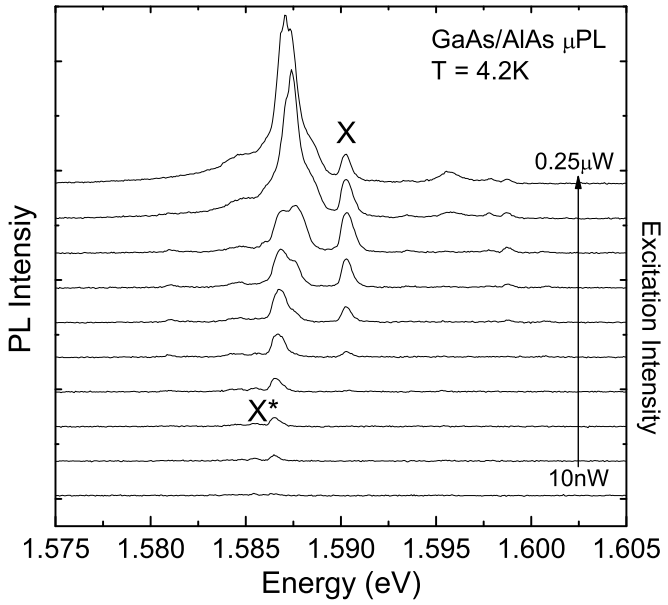

Figure 6.10: *μ-PL spectra of a single quantum dot for different excitation powers in the low excitation regime. Spectrum of a "charged" dot is illustrated for comparison with Fig.6.7, where the spectrum of "neutral" dot is presented.*

The emission from different quantum dots, i.e. shape of the spectra and the pattern of the X and X* emission, is very similar at relatively low excitation powers (see Fig.6.4). For the lowest excitation power the spectrum is composed of a single emission line. But apparently it is either neutral exciton, line X, (as it was discussed up to now, see Fig.6.7), or a charged exciton, line X*. Fig.6.10 illustrates the excitation power evolution of different quantum dot than those presented in Fig.6.7 in the same range of excitation powers. It is observed that the X* emission is the simplest excitation in the case of the lowest excitation power.

Depending which of the lines X or X* appears first in the spectra, we can observe that the dot was empty or already occupied by a single particle, respectively. This additional charge is probably due to the presence of an impurity in the vicinity of the quantum dot of particular charge. At high excitation powers the huge number of carriers that are captured and annihilated in the dot causes fast charge variations. Therefore the spectra at high excitation of "neutral" and "charged" dots are very similar and cannot be distinguished.

μ-PL maps taken for "charged" dots are very similar to those of a neutral dot (described in section 6.1). Fig.6.11 illustrates the X and X* intensity maps together with spectra corresponding to x- and y- cross sections of a "charged" quantum dot. The only difference (compare with Fig.6.2) is that when the quantum dot is excited from large distances the first exciton state that is bound is the charged exciton. This is very well visible in the X* intensity map, where the X* emission extends more than the X emission and this is in contrast to a "neutral" quantum dot.

The charge, negative or positive, of the X* state is not known. It is believed that in most cases it is a negatively charged exciton. This is because the confining potential for the electrons is much deeper than for holes (compare with Fig.2.4). However, in the experiment it is not possible to distinguish between negative and positive charge state recombination.

It is observed that quantum dots can be of two types: "neutral" and "charged". The identification is based on the very low excitation power spectrum, where either a single X emission line is visible, or a single X* line. This indicates that a source of charge fluctuation is present in the vicinity of the quantum dot, and single carriers can be captured from the surroundings of the dot.

6.3 Magnetic field effect

The application of a magnetic field to a zero dimensional system imposes an interplay between spatial and magnetically induced confinement. The theoretical approach to this effect is given in chapter 2 in section 2.3.1. In the following sections, the experimental results of single exciton, charged exciton and biexciton exposed on magnetic field are shown. The effects of:

- emission line energy splitting
- intensity changes

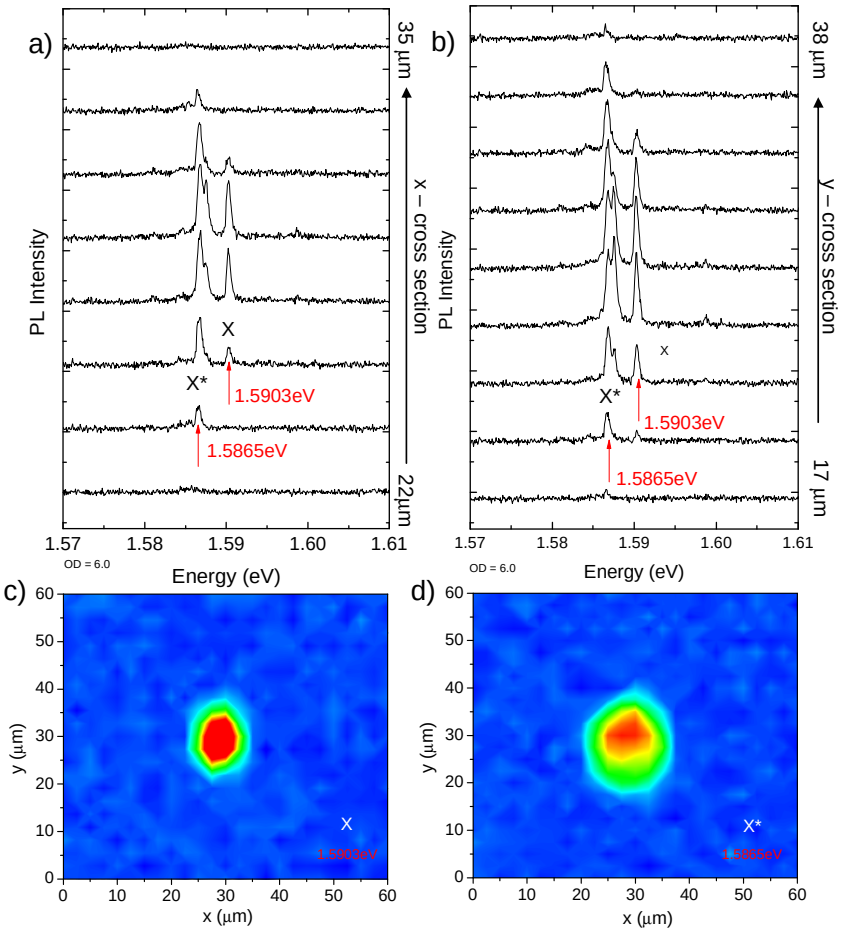

Figure 6.11: *µ-PL spectra of the single quantum dot scanned in the a) x- and b)y- directions. µ-PL intensity maps for the (c) X and (d) X* emission lines. The excitation power evolution of the emission spectra for this particular dot is illustrated in Fig.6.10.*

are discussed.

6.3.1 μ-magneto-PL spectra of X, X* and XX excitonic states

Fig.6.12 illustrates the typical magnetic field behavior of the emission of four different single quantum dots at an excitation power where the excitonic X and X* lines are observed. All emission lines show a significant and very similar diamagnetic shift. The X line attributed to the neutral exciton splits into two well resolved Zeeman components. The effective g-factor of the observed transitions varies from object to object and this effect is discussed in section 6.3.3.

The magnetic field behavior of the low energy part of the spectrum, related to other excitonic complexes, is more complicated. They split into several components. Some of them gain in intensity, and very often in a strong magnetic field become dominant in the spectrum.

It is well visible in the spectra that the total emission intensity from the quantum dots is oscillating in magnetic field. This effect was carefully investigated in this work to prove that this effect is a physical effect, not caused by the excitation power variation during the measurements in magnetic field. This effect is described and discussed in more details in Appendix.
In short, the results that strongly suggest that the oscillations are due to sample effects are:

- the spectra are stable and very well reproducible at a given magnetic field
- the magnetic field positions of observed maxima and minima, plotted versus consecutive integer numbers, were found to be a linear function (in contrast to Shubnikov de Haas oscillations of Fermi energy, where a linear dependence is shown on the inverse of the magnetic field).

The magnetic field evolution of X, X* and XX is typical for a quantum dot. A splitting into two well-resolved Zeeman components and a sub-linear increase in the energy of both spin-split energy levels with magnetic field is observed.

6.3.2 Diamagnetic shift

The value of the diamagnetic shift is evaluated from the energy shift of the exciton emission energy in magnetic field according to eq.2.10. The fitting was done over a full magnetic field range from 0T to 14T. Diamagnetic coefficients of different quantum dots studied are summarized in Fig.6.13.

According to eq.2.11, the diamagnetic coefficient represents the electron and hole wave function extensions in the quantum dot plane. In the first approximation it can be assumed that the quantum dots are isotropic with equal extensions of electron and hole. The electron and hole effective masses are $m*_e$=0.0665$m*_0$ and $m*_h$=0.475$m*_0$, respectively. For the lowest values of diamagnetic shift d=10μeV/T^2 it is obtained that $< r^2_{e,h} >^{1/2} \simeq$5nm and for the highest value of d=20μeV/T^2

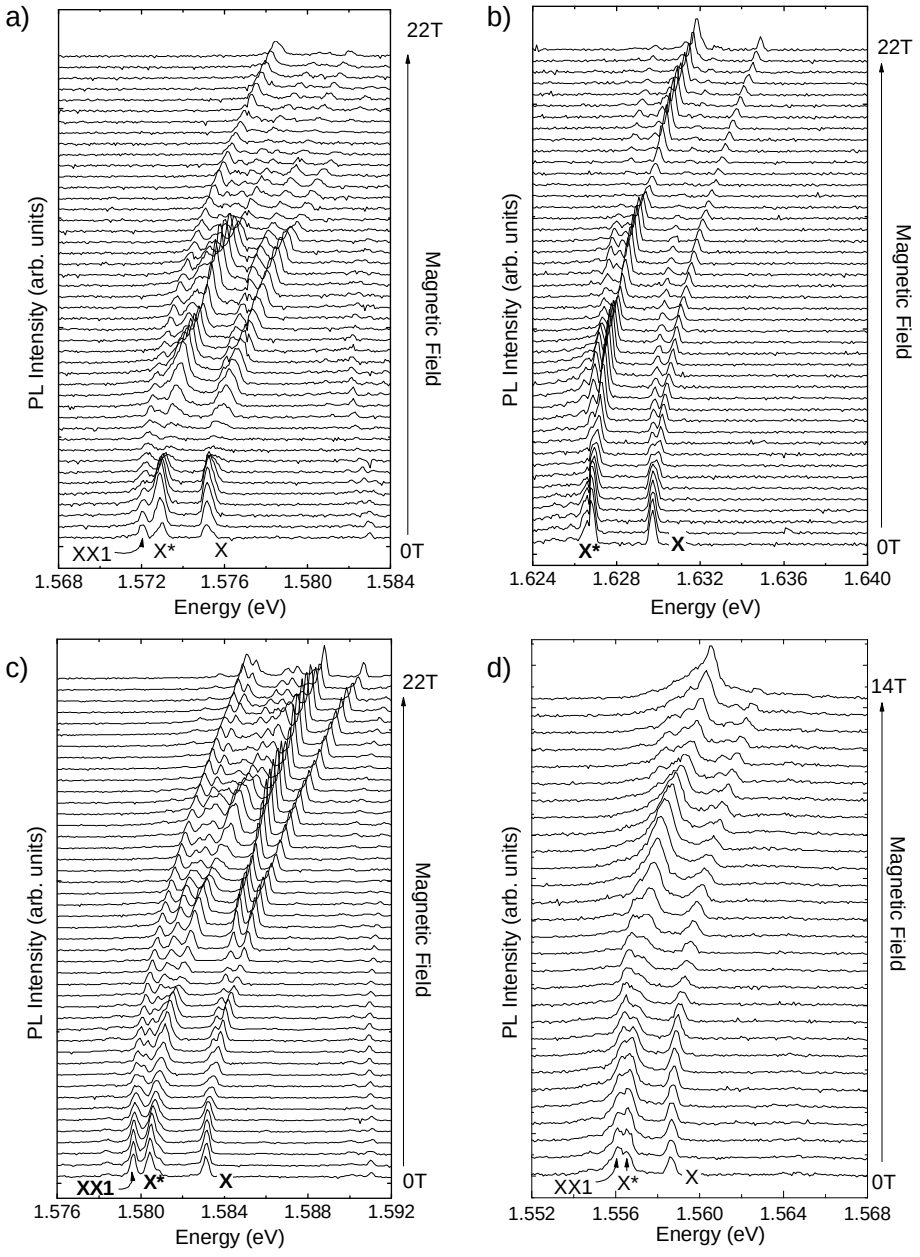

Figure 6.12: *The magnetic field evolution of the single quantum dots emission measured at low excitation power. The results for four different dots are shown in panels a) - d).*

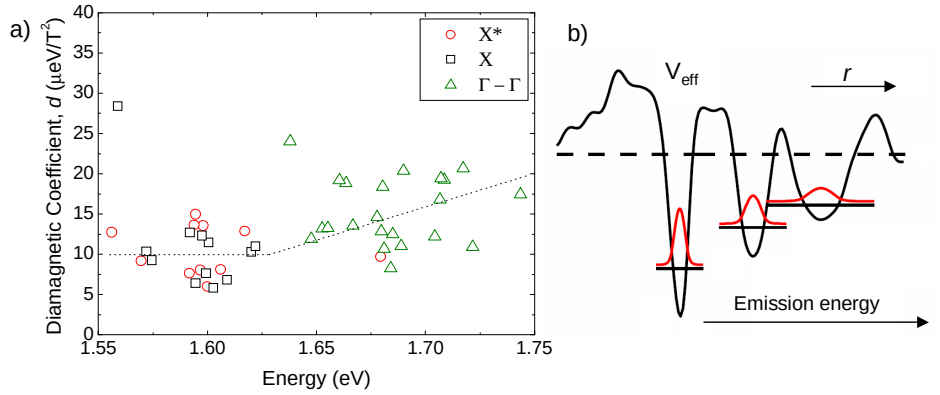

Figure 6.13: *a) The diamagnetic coefficient of X (squares) and X* (circles) for different quantum dots versus emission energy. The diamagnetic coefficient of sharp emission lines observed in the energy region of the phonon replica and the* $\Gamma - \Gamma$ *transition energy is also marked (triangles). b) The model of exciton localization by short-range disorder proposed in Ref.[14]. The deep-lying exciton states have small wave functions.*

$< r_{e,h}^2 >^{1/2} \simeq 7$nm. This is in very good agreement with the dot radius of the first s electronic level estimated from the harmonic confining potential model illustrated in Fig.2.4.

A systematic decrease of the diamagnetic coefficient is found with the decrease of the exciton emission energy. This effect contradicts results obtained in other papers [15] that investigate the effects of diamagnetic shift on the quantum dot size. In general, the diamagnetic coefficient is expected to decrease with decreasing dot size. In the case of the investigated quantum dots, the exciton emission energy is a complicated function of the dot size and potential barriers, which was discussed in section 6.2.1).

However, the general tendency of the positive slope observed in the diamagnetic shift distribution as a function of transition energy shows that the lowest exciton tail states have the smallest diamagnetic coefficients, corresponding to small relative wave functions. Consequently, the lowest exciton states are laterally strongly confined states. A model to describe this effect was proposed in Ref.[14] and was based on calculations of exciton localization on Gaussian disorder. Fig.6.13b) illustrates several minima in the effective potential for the exciton ground states resulting from an assumption of short-range disorder (Ref.[14]). In the investigated structure, this can be the case for the emission observed in the high energy region of the spectra, in the $\Gamma - \Gamma$ transition and its phonon replica regime, where the diamagnetic shift is observed to increase (marked by a dotted line in Fig.6.13(a) for results denoted by triangles).

Experimental evidence shows that the investigated quantum dots, whose emission energy is observed from 1.55eV to 1.65eV, are not due to the localization of

an exciton on interface fluctuations (see chapter 1.2 for details). In this region it can be concluded that no dependence on the diamagnetic coefficient and emission energy is found.

As the diamagnetic coefficient (d) represents the in-plane carrier wave function extension, dependence of d on the characteristic energy, $\hbar\omega_0$, of the in-plane confining potential is expected. Indeed, a decrease of the diamagnetic coefficient with the difference between X and p-shell emission energies is found, which is illustrated in Fig.6.14. High values of the s - p-shell splitting mean that the in-plane dot confining potential are narrow, therefore the observed values of diamagnetic coefficient of X are smaller.

In general, it can be concluded, that the diamagnetic coefficient does not depend on the X emission energy, but is related to the size of in-plane confining potential. This confirms that the exciton emission energy is determined rather by the alloy composition variation than by the quantum dot in-plane dimensions.

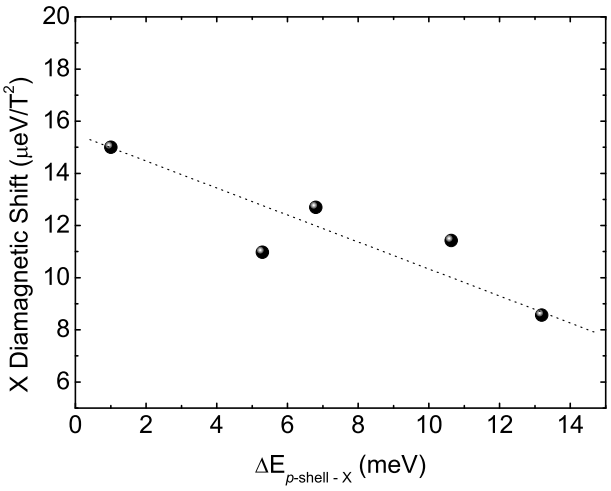

Figure 6.14: *Values of the diamagnetic coefficient versus X and p-shell emission energy difference, for different quantum dots. The dotted line is an eye-guide.*

The diamagnetic coefficient of an exciton is almost constant, approx. $10\mu eV/T^2$, for dots emitting at low energies. It increases up to $20\mu eV/T^2$ for excitons emitting in the high energy range, where the emission is due to excitons localized at quantum well potential fluctuations.
The value of the diamagnetic coefficient allowed to determine the size of the $1s$ exciton wave function as being approx. 5nm, in agrement with the estimated size of the first electronic level in a harmonic confining potential.

6.3.3 g-factor

The Zeeman energy (compare with eq.2.10) reveal a systematic change of the g* value with the exciton emission energy from different quantum dots. This effects is illustrated in Fig.6.15. It is observed that the exciton of higher recombination energy shows higher values of effective g-factors.

The values of the g*-factor are observed not to depend on the size of the lateral confining potential, what is illustrated in Fig.6.16. The results confirm, therefore, that the g*-factor is related more to alloy composition in the dot and barrier material than to the dot size.

The g*-factor obtained in this study is the effective g-factor of the whole exciton. The electron g-factors, g_e, in a GaAlAs alloy are relatively small, from -0.4 to 0.4, depending on the alloy composition. Therefore the g*-factor of the investigated quantum dots depends mostly on the hole g-factor, g_h. The value of g_h is not easy to evaluate due to the mixing of valence energy levels. In general, it is very difficult to determine the electron and hole g-factors separately as they are very sensitive to the band mixing and furnish detailed insight into the confined electronic structure.

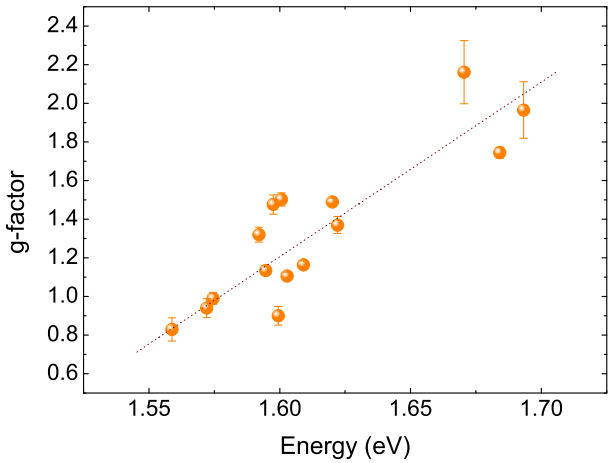

Figure 6.15: *The values of g*-factors of excitonic emission versus emission energy for different quantum dots.*

Some insight to this problem would be given by an experiment where the exciton bright and dark states from the same quantum dot are observed. In the ideal case of an isotropic quantum dot, the exciton state is split into bright and dark states. Only the bright states can emit a photon as a consequence of selection rules

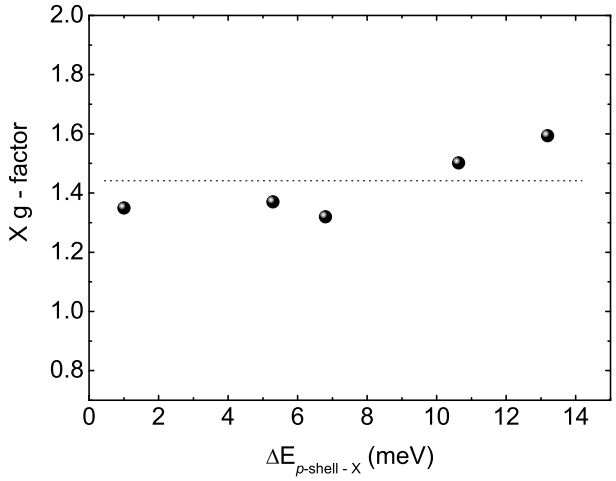

Figure 6.16: *The values of exciton g*-factor versus X and p-shell emission energy difference for different quantum dots. The dotted line is an eye-guide.*

concerning the spin angular momentum. The ideal case can be, however, broken with strong magnetic field or with a highly anisotropic strain field, that would mix the bright and dark states.

The effective g*-factor of an exciton in the investigated quantum dots varies from dot to dot from 0.8 to 2.2. The values are mostly determined by the hole g-factor. An increase of the g* factor was found for excitons emitting in higher energies.

6.3.4 Thermalization effects

Upon increasing the magnetic field, the intensity of the high energy component of the X emission line decreases (Fig.6.12 a) and c)), exhibiting a thermalization dependence:

$$\frac{I_{up}}{I_{down}} = exp[-\frac{g * \mu_B B}{k_B T_{eff}}] \tag{6.1}$$

with an effective temperature of $T_{eff} \sim 10K$, slightly different from dot to dot.

However, it is often seen in the spectra that at high magnetic field it is the high energy component of split exciton emission lines that has a higher emission intensity (Fig.6.12 b) and c). The observed population inversion of the Zeeman split levels in the quantum dots is an intriguing effect. It suggests that the spin relaxation is for some reasons blocked in the system.

One of the possible mechanisms of such effect is the following: the photo-created carriers first thermalize on the X-type, indirect, states; further on the carriers are

captured in the quantum dot levels. In the process of capturing the carriers preserve the spin. With different band structure, GaAs and AlAs totaly different inverse g-factors for conduction band electrons. Therefore, for some quantum dots (of mixed alloy composition) the electron g-factors in the dot and surrounding system is inverted. Consequently, spin conserving capture process from a thermalized spin system leads to an effective higher occupation of the high-energy Zeeman component with corresponding spin orientation. Similar effect was also observed in Ref.[16], on similar structures for excitons localized in the GaAs/AlAs interface fluctuations.

6.3.5 X as bound state

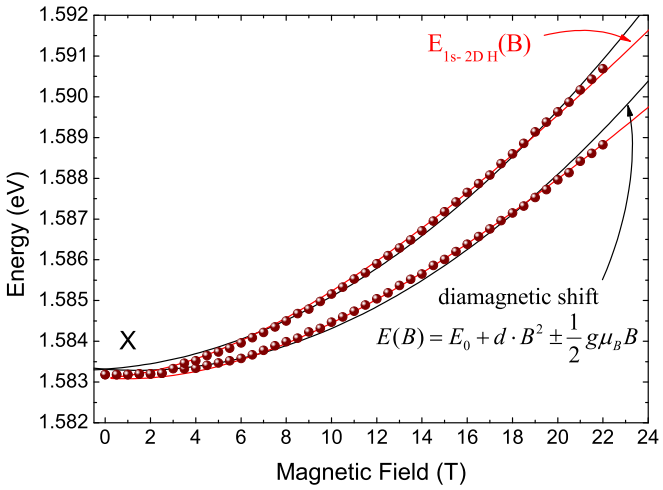

Figure 6.17: *Typical emission energy shift of a single exciton emission line up to high magnetic fields. The models of diamagnetic shift and of 2D hydrogen atom 1s state energy shift are fit to the data as described in the text.*

The PL peak energy of the X emission from a representative quantum dot (whose emission is illustrated in Fig.6.12c) is plotted as a function of applied magnetic field in Fig.6.17.

The PL peak energies fitted according to eq.2.10 and eq.2.12 are compared. It is well seen that the quantum dot exciton energy shift is much better described by the model of a two-dimensional hydrogen atom than a standard diamagnetic shift, especially in the high magnetic field regime. The theoretical aspect of this problem is widely discussed in chapter 2.3.1.

The fitting parameter in the case of eq.2.12 is the exciton binding energy. For the exciton emission illustrated in Fig.6.17 a value of E_B=18.1meV was obtained,

for the exciton effective mass set to $m* = 0.058m_0$. This values is very reasonable, although slightly higher than that obtained from the model of band gap renormalisation described in section 7.2.1.

At high magnetic field the description of the energy shift of both spin-split energy levels of exciton in terms of a diamagnetic shift with quadratic dependence on magnetic field is no longer valid. A better approach to the problem of energy shift with magnetic field of a strongly confined exciton is given by the model of a two dimensional hydrogen atom.
The binding energy of an exciton in a quantum dot could be evaluated to be approx. 18meV.

Bibliography

[1] J. G. Tischler, A. S. Bracker, D. Gammon, and D. Park, "Fine structure of trions and excitons in single GaAs quantum dots," *Phys. Rev. B*, vol. 66, p. 081310, 2002.

[2] Q. Wu, R. D. Grober, D. Gammon, and D. S. Katzer, "Imaging spectroscopy of two-dimensional excitons in a narrow GaAs/AlGaAs quantum well," *Phys. Rev. Lett*, vol. 83, p. 2652, 1999.

[3] Q. Wu, R. D. Grober, D. Gammon, and D. S. Katzer, "Excitons, biexcitons, and electron-hole plasma in a narrow 2.8nm GaAs/$Al_xGa_{1-x}As$ quantum well," *Phys. Rev. B*, vol. 62, p. 13022, 2000.

[4] K. Brunner, G. Abstreiter, G. Böhm, G. Tränkle, and G. Weimann, "Sharp-line photoluminescence and two-photon absorption of zero-dimensional biexcitons in a GaAs/AlGaAs structure," *Phys. Rev. Lett.*, vol. 73, p. 1138, 1994.

[5] K. Matsuda, T. Saiki, S. Nomura, M. Mihara, Y. Aoyagi, S. Nair, and T. Takagahara, "Near-field optical mapping of exciton wave functions in a gaas quantum dot," *Phys. Rev. Lett.*, vol. 91, p. 177401, 2003.

[6] K. Brunner, G. Abstreiter, G. Böhm, G. Tränkle, and G. Weimann, "Sharp-line photoluminescence of excitons localized at GaAs/AlGaAs quantum well inhomogeneities," *Appl. Phys. Lett.*, vol. 64, p. 3320, 1994.

[7] D. Gammon, E. S. Snow, and D. S. Katzer, "Excited state spectroscopy of excitons in single quantum dots," *Appl. Phys. Lett*, vol. 67, p. 2391, 1995.

[8] S. V. Nair and Y. Masumoto, "Multi-exciton states and many-body correlations in quantum dots," *phys. stat. sol. b*, vol. 224, p. 739, 2001.

[9] E. Tokunaga, A. L. Ivanov, S. V. Nair, and Y. Masumoto, "Inverse exciton series in the optical decay of an excitonic molecule.," *Phys. Rev. B*, vol. 56, 1999.

[10] P. Hawrylak, "Excitonic artificial atoms: Engineering optical properties of quantum dots," *Phys. Rev. B*, vol. 60, p. 5597, 1999.

[11] M. Bayer, O. Stern, P. Hawrylak, S. Fafard, and A. Forchel, "Hidden symetries in the energy levels of excitonic 'artificial atoms'," *Nature*, vol. 405, p. 923, 2000.

[12] P. Michler(Ed.), "Single quantum dots. Fundamentals, applications and new concepts," *Topics in Applied Physics, Springer*, vol. 60, 2003.

[13] H. van Kesteren, E. Cosman, P. Dawson, K. Moore, and C. Foxon, "Order of the x conduction-band valleys in type-II GaAs/AlAs quantum wells," *Phys. Rev. B*, vol. 39, p. 13426, 1989.

[14] M. Erdmann, C. Ropers, M. Wenderoth, R. G. Ulbrich, S. Malzer, and G. H. Döhler, "Diamagnetic shift of disorder-localized excitons in narrow GaAs/AlGaAs quantum wells," *Phys. Rev. B*, vol. 74, p. 125412, 1997.

[15] M. Sugisaki, H.-W. Ren, S. V. Nair, K. Nishi, and Y. Masumoto, "External-field effects on the optical spectra of self-assembled InP quantum dots," *Phys. Rev. B*, vol. 66, p. 235309, 2002.

[16] A. Schaller, A. Zrenner, G. Abstreiter, and G. Böhm, "Spectroscopy of excitonic Zeeman levels in single quantum dots," *Physica E*, vol. 2, p. 609, 1998.

Chapter 7

Highly Excited Single Quantum Dot

La spectroscopie de boîte quantique unique sous forte excitation optique permet d'étudier la structure riche des états excités. L'observation et l'analyse des spectres d'une boîte quantique unique en fonction de la puissance du laser, donc du nombre des porteurs confinés, dans un régime de puissance très large, donnent accès aux propriétés optiques et structurales de la boîte. Grâce à ces expériences, nous avons évalué une forme de potentiel de confinement et extrait les dimensions des boîtes. L'application d'un champ magnétique intense et la comparaison de l'évolution des spectres d'émission multi-excitoniques en fonction du champ magnétique avec le spectre de Fock-Darwin nous ont permis d'une part de démontrer les similarités de ces systèmes avec une boîte quantique idéale, d'autre part, les résultats obtenus ont permis de mettre en évidence de fortes interactions avec des niveaux énergétiques complètement occupés.

A special property of a zero dimensional structure is the particular degeneracy of the energy levels (see chapter 2 for details). When a more complicated exciton complex than the biexciton is formed in a single quantum dot, the excess particles are confined in the excited shells. Depending on the number of particles in the dot, they occupy a certain number of excited levels, what is reflected in the emission as the appearance of additional structures on the high energy side of the PL spectra. The effects of a large number of carriers in a single quantum dot are discussed in the following sections.

In first part, the general effects of the increase of the excitation power on the PL are shown. The shape of the confining potential and the dot size are evaluated.

In the second part, the interactions in this dense electron - hole system are considered. The effects of the emission energy shift observed from the ground state are discussed in terms of the band gap renormalisation effects known from bulk materials.

Then, the effects of applying a magnetic fields are investigated. The Fock - Darwin energy diagram, typical for a single particle confined in harmonic potential, is

observed. The limitations and advantages of this simple description are discussed in terms of hidden symmetry effects and many-body type interactions.

7.1 Highly excited states: s, p, d, . . . , emission

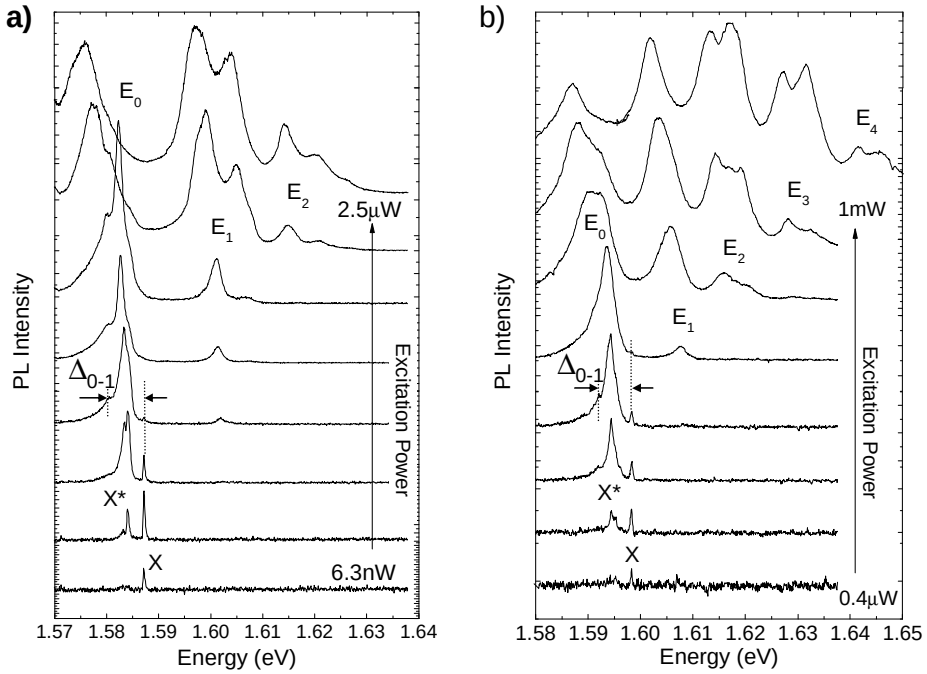

Figure 7.1: *PL spectra of two different single quantum dots a) and b) in the whole spectral range and for all accessible excitation powers.*

It was shown in the previous chapter that, above a certain excitation power, the single exciton emission saturates then vanishes, and further on the complex, low energy multi-excitonic emission dominates the spectra in the low energy range (Fig.6.7 and Fig.6.10). With further increase of the excitation power the spectra become more complicated and the emission from the excited states becomes visible.

The excitation power evolution of several single quantum dot spectra in the whole spectral range and for all accessible excitation powers is illustrated in Fig.7.1 and Fig.7.2. Fig.7.1a) and Fig.7.2a) illustrates the spectra for the same quantum dots as discussed in chapter 6 and illustrated in Fig.6.7 and Fig.6.10, respectively, but for higher excitation powers and in a wider spectral range.

At the excitation power for which the excitonic emission vanishes from the spectra, the low energy region dominates the intensity and forms a complicated structure of the ground state emission. In Fig.7.1 this emission is denoted by E_0.

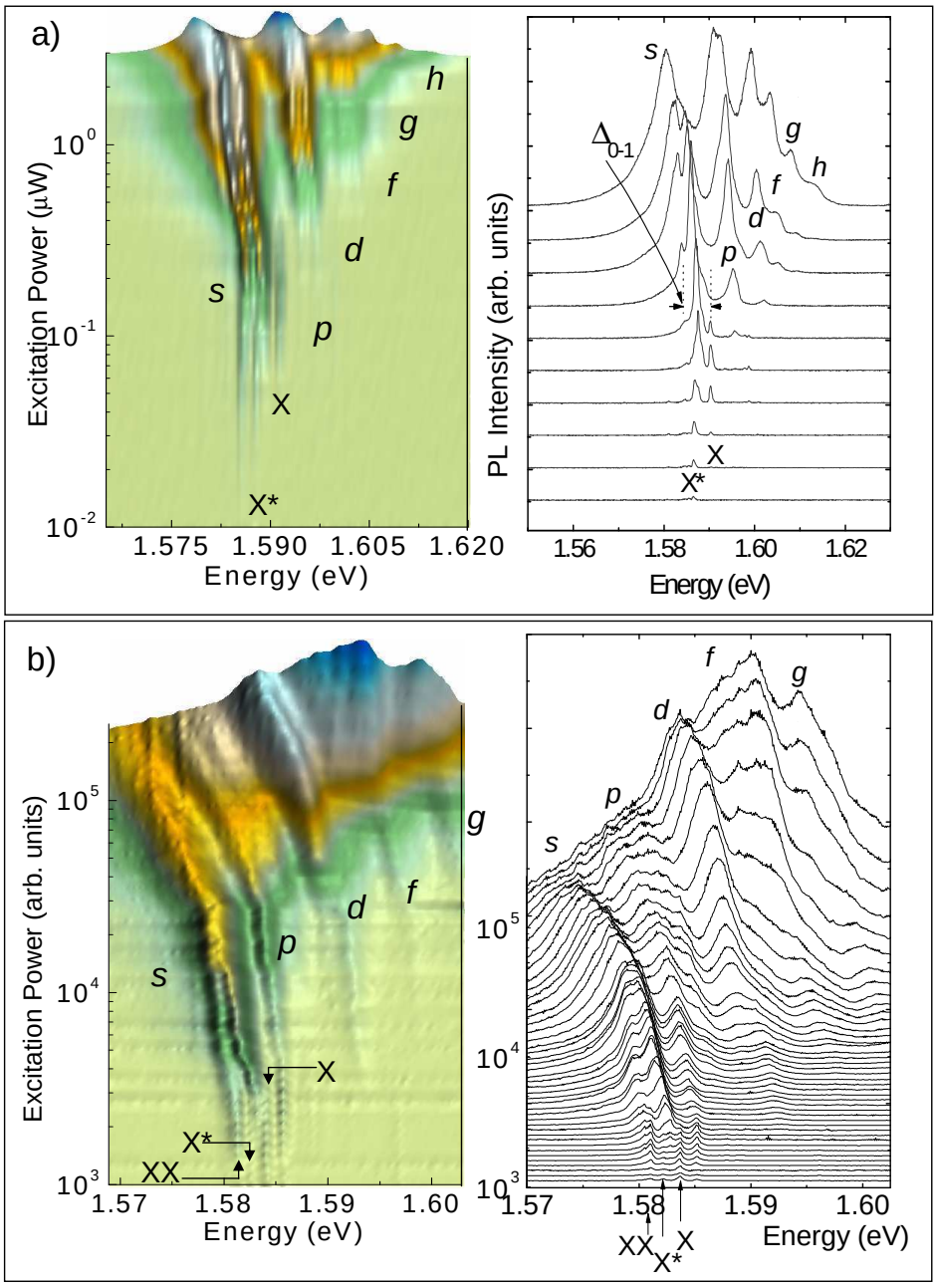

Figure 7.2: *PL intensity maps (left panels) and several corresponding spectra (right panels) of two single quantum dots a) and b) in the whole spectral range and for all accessible excitation powers.*

Simultaneously, the appearance of broad emission approx. tens of meV above the E_0 line is observed. This emission is attributed to the recombination of carriers from the first excited electronic state, E_1, of the quantum dot. In the μ-PL spectra from a different dot, illustrated in Fig.7.1b), up to four excited states were observed (marked as E_1, E_2, E_3 ...).

With further increase of the excitation power (not shown), above that for which the corresponding spectra are shown in the figures, the whole spectrum transforms into a broad band, however, no additional structures appear. This indicates that there exists a finite and precise number of excited states, what sets a limit to the quantum dots dimensions (compare with the discussion in chapter 2.1.1, where the dot dimensions are evaluated).

The possibility of filling such a large number of excited states suggests that the confining potential of the quantum dots is very deep. This is a particular property of the investigated quantum dot system. Especially, this distinguishes this system from the usually investigated GaAs quantum dots that are formed at the quantum well interface fluctuations (see chapter 1.2).

The characteristic feature for all the dots investigated in this sample is that their emission from excited states is almost equally spaced in energy. This is a typical effect for harmonic confining potential. As it was discussed already in chapter 2 and is shown experimentally in section 7.3, the application of a magnetic field splits the observed energy levels in the way characteristic for s, p, d, ... and higher atomic-like shells. Thus, due to the similarity of the effects $E_0 \equiv s$, $E_1 \equiv p$ and so on. Both notations are used in this work.

The inter-shell energy separation, $\hbar\omega_{e-h}$, varies from object to object from 5meV to 20meV. This corresponds to the diameter of the first electronic state from $\sim$30nm to $\sim$15nm for GaAs dots (compare with chapter 2.1.1, Fig.2.4). Taking into account the number of bound electronic shells the average dot dimensions in this sample are tens of nm.

The splitting of the emission lines of the excited shells is observed very often (compare with E_1 state in Fig.7.1a). It is assigned as being most probably due to the shape anisotropy of the dot, what is illustrated in Fig.2.2. A splitting of a few meV corresponds to a deformation of approx. δ=1.7, what gives the ratio of x and y dot lengths, i.e. the dot elongation.

The observation of a number of excited state emission lines from a single quantum dot reveals that the investigated dots are strongly confined systems. The emission is typically zero-dimensional and exhibits a multiple "atomic-like" shell structure.

7.1.1 Mapping experiment

To prove that even at high excitation powers the observed emission comes from the same quantum dot, a μ-PL mapping experiment was performed.

The experimental setup is presented in chapter 4.3.2.

The quantum dot whose emission is illustrated in Fig.6.11 is in this experiment excited with a high excitation power. Fig.7.3 illustrates the spectra corresponding to a cross section of the quantum dot in the x- (a) and y- (b) direction, and PL-maps for the energies of X (a), X* and s (b), p (c) and d (d) emission lines.

If the quantum dot is excited in the center, the emission spectrum is composed of several broad lines, corresponding to recombination from s, p, and d levels, and even traces of higher excited states are visible. When the excitation spot is moved away from the center of the quantum dot, the spectrum changes as it would have been by reducing the excitation power. This effect is well seen when the spectra in Fig.7.3a) and b) are compared with those in Fig.7.2. When the exciting laser spot is approx. 20μm from the center of the dot, the emission spectrum is similar to those observed for small excitation powers and is composed of X and X* sharp lines.

The μ-PL maps of the sample taken for the energies of X, X* and s, p and d lines show that all emissions are coming from the same place on the sample. Moreover, the emission is symmetric in x and y spatial directions. The ring shape of the X emission is due to the fact that at high excitations, i.e. when the laser spot is approaching the dot, the X saturates and vanishes from the spectra, as the X emission is only visible for weak excitations. The same ring shape on the μ-PL map should be observed for X* emission. However, in the same energy as X* line, the strong emission from the s state is visible, this affects the PL-map for X* emission energy and the ring shape is not observed.

The fact that the investigated quantum dots can be excited at such large distances from the excitation spot is due to strong diffusion properties of the indirect barrier material. The carriers that are created in the surroundings of quantum dots by above band gap excitation spread up to 100μm (as it was shown in chapter 5.4) before they recombine in the quantum dot. This effect was already discussed in chapter 6.1.

The μ-PL mapping experiment at high excitation power shown that X, X*, and s, p, d, . . . excited state emissions are well defined in space. All observed emissions are due to multi-exciton complexes recombination confined in the same quantum dot, well isolated from surrounding objects.

7.1.2 Hidden symmetry properties of the system

Two particular effects are observed with the increase of the excitation power above the observed saturation of the X emission line. First, a discrete emission from the E_1 level is visible. Second, the E_0, ground state emission becomes broad and a low energy structure appears, approx. 5.6meV below the X emission. They are denoted by Δ_{0-1} in Fig.7.1 and Fig.7.2.

This low energy emission is the effect of the recombination of excitons confined in the E_0 state in the presence of excitons in the partially filled excited E_1 state.

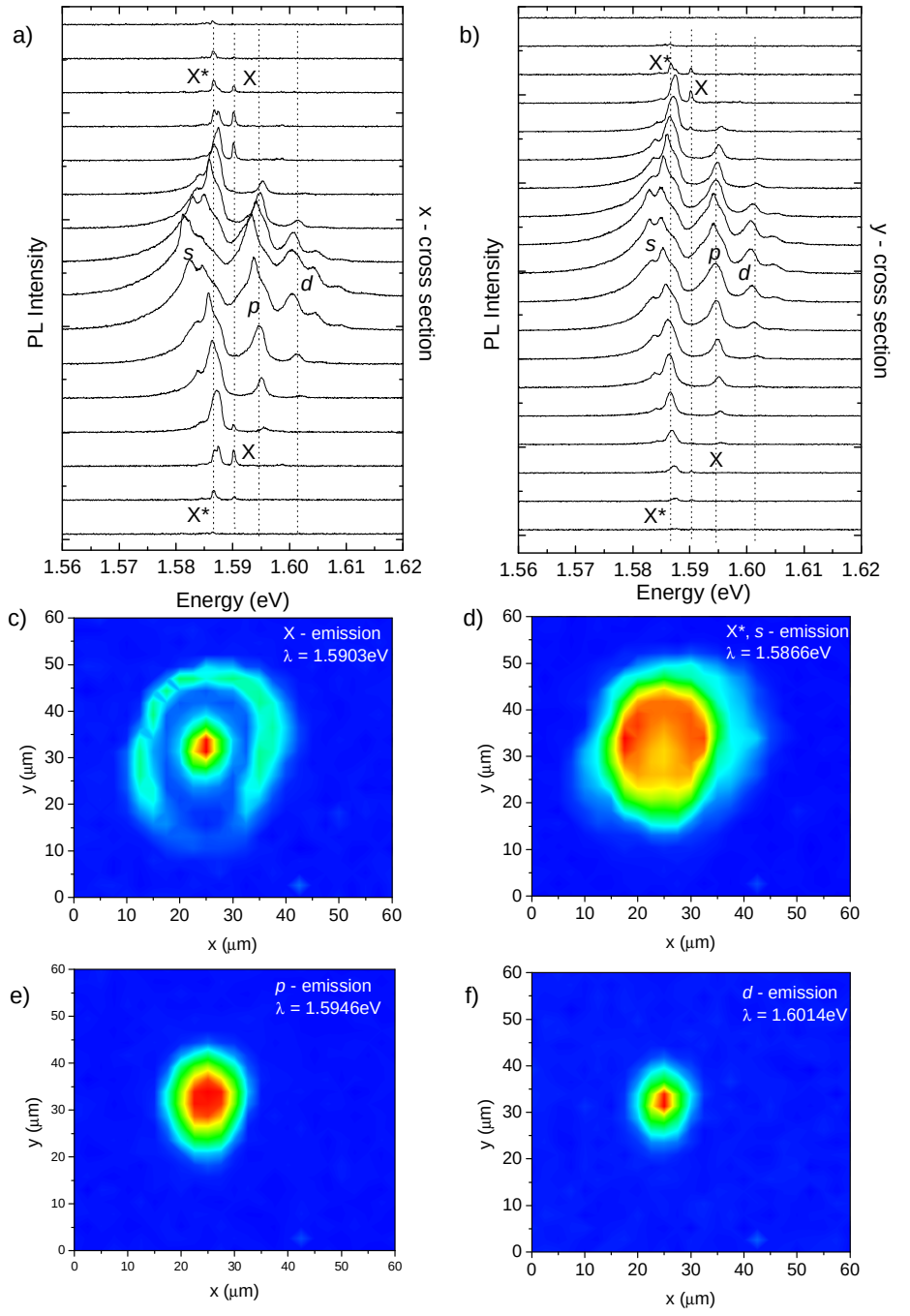

Figure 7.3: *a) x-cross section and b) y-cross section μ-PL spectra of the quantum dot whose emission is illustrated in Fig.7.2a) excited with an excitation power of 1.6μW. c)- f) μ-PL maps corresponding to the energies as marked by vertical dotted lines in the spectra.*

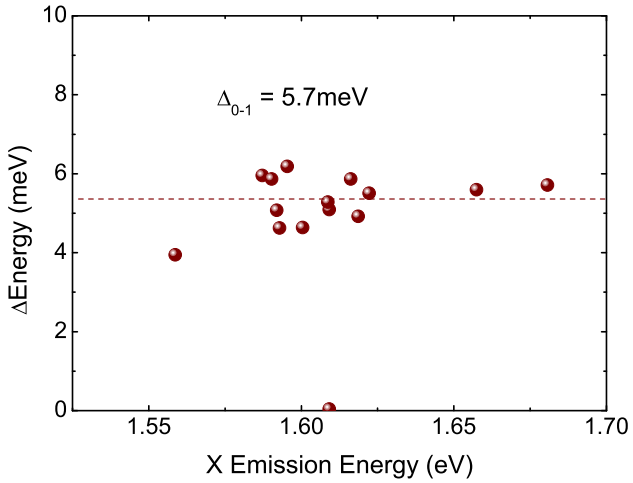

Figure 7.4: Δ_{0-1} *Energy difference between the X emission line and that which forms the ground state emission* E_0 *in the moderate excitation power regime for different quantum dots.*

The value is determined by the inter-level interaction strength.

Fig.7.4 illustrates the values of Δ_{0-1} for different quantum dots. The emission energy of X varies from dot to dot depending on their dimensions, composition and surroundings. As may be seen in Fig.7.4, Δ_{0-1} is not observed to depend on the X emission energy and the average value is approx. 5.6meV. It is believed that it is a general value for GaAs that determines the strength of interactions between ground and excited shell excitons.

This effect is theoretically treated by Nair [1], Wojs [2] and Hawrylak [3]. An experimental demonstration and theoretical discussion on this subject can be also found in Ref.[4].

A similar effect is observed with filling of the subsequent excited energy levels. Each time the carriers start to fill the next excited shell, an additional, low energy emission appears from the lower completely filled shell. This effect is marked by vertical dotted lines in Fig.7.5. The figure illustrates the same results as those presented in Fig.7.2a) but as a map of intensity in logarithmic scale.

Interestingly, the inter-particle Coulomb interactions between the excitons in the partially filled shell and the excitons filling the underlying shells do not affect significantly the recombination energy until the shell is completely occupied, i.e the E_n emission energy does not change until the E_{n+1} state is occupied. This effect is schematically marked by horizontal dotted lines in Fig.7.5. It is speculated that

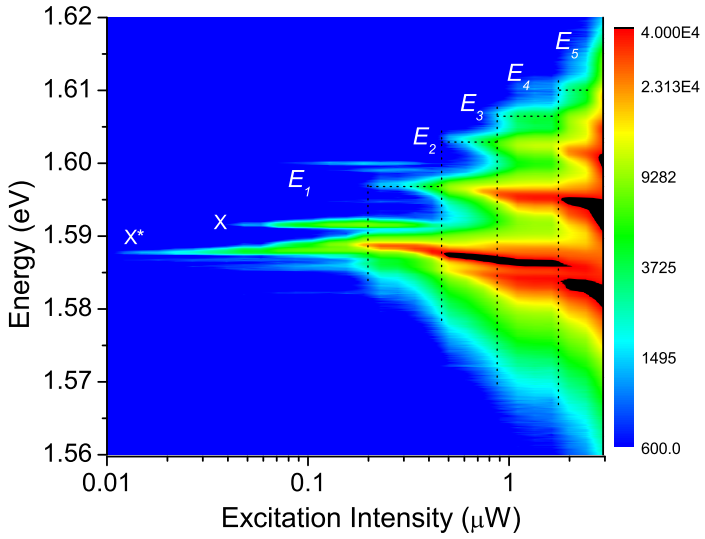

Figure 7.5: *Excitation power evolution μ-PL intensity map of a single quantum dot (the same results as illustrated in Fig.7.2a), presented on a different type of graph). The intensity is in logarithmic colour scale.*

this property of the system is associated with degeneracies of electronic shells and with the equal strength of electron - electron, electron - hole, and hole - hole interactions due to the exact overlapping of electron and hole orbitals, what is often referred [2, 3, 5] to as the hidden symmetry property of the system.

The effects of interactions between particles from different energy shells are visible in the excitation power dependent spectra as the appearance of additional emission lines when the number of carriers in the quantum dot is increased. Simultaneously, the energy shift of lower lying shells is observed only when the presence of carriers on the higher excited shell is noted. This is assigned as the hidden symmetry property of the investigated system.

7.2 Many-body type effects

The modification of single-particle properties in densely occupied quantum dots is of fundamental interest. Although the change of the semiconductor band gap in bulk materials or even in quantum wells is widely known, the effects of many body exchange-correlation interactions in a single quantum dot are still under investigation. Recent theoretical studies [1, 2] and experiments performed on quantum dots [6, 7] show effects of the exchange-correlation interaction and an emission energy shift of a few 10 meV in the many-body regime.

The average dimensions of the investigated quantum dots can be estimated as height $h =\sim$12.4nm and an radius $r =\sim$50nm. For example 10 excitons confined inside a dot correspond to an effective carrier density of $\varrho = 10/(\pi r^2 h) \sim 10^{17}\mathrm{cm}^{-3}$ or in 2D: $\varrho = 10/(\pi r^2) \sim 10^{11}\mathrm{cm}^{-2}$. Thus it is a quite dense electron-hole system in comparison to bulk or quantum well materials. In the high density regime the Coulomb interactions between the carriers become important. This should be reflected in the PL spectra as a significant modification of the emission energy.

As the number of electron - hole pairs in a quantum dot is increased, the carriers are subsequently added to the next discrete and degenerate energy levels (as it was discussed theoretically in chapter 2.1.2 and shown experimentally in the previous section). The carriers confined at fully occupied levels interact and thus the emission energy is expected to gradually change. This effect is observed in the emission spectra as the red shift of the subsequent emission lines. This is especially well visible in Fig.7.2 in the intensity maps, but is a general effect for all investigated dots. Particulary, as the emission from the first excited state is observed the ground state emission start to shifts to the low energy side and gradually broadens. Further on, as the emission from the second excited state becomes visible, the first excites emission line is observed to shift. The process is similar for the following excited states. In order to understand the physical properties of carriers confined in a highly excited single quantum dot, the band gap renormalisation formalism from bulk materials was directly applied. The following sections demonstrate how the two systems are compared and discuss the obtained results.

7.2.1 Band gap renormalisation

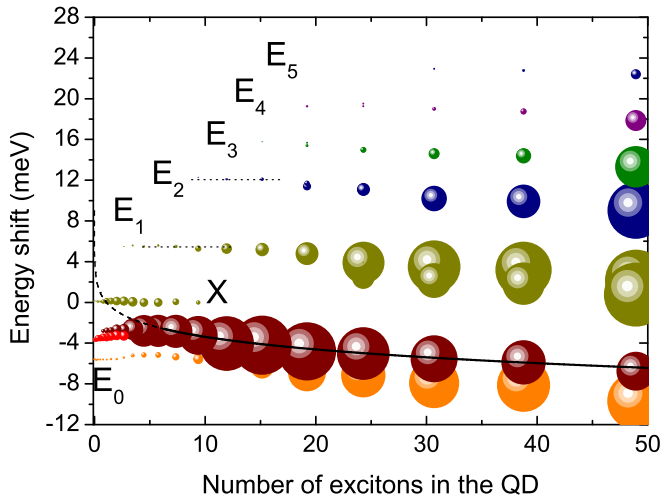

Figure 7.6: *Emission energy shift with increasing number of carriers in the quantum dot. The results for the quantum dot that emission is illustrated in Fig.7.2a) are presented. The excitation intensity is evaluated for the number of carriers in the dot as described in the text and illustrated in Fig.7.7. The solid line corresponds to the energy shift evaluated from model of band gap renormalisation. As the model is valid only for high excitations, the doted line represents the evaluation in low density regime.*

Many theoretical discussions have been given to describe the properties of a three dimensional electron-hole liquid in semiconductors [8, 9, 10]. In general, the effect of exchange-correlation energy is shown to be independent on different band characteristic of semiconductors and is driven mainly by the number of carriers in the system. The carrier density ν can be characterized by the dimensionless parameter r_s, the radius of the sphere whose volume is equal to the inverse density measured in units of the Bohr radius of an exciton a_B:

$$\frac{4}{3}\pi r_s^3 a_B^3 = \frac{1}{\nu} \tag{7.1}$$

To estimate the effective ground state emission energy shift in a quantum dot the T=0 simple function from Ref.[9] for a bulk material was directly applied. In the units of Ry:

$$\varepsilon_{exc}(r_s) = \frac{a + br_s}{c + dr_s + r_s^2} \tag{7.2}$$

where a=-4.83, b=-5.09, c=0.015, and d=3.0426 with the parameters for GaAs taken from Ref.[11]: effective Bohr radius for the exciton a_B^*=146$\mathring{A}$ and the effective Rydberg : R_y^*=3.9meV.

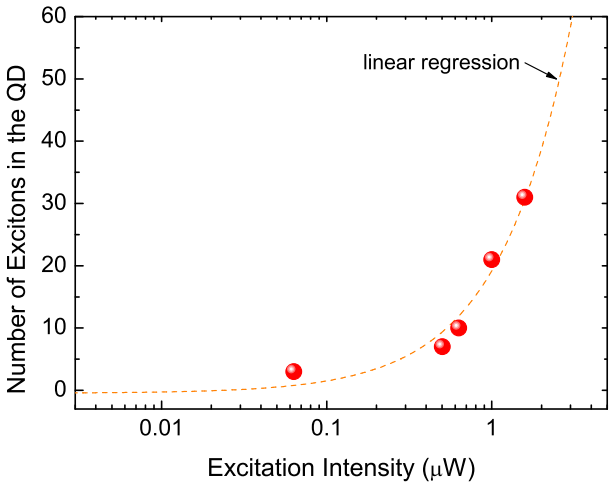

Figure 7.7: *The changes of number of excitons in the dot with increased excitation intensity evaluated for the quantum dot from Fig.7.2a).*

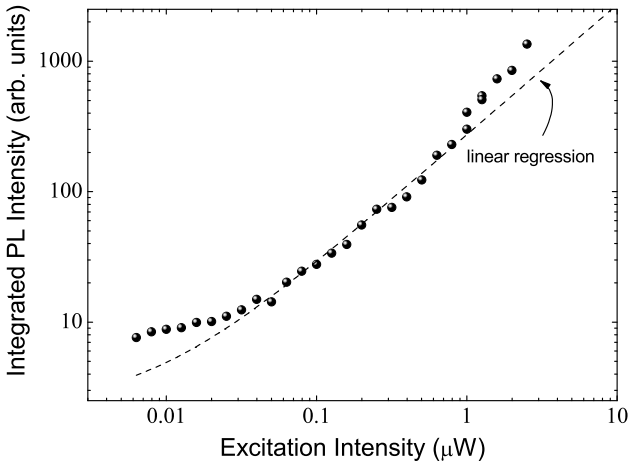

Figure 7.8: *Integrated PL intensity of the quantum dot that emission is shown in Fig.7.2a) for different excitation powers.*

The effective carrier density in the dot ν is calculated as the number of confined carriers, N, in a dot of radius r and the height h. It can be therefore expressed as:

$$\nu = \frac{N}{\pi r^2 h} \tag{7.3}$$

Assuming an ideal harmonic potential as the confining potential for the quantum dot, the rule that only $2(2n+1)$ particles can occupy the n^{th} level (n=0,1,2,...) has to be satisfied (compare with chapter 2 section 2.1.2). As n increases the carriers occupy the energy levels of different diameter r. This is schematically illustrated in Fig.7.7. The relation $r = r(N)$ is obtained from the set of equations:

$$\hbar\omega_{e-h}(n + \frac{1}{2}) = \frac{1}{2}\omega_{e-h}^2 m^* r^2 \tag{7.4}$$

$$N = n^2 + 3n + 2 \tag{7.5}$$

where n, the number of degenerate energy levels, is assumed in further calculations to be continuous for simplicity.

The curve in Fig.7.6 shows the results of calculations for $\hbar\omega_{e-h}$=6meV and the exciton binding energy of 10meV, what gives a very good qualitative agreement especially for high carrier concentrations where the simple formula gives a better approximation. The obtained value for the exciton binding energy is reasonable, although slightly lower than that evaluated in 6.3.5.

The evaluation of the excitation intensity for the number of carriers in the dot is approximate in this case. It is assumed that, at the excitation power when the first excited state emission is visible in the spectra, the occupation of the quantum dot is of approx. three excitons. Similarly for higher states, i.e. when the emission from the second excited state is visible, at least eight excitons must be confined in the dot, and so on. The resulting values for the quantum dot whose emission is illustrated in Fig.7.2a) are shown in Fig.7.7. The number of excitons in the quantum dot is assumed to linearly increase with the excitation power. This is in general a good assumption as the PL intensity from a single dot also changes linearly with the excitation intensity, what is illustrated in Fig.7.8.

A similar evolution of the energy shift is obtained when applying direct calculations for quantum dots as described in Ref.[1].

With the increase of the number of carriers in a quantum dot the emission energy shifts towards lower energies. This tendency is especially well visible for the ground state emission and can be very well approximated by the model of band-gap renormalisation including exchange and correlation effects. The exciton binding energy can be evaluated from the model and is around 10meV.

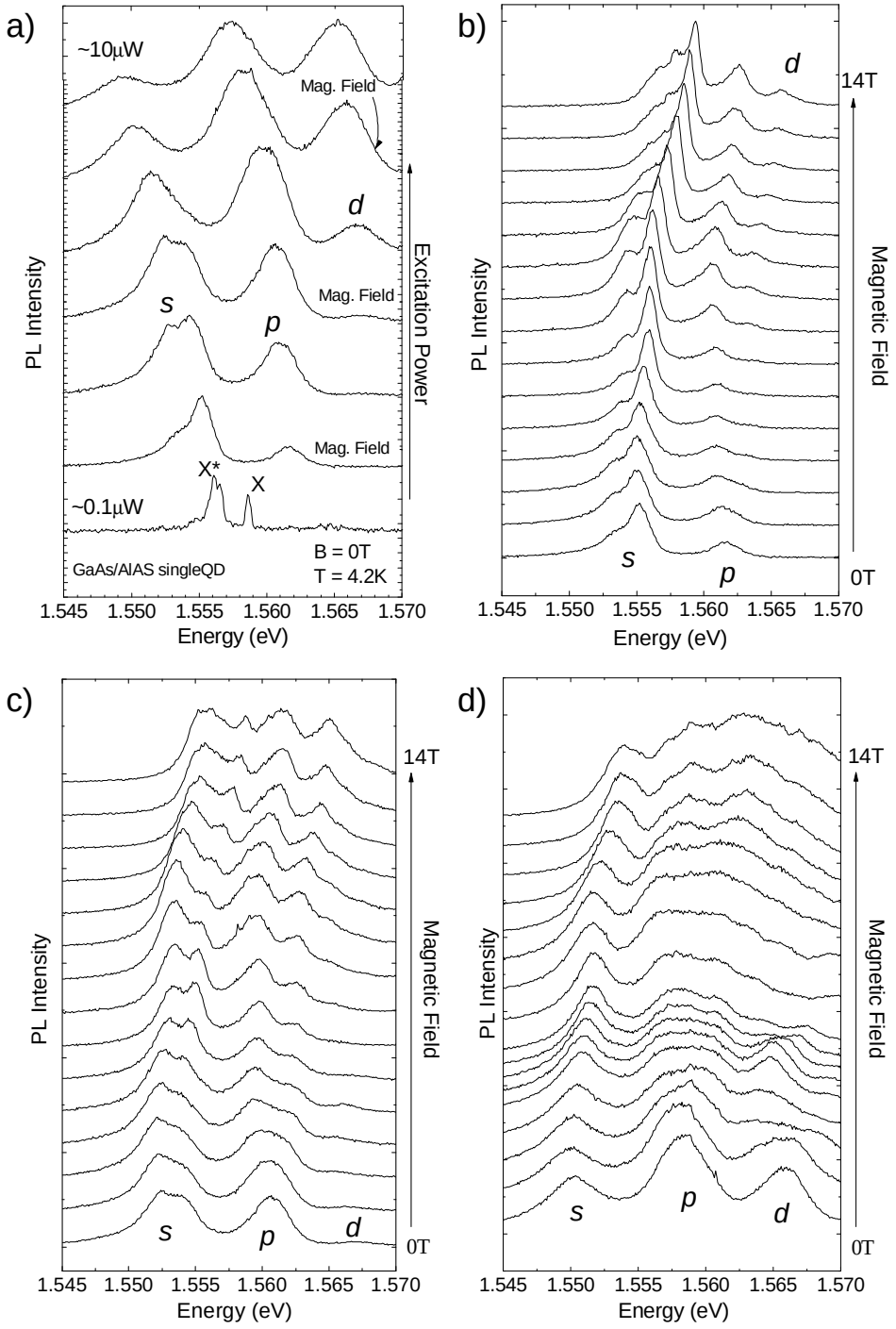

Figure 7.9: *a) Excitation power dependence of the emission from a single quantum dot. The excitation power at which magnetic field was applied is marked in the figure and corresponding magneto-μ-PL spectra are illustrated in b) - d).*

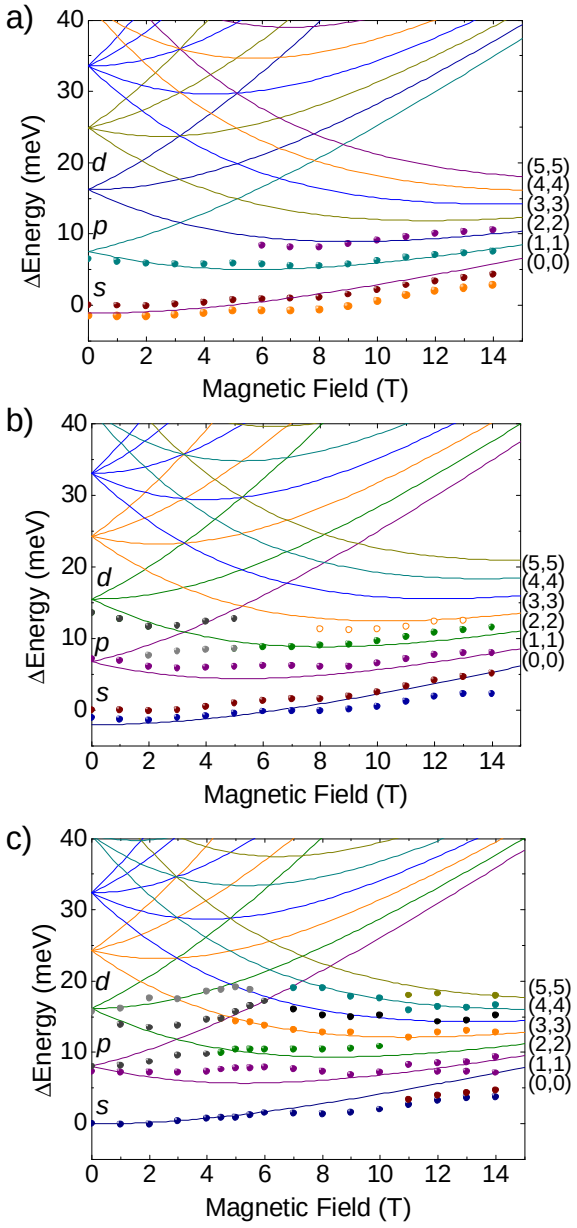

Figure 7.10: *Fan-chart diagrams of the emission energy shifts with respect to the ground state emission at B=0T for three different excitation powers a), b) and c). The corresponding spectra are illustrated in Fig.7.9 b) - d), respectively. The Fock - Darwin energy level evolution was fitted according to eq.7.6.*

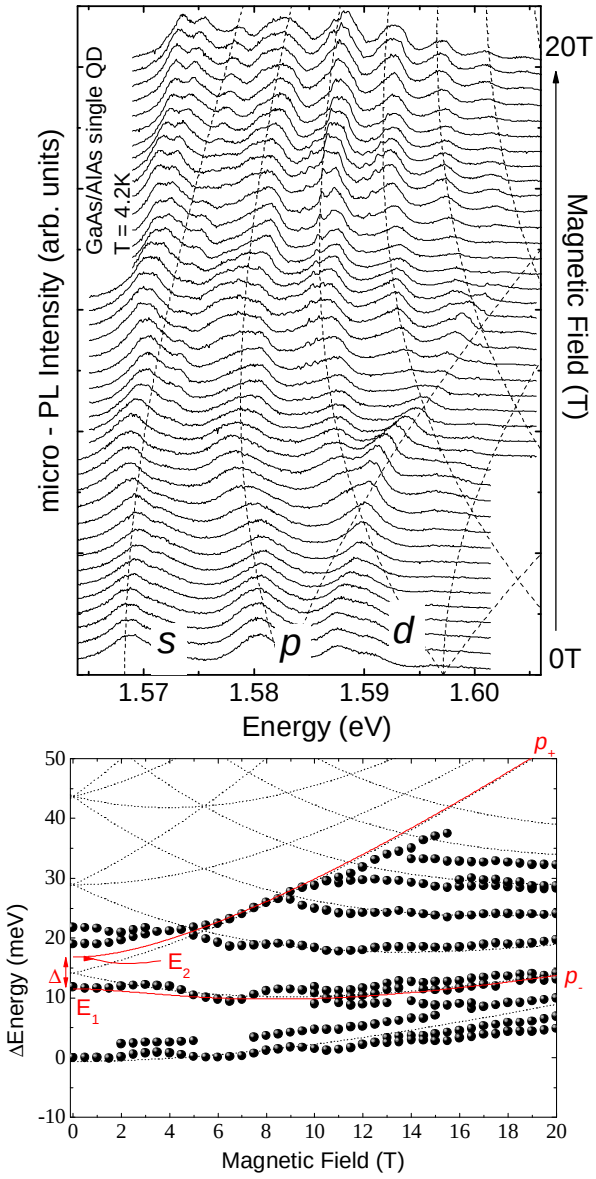

Figure 7.11: *Magneto-μ-Pl spectra of single quantum dot with corresponding fan-chart diagrams of the emission energy shifts with respect to the ground state emission at B=0T. The Fock - Darwin energy level evolution (dotted lines) was fitted according to eq.7.6 with* m^**=0.058*m_0 *and* $\hbar\omega_{e-h}$*=16meV. Red lines illustrate the interactions of* p_- *and* p_+ *levels calculated by eq.7.8 with* Δ*=2.66meV.*

7.3 Confining magnetic field - Fock-Darwin diagram

The application of a magnetic field in the direction perpendicular to the growth direction leads to distinct effects in the energy structures of the quantum dots. When the emission from the quantum dot is determined by X, X* and XX resonances, a Zeeman splitting of the emission lines is observed and the energy shift can be successfully described by the typical diamagnetic shift model (see chapter 6.3.2 and 2.3.1). However, at high excitation powers, when the emission from the ground state and a number of higher excited states is visible, a splitting of the excited states is expected to follow the Fock - Darwin diagram (see chapter 2.3.2).

The excitation power evolution of the emission spectra from a single quantum dot is plotted in Fig.7.9. The results are illustrated for a typical quantum dot. The characteristic energy $\hbar\omega_0$=8meV and the dot has three bound states.

A magneto-μ-PL experiment was performed in the setup illustrated and described in section 4.3.4.

Fig.7.10 illustrates spectra in a magnetic field of the excited energy levels of the quantum dot. Spectra taken for three different excitation powers are illustrated: a) lower excitation power, b) intermediate excitation power, and c) very high excitation power, when excited states emission is visible, as it is marked in Fig.7.9.

For all spectra the energy shift with respect to ground state emission at zero magnetic field is presented in the fan chart diagram below the spectra. The solid curves represent fitted Fock - Darwin energy levels according to equation (compare with eq.2.18 expression in chap.2.3.2):

$$\epsilon'(n,m) = E_0 + \hbar\Omega(n+1) - \frac{1}{2}\hbar\omega_c m \tag{7.6}$$

$$\Omega^2 = \omega_0^2 + \frac{1}{4}\omega_c^2 \tag{7.7}$$

The effective mass - $m*$, the characteristic energy $\hbar\omega_0$ and the relative energy E_0 are fitting parameters in this case. E_0 is the experimental parameter used to shift the whole Fock - Darwin fan chart along the energy scale to set $\epsilon'(0,0) = 0$. In general: E_0-$\hbar\omega_0 \approx 0$.

The Fock - Darwin fan chart illustrated in Fig.7.10 is fitted with slightly different parameters, however, the average values are m^*=0.06m_0, very close to the electron-hole reduced effective mass in GaAs, and $\hbar\omega_{e-h}$=8meV.

The excitonic effects are included in the picture that the same Fock - Darwin fan chart is considered for electrons and for holes. The sum of the two behaviors gives the excitonic Fock - Darwin diagram. Thus, the value $\hbar\omega_{e-h}$=8meV is in a first approximation the sum of electron $\hbar\omega_e$ and hole $\hbar\omega_h$ characteristic energies. If the electron and hole model is fitted separately, the resulting values for the quantum dot illustrated in Fig.7.10 are $\hbar\omega_e$=7meV and $\hbar\omega_h$=1meV. This qualitatively gives

a good estimation of the respective electron and hole energies, which, according to the results, have a ratio of approx. 87% - 13%, what is a reasonable value. This proportionality and the resulting shape of the electron and hole potential for this particular quantum dot are illustrated in Fig.2.4.

The first and very important conclusion that can be drawn from the pictures is that the energy shift in magnetic field of the excited states of a quantum dot can be reasonably well reproduce by the Fock-Darwin model. This effect is very well seen especially at high magnetic field, where in each case all emissions are observed from the states of (n, n) symmetry and start to form the first Landau level type band. This is the general effect for all quantum dots investigated in a magnetic field. Fig.7.11 illustrates the magnetic field evolution of the excited energy levels for another quantum dot, for comparison. The magnetic field seems to order the system, so at high magnetic field the levels of one type are populated as it was discussed in chapter 2.3.2.

Fig.7.11 also illustrates, that the Fock - Darwin model (dotted lines) is not sufficient to described the splitting of the p shell at zero magnetic field for this particular dot, as according to the model, the p states are in this case degenerate. The p_- - (1,1) state, and p_+ - (1,-1) state, are mixed as a result of the asymmetry of the lateral potential and electron-electron interactions. In general, the interaction of p_- and p_+ states can be described by simple perturbation theory. The energy evolution in a magnetic field can be expressed as:

$$E_{1,2} = \frac{E_+ + E_-}{2} \pm \sqrt{(\frac{E_+ - E_-}{2})^2 + \Delta^2} \tag{7.8}$$

where E_- and E_+ are the energies of p_- and p_+ levels, respectively, and are expressed by the Fock - Darwin model according to eq.7.6. Red solid lines in Fig.7.11 illustrate the $E_{1,2}$ energy evolution in a magnetic field with a zero field splitting, Δ, of 2.66meV, what is a similar value to those evaluated in section 7.1. In comparison to Fig.2.2, Δ is mostly determined by the quantum dot elongation.

When the three pictures taken for the same quantum dot and different excitation powers (Fg.7.10) are compared it may be seen that there are some deviations from the model, especially at high excitation powers.

Starting from the lowest excitations, when the first excited state is populated (Fig.7.10a), the evolution of the (1,1) and (2,2) states follows the experimental behavior very well.

In the excitation regime, where the carriers start to occupy the second excited state at zero magnetic field (Fig.7.10), it is observed that with the increase of magnetic field the highest occupied level is of (2,2) symmetry up to ∼3T. Then the situation seems to change and the (1,-1) level takes the role of the highest populated level. Above approx. 5.5T - 6T the (3,3) state is the highest occupied level. This effect resembles the typical evolution of Fermi energy at Landau Levels. As both, the two-dimensional electron gas and quantum dot have degenerate energy levels in a magnetic field, the oscillatory behavior of the Fermi energy is the same type of effect in both cases.

Although, as for the valence states, the energy seems to agree with the model quite well, small deviations from the Fock - Darwin evolution of lower lying states with completely filled shells are observed. This effect is very well visible at higher excitation powers (compare with Fig.7.10c). The first excited state no longer matches the presumed evolution and its emission energy is slightly higher than the theory would expect.

7.3.1 Conclusions from the Fock - Darwin model

The Fock - Darwin energy levels are the simplest solution of the problem of carriers confined in an ideal, parabolic confining potential in a magnetic field. Moreover, the important statement is that the system is composed of ensembles of non - interacting carriers. The model can, however, be applied in the case of highly excited quantum dot with some limitations.

First, it was concluded from Fig.7.10, that the interactions between the carriers become important at completely filled discrete energy levels, while at partially filled level the carriers seem to behave as a non-interacting system. The carriers on valence levels form a kind of independent system with motion determined by a mean potential of the surroundings and the levels below. Thus, with the increased occupation of higher excited levels the rearrangement of lower lying levels (completely filled) is evidently expected, what is indeed observed. Therefore, apart from the inter level carrier interaction (as it was discussed in section 7.1.2), the effects of interactions of carriers in the same shell are well visible when the shell is fully populated.

Second, one can conclude that the parabolic potential is a relatively good approximation of the confining potential in the system in question. The characteristic feature of the ideal parabolic potential is that the emission energy does not depend of the number of interacting carriers. Thus, the slight disagreement observed in the experiment, particularly under high excitations, may be the result of deviation from the parabolic potential. However, the valence band holes, where we can expect strong interaction between the bands of different orbital momentum, can influence the situation. The same concerns other additional interactions (for example spin - orbit interactions [12] that the effect is increasing with the number of carriers) that can occur in the system.

Generally speaking, with a lack of strong inter-particle interactions the Fock - Darwin picture is not so far from the situation that we are dealing in the structure. However, under very strong excitation power the spectra become more complicated, additional transitions are observed and almost no correlations with the Fock - Darwin model are observed.

The magnetic field evolution of excited energy levels in a single quantum dot can be understood in terms of the Fock - Darwin energy diagram. The effects of strong intra-shell carrier interactions on excited states are observed for completely populated, closed shells. At the same

time, almost perfect agreement with the Fock - Darvon model was found for the valence shells, suggesting very weak interactions between carriers confined on open shells.

Bibliography

[1] S. V. Nair and Y. Masumoto, "Culomb effects in the optical spectra of highly excited semiconductor quantum dots," *Journal of Luminescence*, vol. 87, p. 438, 2000.

[2] A. Wojs, P. Hawrylak, S. Fafard, and L. Jacak, "Theory of the luminescence from highly excited self-assembled quantum dots," *Physica E*, vol. 2, p. 603, 1998.

[3] P. Hawrylak and M. Korkusiński, "Electronic and optical properties of self-assembled quantum dots" in "Single quantum dots: Fundamentals, applications, and new concepts.," *P.Michler, Editor, Topics in Applied Physics, Springer-Verlag*, vol. 90, p. 25, 2003.

[4] M. Bayer, O. Stern, P. Hawrylak, S. Fafard, and A. Forchel, "Hidden symetries in the energy levels of excitonic 'artificial atoms'," *Nature*, vol. 405, p. 923, 2000.

[5] A. Wojs and P. Hawrylak, "Exciton-exciotn interaction in highly excited quantum dots in a magnetic field," *Solid State Communications*, vol. 100, p. 487, 1996.

[6] R. Heitz, F. Guffarth, I. Mukhametzhanov, M. Grundmann, A. Madhukar, and D. Bimberg, "Many-body effects on the optical spectra of InAs/GaAs quantum dots," *Phys. Rev. B*, vol. 62, p. 16881, 2000.

[7] L. Landin, M. S. Miller, M.-E. Pistol, C. E. Pryor, and L. Samuelson, "Optical studies of individual InAs quantum dots in GaAs: Few-particle effects," *Science*, vol. 280, p. 262, 1998.

[8] W. F. Brinkman and T. M. Rice, "Electron-hole liquids in semiconductors," *Phys. Rev. B*, vol. 7, p. 1508, 1973.

[9] P. Vashishta and R. K. Kalia, "Universal behavior of exchange-correlation energy in electron-hole liquid," *Phys. Rev. B*, vol. 25, p. 6492, 1982.

[10] O. Gunnarsson and B. I. Lundqvist, "Exchange and correlation in atoms, molecules, and solids by spin-density-functional formalism," *Phys. Rev. B*, vol. 13, p. 4274, 1976.

[11] M. Capizzi, S. Modesti, A. Frova, J. L. Staehli, M. Guzzi, and R. A. Logan, "Electron-hole plasma in direct-gap $Ga_{1-x}Al_xAs$ and k-selection rule," *Phys. Rev. B*, vol. 29, p. 2028, 1984.

[12] P. Pietiläinen and T. Chakraborty, "Energy levels and magneto-optical transitions in parabolic quantum dots with spin-orbit coupling," *Phys. Rev. B*, vol. 73, p. 155315, 2006.

Chapter 8

Effects of Temperature

Ce chapitre est consacré à l'étude de l'émission d'une boîte quantique unique en fonction de la température (de l'hélium liquide à une température d'environ 140 K). L'influence de la température permet d'observer les effets des processus non radiatifs activés thermiquement et permet ainsi de discuter les propriétés des matériaux constituant les boîtes quantiques en déterminant les évolutions de la bandes interdite en fonction de la température. Les mécanismes responsables des variations de l'intensité, de l'énergie d'émission et de l'élargissement des lignes d'émissions sont analysés. En particulier, nous discutons l'interaction entre un exciton confiné et les phonons acoustiques de faible énergie. Ce couplage, si présent, apparaît sous la forme d'une raie non Lorentzienne bien spécifique.

Studies of the effects induced by temperature in single excitons and exciton complexes give important information about the interplay between radiative and non-radiative processes and the role of electron-phonon interactions [1, 2, 3, 4, 5]. The strong localization of carriers in a quantum dot material allows for a direct and precise probing of the dot matrix and surrounding disorder and thus a determination of the temperature shift of the band-gap and carrier thermal activation energy.

The following chapter illustrates the effects of increasing the temperature, above that of liquid helium, on single exciton and exciton complex emission from GaAs/AlAs single quantum dots.

The experimental results are illustrated in the first part, 8.2. The spectra of single quantum dots taken for different temperatures and with various excitation powers are shown. The main temperature effects on exciton-complexes emission are pointed out.

The effects of emission energy shift, thermal line broadening and change of PL intensity are discussed in the subsequent chapters, 8.2, 8.4 and 8.3, respectively.

The experiment was performed in the setup described in chapter 4.3.1.

8.1 General description of the temperature dependence of the emission spectra

The temperature evolution of several quantum dot emission spectra are illustrated in Fig.8.1 a) - d). The spectra are taken at an excitation power close to the limit of exciton emission intensity saturation, to observe only sharp emission from the *s*-shell.

Several major effects are observed in the spectra with temperature increasing:

- The energy of all emission lines shifts to the red. This effect is discussed in section 8.2 in terms of semiconductor band-gap shrinkage.
- The total emission intensity decreases and the emission lines are not visible at very high temperatures above approx. 120K, due to temperature activated nonradiative processes. For some emission lines (for example X) a recovery at a certain temperature is observed before the emission is quenched. This effect is discussed in section 8.3.
- A successive disappearance of the emission lines is observed. First it is the trion emission line. The X* peaks disappear very quickly with increasing temperature. This effect was also observed in Ref.[6]. The X emission line is visible up to relatively high temperatures, up to ∼80K.
- Surprisingly, new emission lines (XX3, XX4) appear in the lowest emission energy region, below the X* and XX1 transitions. The possible origin of these low energy lines is discussed in section 8.3.1.
- Broadening of the emission lines is hardly observed. Within the experimental resolution the width of the X line is stable up to 70K when the emission line is quenched, as discussed in section 8.4.

At higher excitation power, when the emission from more complicated excitonic complexes is observed, the temperature evolution of the spectra is very similar to that described previously and most of the effects pointed above are still visible.

Fig.8.2, Fig.8.3 and Fig.8.4 illustrates a series of results taken for the same quantum dot but excited with different excitation powers and at different temperatures.

When the excitation power is slightly increased above the saturation of the X peak (Fig.8.3 c) and d), the temperature dependence of the low energy tail is very similar to the previously observed at lower excitation powers. New emission lines appear with increasing temperature. As the emission intensity decreases, the recovery of the X emission line is observed around 70K in Fig.8.3 c).

At very high excitation powers, when the emission from the s, p and d shells is visible, the intensity of the emission lines with increasing temperature is thermally quenched and subsequently, starting from the highest occupied state, an emptying of the high energy levels is observed.

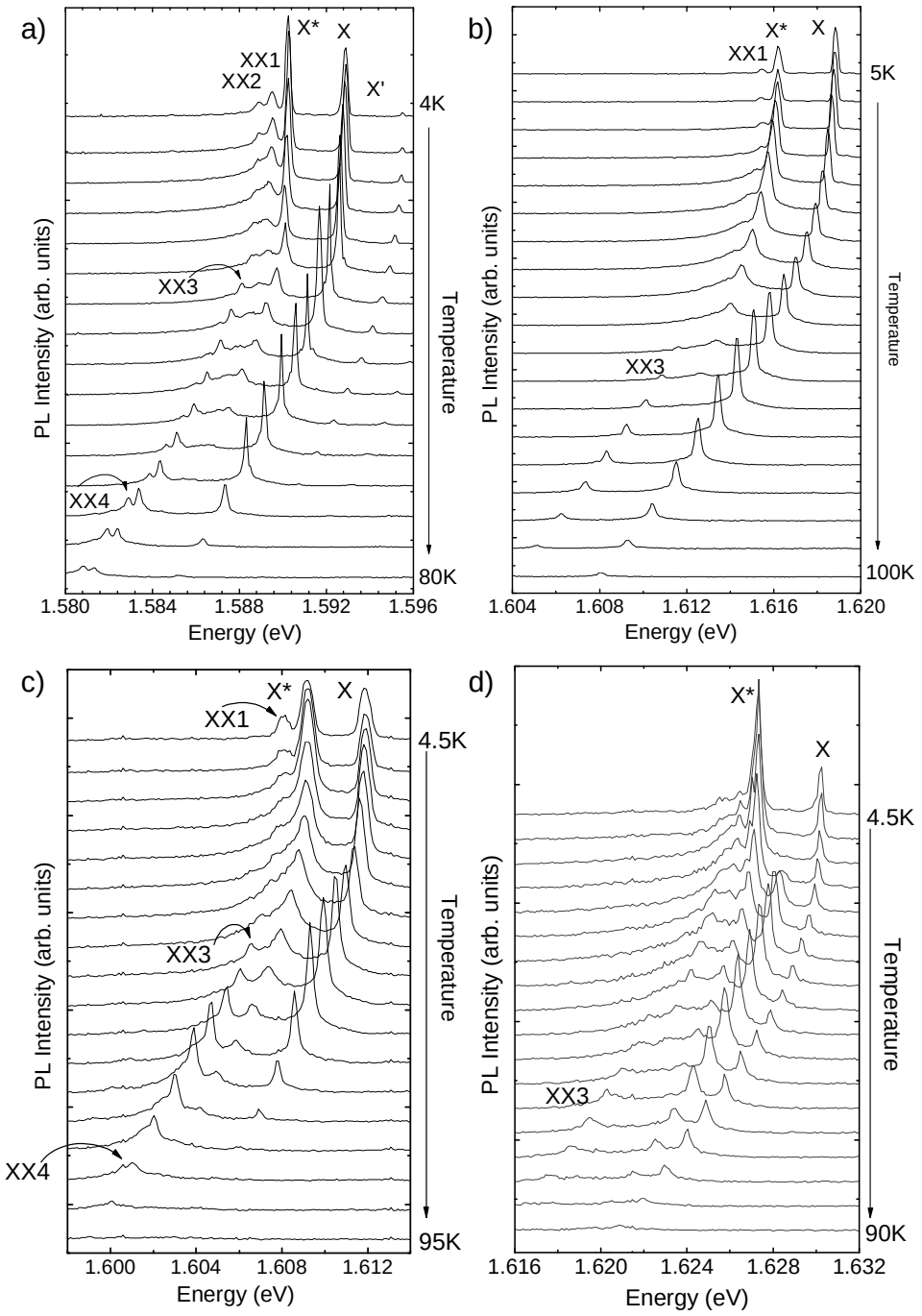

Figure 8.1: *Typical μ-PL spectra of four different quantum dots (a - d) excited with small excitation power to observe single excitonic emission lines.*

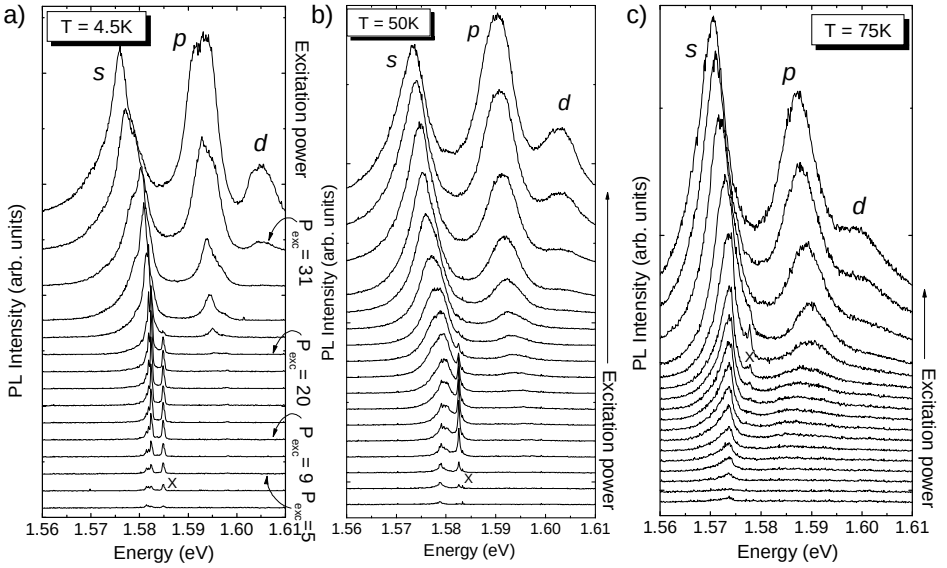

Figure 8.2: *The excitation power evolution of the emission spectra for the same quantum dot taken at temperatures a) 4.2K, b) 50K, c) 75K (in the same excitation power range). The excitation power units are arbitrary and are marked in figure a) for several spectra.*

In general, the emission intensity from all dots decreases with increasing temperature because the interactions between the confined excitons and phonons become stronger at higher temperatures, resulting in the increase of non-radiative decay of excitons. Fewer carriers are therefore trapped in the "radiative" levels of quantum dot and the resulting emission is similar to that caused by reducing the excitation power with some additional high-temperature features (energy shift, appearance of new emission lines).

The emission from single quantum dots was traced with increasing lattice temperature up to 100K, giving information about the properties of single exciton, simple exciton complexes and excited states of quantum dot. Series of excitation power dependent spectra versus temperature were shown for the same quantum dot. The effects of the temperature increase on the emission properties are: the quenching of PL intensity, emission energy shift, appearance of low energy emission lines and small line broadening effects.

8.2 Band-gap shrinkage

The band gap of a semiconductor may change because of two contributions. First, the change of lattice constants causes a change in the atomic wave-function overlap. The second contribution is caused by the electron-phonon interaction. At high temperatures both contributions lead to a linear change of the band gap energy.

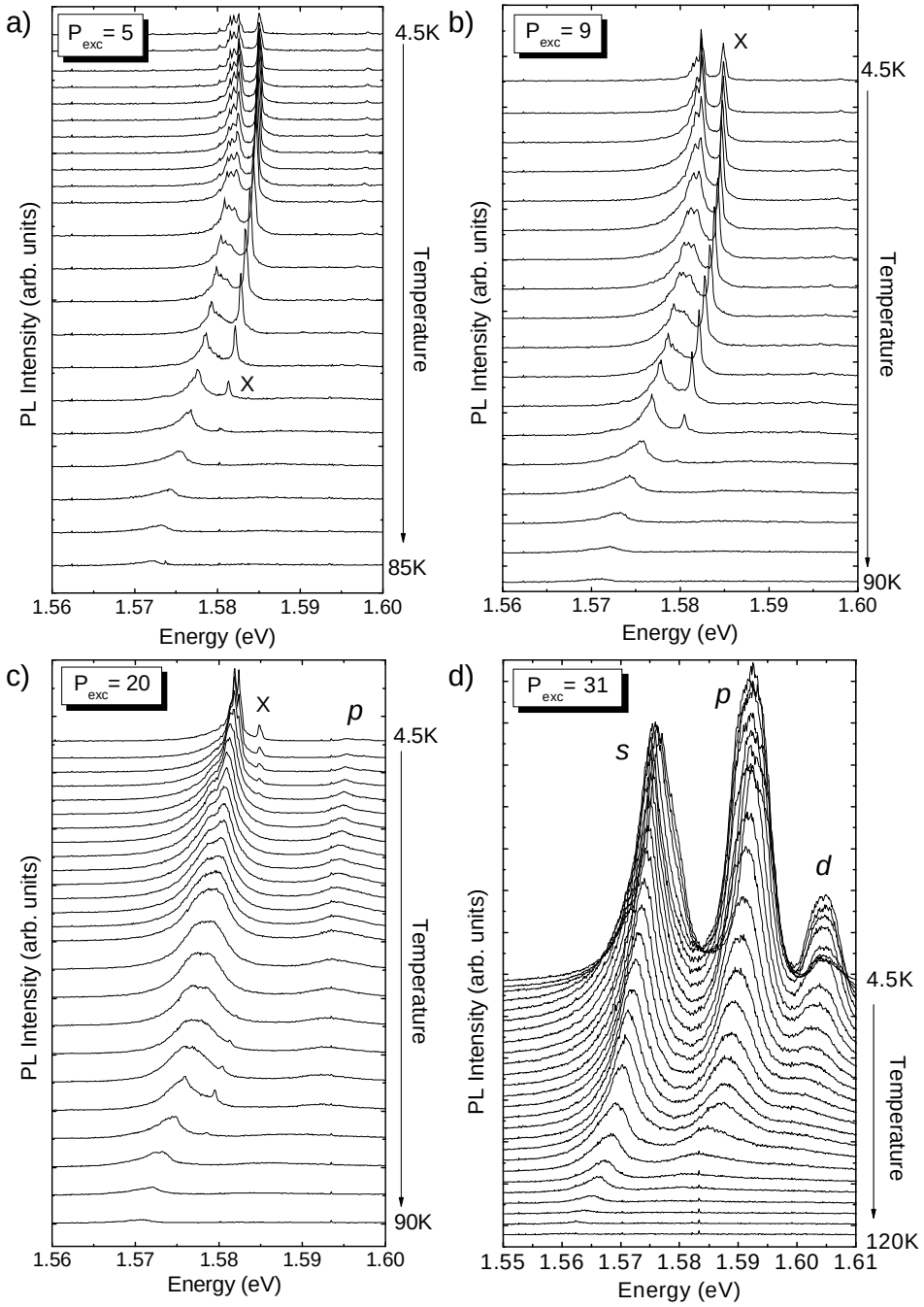

Figure 8.3: *The temperature evolution of the emission spectra for the same quantum dot taken with different excitation powers* a) $P_{exc} = 5$, b) $P_{exc} = 9$, c) $P_{exc} = 20$ *and* c) $P_{exc} = 31$. *The excitation power units are arbitrary. The spectra of corresponding excitation powers at 4.2K are illustrated in Fig.8.2.*

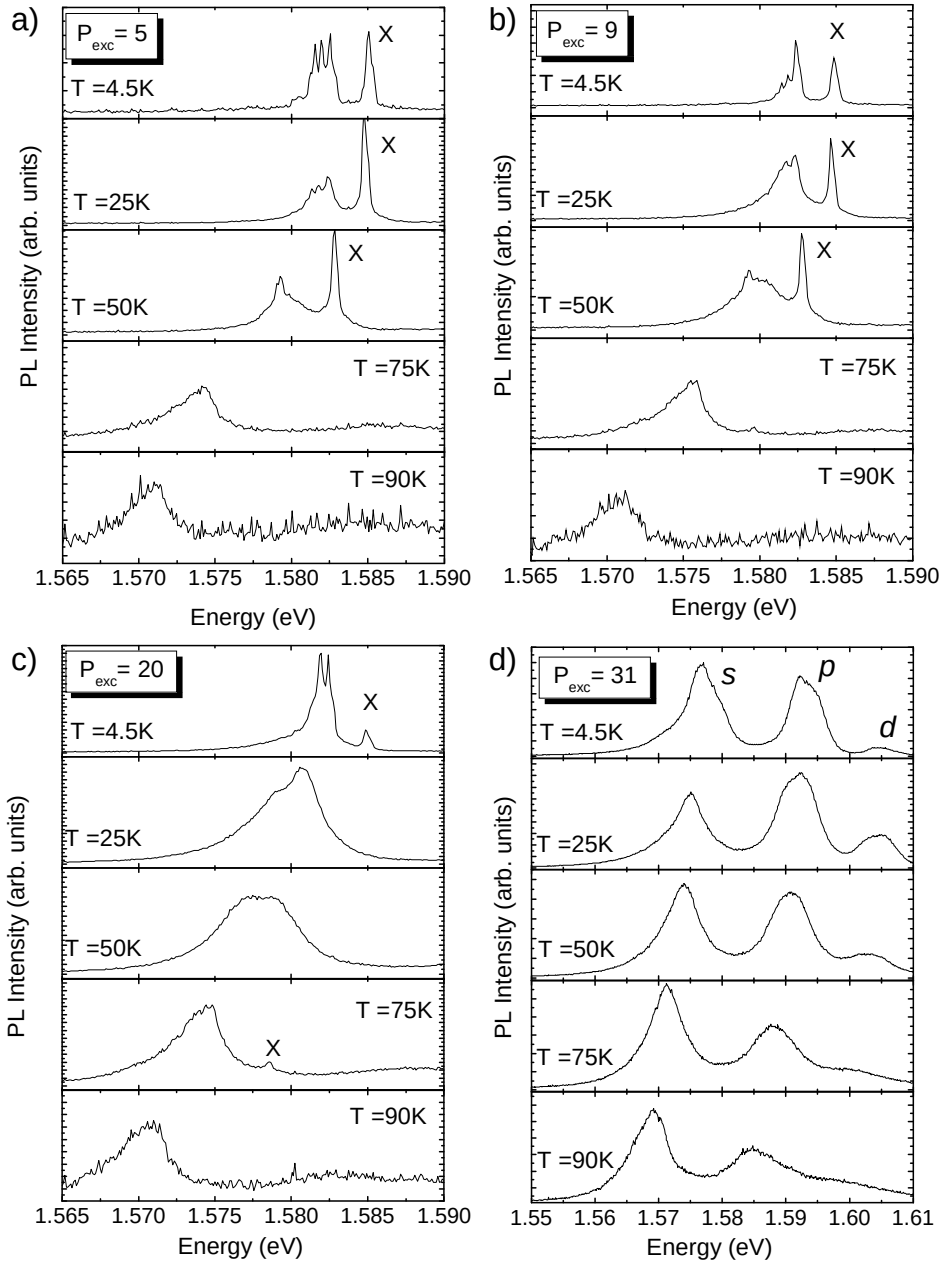

Figure 8.4: *Several corresponding spectra of the temperature evolution illustrated in Fig.8.2. The emissions in each picture are normalized in the intensity to compare the change of the line shape with increasing temperature.*

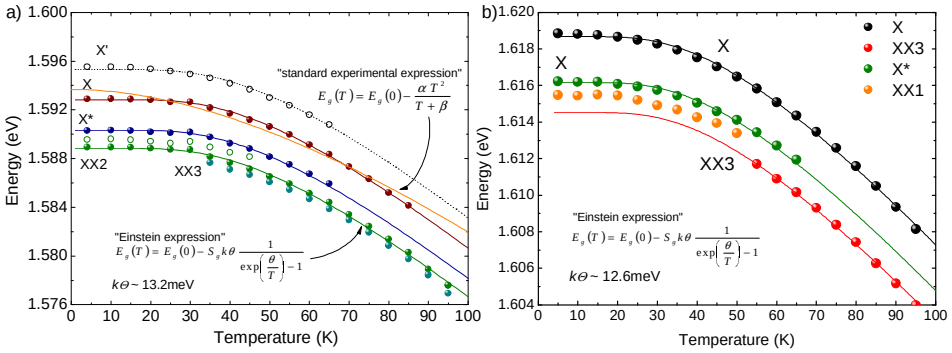

Figure 8.5: *The typical emission energy shift of single excitonic emission lines. The example of two different quantum dots a) and b) is shown. The corresponding emission spectra are presented in Fig.8.1 a) and b), respectively. The lines illustrate the fitting according to eq.8.2 and eq.8.3, as shown in the figure.*

At low temperatures the electron-phonon interaction clearly dominates.

There have been many theoretical attempts to calculate the band-gap energy shift in semiconductors [7, 8].

In general, the whole series of formulas can be traced to an expression:

$$E_g(T) = E_g(0) - \int d(\hbar\omega) f(\omega) \overline{n}(\omega, T) \tag{8.1}$$

with the electron-phonon spectral function $f(\omega)$ and the phonon occupation number $\overline{n}(\omega, T)$ (given by the Bose - Einstein distribution). The $f(\omega)$ function is not known a priori. Different expressions are given in many papers [9, 10, 11] and lead to various fitting formulas of Viña [12], O'Donnell and Chen [13] or Pässler [14, 15]. All these formulas aim at a simple description for the shift of the band gap energy over the temperature range from below liquid helium temperature to above room temperature for a whole class of semiconductors.

Among all fitting formulas there are two most widely used: the Varshni formula [9] and the so-called "Einstein expression".

The Varshni formula is often used due to its simplicity. It is expressed as:

$$E_g(T) = E_g(0) - \frac{\alpha T^2}{T + \beta} \tag{8.2}$$

where α and β are constants.

In the "Einstein expression", namely [12]:

$$E_g(T) = E_g(0) - S_g k_B \Theta \frac{1}{exp(\frac{\Theta}{T}) - 1} \tag{8.3}$$

the phonon population is calculated in the Einstein single oscillator model, where $k_B\Theta$ is an energy which describes the average phonon frequency for the lattice. S_g is a dimensionless coupling constant which describes the slope of E_g as a function of the temperature for $T \rightarrow \infty$.

In this work, eq.8.3 was used as it applies better to the experimental results, as illustrated in Fig.8.5, where both formulas are fitted to the X emission energy shift.

It is observed that the temperature evolution of all emission lines (X, X*, XX1,...) can be very well described by the "Einstein expression". Moreover the same fitting parameters are obtained for all emission lines. This confirms that all emissions are from the same dot and the electron-phonon interaction is the same in each case.

From the fits, the parameter of $k_B\Theta$ was found to vary from 12.5meV to 13.5meV from dot to dot. This corresponds to a Θ of 145K - 156K. The obtained values are slightly bigger than those in Ref.[3] for GaAs excitons localized at the interface potential fluctuations, namely 120K.

The temperature induced energy shift of the emission lines is well described by the band-gap energy shift in the Einstein model due to the change of atomic constants and electron-phonon interaction. The average phonon frequency for the lattice was evaluated at $k_B\Theta \sim$13meV.

8.3 Role of radiative and non-radiative processes

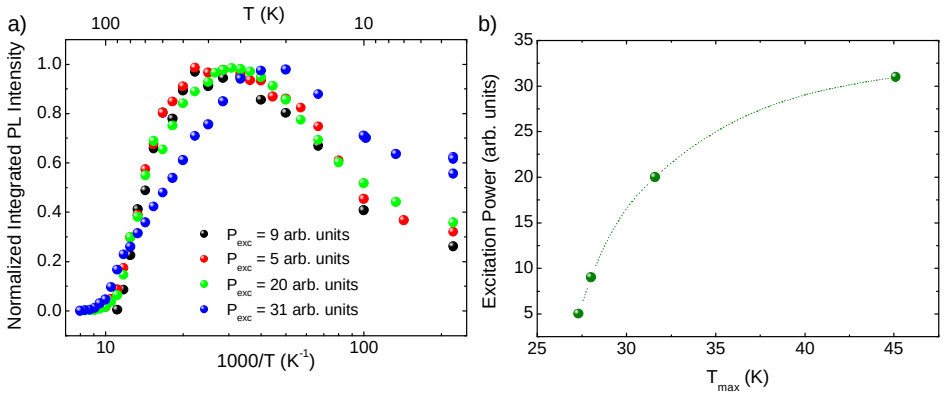

Figure 8.6: *a) Integrated μ-PL intensities from the quantum dot for which the emission spectra are illustrated in Fig.8.3 for different excitation powers. The data are normalized to highest intensities. b) The temperatures corresponding to the maximum of the intensity vs. excitation power. The dotted line is an eye-guide.*

A general feature of the emission from quantum dots with increasing temperature is that the intensity is gradually quenched. Fig.8.6a) illustrates the integrated

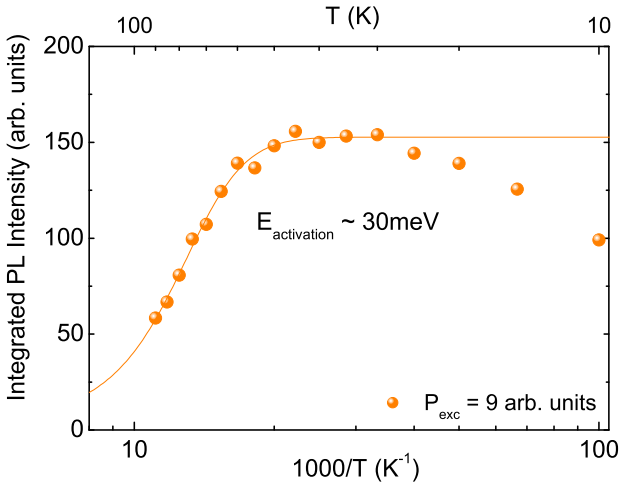

Figure 8.7: *Integrated μ-PL intensity from the quantum dot whose emission spectra are illustrated in Fig.8.3b). The solid line illustrates the fitting of eq.8.9 to the experimental points.*

μ-PL intensity changes with increasing temperature for the spectra demonstrated in Fig.8.3. The different experimental points are the results for different excitation powers for the same quantum dot. It is observed that starting from low temperatures, the emission intensity increases slightly, reaches a maximum point, and then decreases. The temperature at which the maximum PL intensity is reached depends slightly on the excitation power, as illustrated in Fig.8.6b). The higher the excitation power, the higher the temperature of the maximum PL intensity.

The quenching of the PL at high temperature is caused by the increased role of non-radiative processes. The behavior can be well reproduced assuming a thermal activation model of non-radiative processes. The carrier population in the quantum dot under above-barrier excitation is determined mainly by the concentration in the 2D quantum well system (compare with the discussion in chapter 10.3). The carrier concentration in the quantum dot n_{QD} is proportional to the carrier concentration in the 2D reservoir n_{2D}:

$$n_{QD}(T) \sim n_{2D}(T) \tag{8.4}$$

The thermal dependence of n_{2D} is determined by radiative and non-radiative processes, where the latter are assumed in the model to be thermally activated, with an activation energy E_{act}:

$$P = \frac{n_{2D}(T)}{\tau_{2D}} + n_{2D}(T)\alpha e^{\frac{-E_{act}}{k_B T}} \tag{8.5}$$

with P proportional to excitation power, τ_{2D} the radiative decay time in the quantum well, α proportionality constant, and k_B Boltzman constant.

The T=0K condition sets the emission intensity at 0K, I(0):

$$P = \frac{n_{2D}(0)}{\tau_{2D}} = I(0) \tag{8.6}$$

The temperature dependent PL intensity is given by

$$I(T) = \frac{n_{2D}(T)}{\tau_{2D}} \tag{8.7}$$

Therefore the relation 8.5 takes the form:

$$I(0) = I(T) + I(T)\tau_{2D}\alpha e^{\frac{-E_{act}}{k_B T}} \tag{8.8}$$

Rewriting eq.8.8, the emission intensity is expected to decay with temperature according to:

$$I(T) = \frac{I(0)}{1 + aexp(-E/k_B T)} \tag{8.9}$$

where $a = \tau_{2D}\alpha$ and E_{act} are temperature-independent constants.

Due to proportionality 8.4, the model expressed by eq.8.9 can be well applied to the quantum dot emission intensity changes with increasing temperature, as illustrated in Fig.8.7.

The fitted thermal activation energy varies slightly from dot to dot and is approx. 30meV. A similar model was applied in Ref.[2] for InP quantum dots, where a similar PL emission intensity behavior with the increasing temperature was observed.

The observed quenching of the total emission intensity from quantum dots with increasing temperature is due to the important role of non-radiative processes at temperatures above ∼30K. The effective carrier density in the dot is observed to decrease with increasing temperature. The changes are well reproduced by a model assuming thermal activation of non-radiative processes in the 2D system constituting of a carrier reservoir for the quantum dots.

8.3.1 Thermally activated emission

Interestingly, when the emission from a single exciton is followed with temperature it is found that its intensity is recovering at certain temperatures. This effect is well visible in the spectra in Fig.8.1. The integrated emission from X versus temperature for different quantum dots is illustrated in Fig.8.8.

This anomalous increase of the X emission intensity is interpreted as an increase of the population of the X level due to the depopulation of X* with increasing temperature. Charge fluctuations in the dot cause a fast decay of X* with increasing temperature and therefore more single excitons are captured in a certain temperature range. The X decay at high temperatures is due to the increased role of non-radiative processes that reduce the carrier population on dot levels (as described in the previous section).

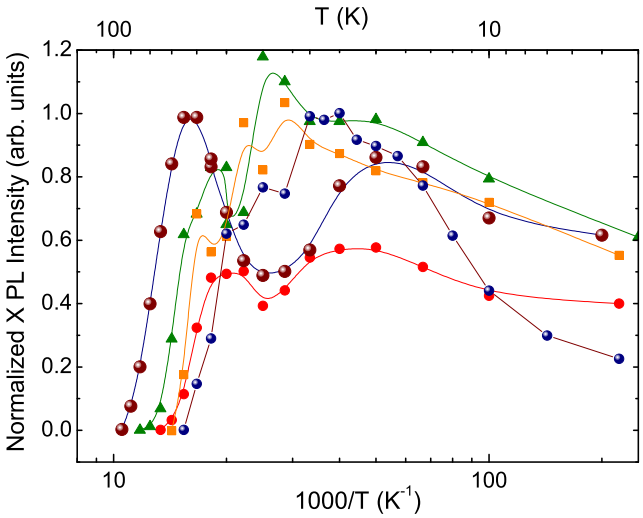

Figure 8.8: *Integrated emission intensity of the single exciton emission line, X, for several quantum dots.*

The appearance of new emission lines in the spectra with increasing temperature at low excitation power, visible in Fig.8.1 as the successive emergence of lines XX3 and XX4, is more complicated in origin. These lines are observed to be temperature activated and appear above ∼30K. A possible scenario is that this recombination involves a number of excited states in the initial and final state of the recombining carriers. A scheme of the proposed diagram is illustrated in Fig.8.9. The initial state of $N+e+h$ carriers populating the s-shell (therefore N is limited to N=0,1,2) is split due to the different carrier configurations; the same happens to the final state of N carriers. At T=4.2K the emission spectrum is composed of emission lines due to the recombination from the initial to the final ground, thermalized states (red arrow in Fig.8.9). The number of observed lines (mostly: X, X^-, X^+, XX) in this case depends on N. When the temperature is increased the carriers start to populate excited levels. Also the recombination processes to excited final states become more probable (green arrow in Fig.8.9) and, as shown by the experiential results, very active in this case. The ladder of final states must be much wider in energy than that of the initial states in order to observe such an effect. This splitting of the final states is assigned, most probably, to the hole left in the excited p-shell state after recombination, as the energy difference between hole shells is smaller (∼1meV) than that for electrons (∼7meV). Therefore, the XX3 and XX4 emissions are probably due to positively charged exciton and/or biexciton recombination in the excited states.

The photoluminescence intensity of X for different quantum dots is found to recover when the temperature is raised above a certain value. This phenomenon is interpreted as an increase in the X level population

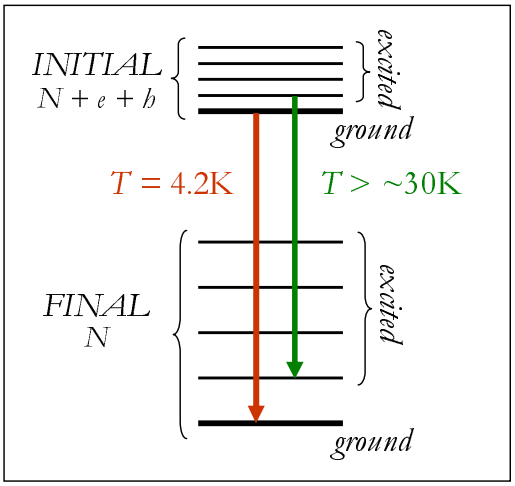

Figure 8.9: *Scheme of the proposed recombination diagram when the temperature is increased (see text for details).*

due to X* decay caused by charge fluctuations in the dot. The additional low energy emission lines, XX3 and XX4, that appear in the spectra above ~30K are most probably due to transitions leaving behind a hole in the excited state.

8.4 Line broadening effects

One major difference between the excitonic emission from a quantum dot and other systems is the origin of the broadening of the emission lines. For example, in a quantum well the broadening is due to possible non-uniformity of the interfaces and to thermal spreading. In a quantum dot, the energy levels are discrete. The temperature dependence is in this case very different, since carriers can only be thermally excited to a limited number of well-separated excited states. Thermal excitation of carriers cannot therefore broaden the states. The homogeneous broadening of the single exciton line that is observed in almost all quantum dot systems [4, 5, 16, 17, 18, 19, 20, 21, 22], is mainly due to interactions with phonons. The inelastic scattering of the exciton by acoustic phonons reduces the exciton lifetime and therefore broadens the emission line. This effect is observed as the appearance of a broad background on both sides of the central, X, emission line and the shape of the line deviates strongly from the Lorentzian with increasing temperature. This broad background is very often referred to as a phonon sideband and becomes visible at temperatures above approx. 30K.

The excitonic emission lines in the investigated system are relatively narrow, approx. 200μeV at 4.2K. Fig.8.10 a) and b) illustrates the Lorentzian fit for several X emission lines (corresponding spectra are shown in Fig.8.1a) in the whole range of investigated temperatures. It is observed that the Lorentzian shape fit very well to the experimental data. Interestingly, in the case of the investigated dot the

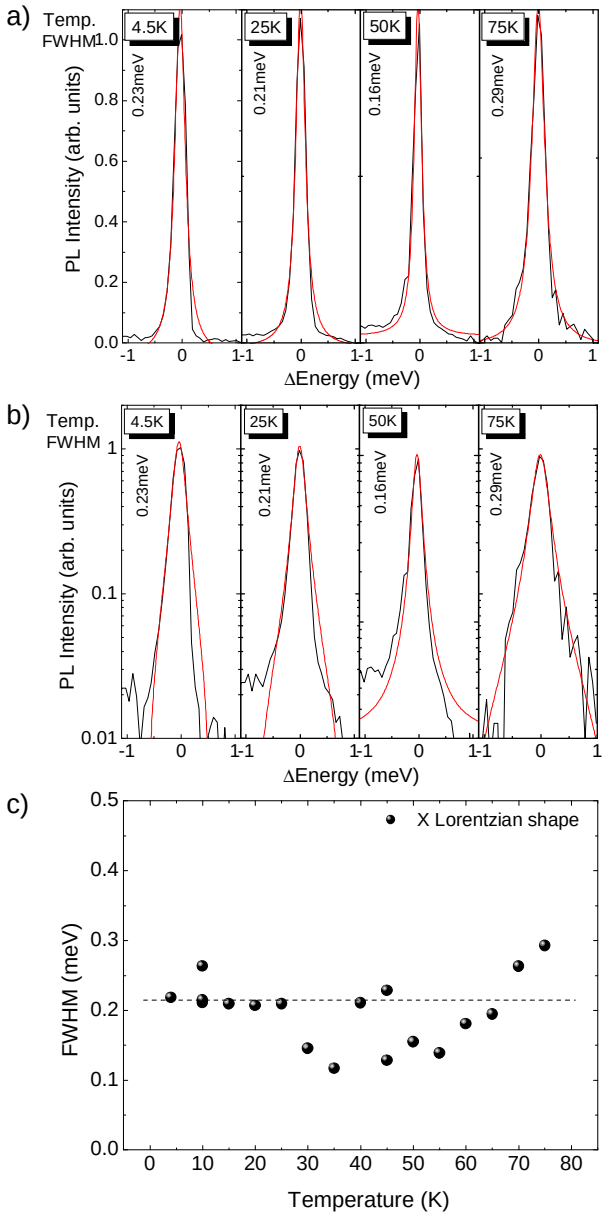

Figure 8.10: *a) Examples of a Lorentzian fit to single X emission lines at temperatures 4.2K (a), 25K (b), 50K (c) and 75K (d) for the quantum dot which emission spectrum is illustrated in Fig.8.1a). b) The same picture as a) but in logarithmic intensity scale. The good agreement of the fit with the data confirms that the emission lines are homogenously broadened. c) Resulting width (FWHM) of the X emission lines for all temperatures. The lines do not broaden significantly in the whole range of the investigated temperatures before disappearing from the spectrum.*

emission lines exhibit no significant broadening even at high temperatures, up to 70K, as illustrated in Fig.8.10c).

A similar effect is observed for the XX1 and XX3 emission lines. No broadening is observed even at high temperatures of 100K. They are, contrary to X, better fit by a Gaussian shape line. This can suggest their identification as the emission of an ensemble of excitons and/or more complicated excitonic state recombination (leaving the residual carriers in an excited state).

The lack of broadening, typical for other quantum dots, shows that in the case of the investigated quantum dots the system is very insensitive to inelastic scattering by phonons. This can be due to the absence of appropriate states between the dot discrete energy levels (bottleneck effect).

However, if looking carefully for the phonon-sidebands in X emission line at high temperatures it can be found that for some quantum dots the effect is indeed visible at high temperatures. Fig.8.11 illustrates the Lorentzian fit of the X emission line for the quantum dot whose emission spectrum is illustrated in Fig.8.1b). The phonon-sidebands are observed to appear in the spectra at temperatures as high as 75K. In this case also a broadening of the emission line is observed from 0.2meV at 4.K up to 0.5meV at 95K.

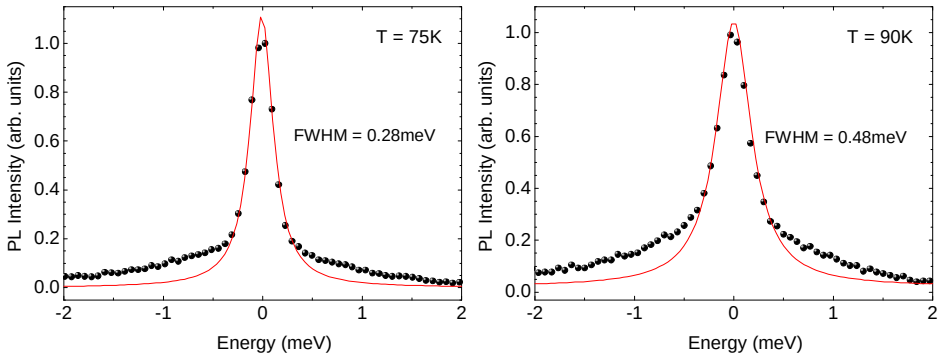

Figure 8.11: *Examples of a Lorentzian fit to a single X emission line at temperatures 75K (left panel) and 90K (right panel) for the quantum dot which emission spectrum is illustrated in Fig.8.1b). Dots: experimental data; solid line: Lorentzian fit.*

The thermal broadening of the X emission line is hardly observed up to a temperature of 70K. This can be due to weak interaction of electrons with acoustic phonons in the case of the investigated quantum dots.

Bibliography

[1] P. Michler(Ed.), "Single quantum dots. Fundamentals, applications and new concepts," *Topics in Applied Physics, Springer*, vol. 60, 2003.

[2] M. Sugisaki, H.-W. Ren, K. Nish, and Y. Masumoto, "Optical properties of InP self-assembled quantum dots studied by imaging and single dot spectroscopy," *Jpn. J. Appl. Phys.*, vol. 41, p. 958, 2002.

[3] D. Lüerssen, R. Bleher, and H. Kalt, "High-precision determination of the temperature-dependent band-gap shrinkage due to the electron-phonon interaction in GaAs," *Phys. Rev. B*, vol. 61, p. 15812, 2000.

[4] L. Besombes, K. Kheng, L. Marsal, and H. Mariette, "Acoustic phonon broadening mechanism in single quantum dot emission," *Phys. Rev. B*, vol. 63, p. 155307, 2001.

[5] I. Favero, G. Cassabois, R. Ferreira, D. Darson, C. Voisin, J. Tignon, C. Delalande, G. Bastard, P. Roussignol, and J. M. Gérard, "Acoustic phonon sidebands in the emission line of single InAs/GaAs quantum dots," *Phys. Rev. B*, vol. 68, p. 233301, 2003.

[6] J. G. Tischler, A. S. Bracker, D. Gammon, and D. Park, "Fine structure of trions and excitons in single GaAs quantum dots," *Phys. Rev. B*, vol. 66, p. 081310, 2002.

[7] P. B. Allen and M. Cardona, "Theory of the temperature dependence of the direct gap of germanium," *Phys. Rev. B*, vol. 23, p. 1495, 1981.

[8] S. Biernacki, U. Scherz, and B. K. Meyer, "Temperature dependence of optical transitions between electronic energy levels in semiconductors," *Phys. Rev. B*, vol. 49, p. 4501, 1994.

[9] Y. Varshni, "Temperature dependence of the energy gap in semiconductors," *Physica (Amsterdam)*, vol. 34, p. 149, 1967.

[10] S. Gopalan, P. Lautenschlager, and M. Cardona, "Temperature dependence of the shifts and broadenings of the critical points in GaAs," *Phys. Rev. B*, vol. 35, p. 5577, 1986.

[11] N. Garro, A. Cantarero, M. Cardona, A. Göbel, T. Ruf, and K. Eberl, "Dependence of the lattice parameters and the energy gap of zinc-blende-type semiconductors on isotopic masses," *Phys. Rev. B*, vol. 54, p. 4732, 1996.

[12] L. Vina, S. Logothetidis, and M. Cardona, "Temperature dependence of the dielectric function of germanium," *Phys. Rev. B*, vol. 30, p. 1970, 1984.

[13] K. P. O'Donnell and X. Chen, "Temperature dependence of semiconductor band gaps," *Appl. Phys. Lett.*, vol. 58, p. 2924, 1991.

[14] R. Pässler, "Basic model relations for temperature dependencies of fundamental energy gaps in semiconductors," *phys. stat. sol. b*, vol. 200, p. 155, 1997.

[15] R. Pässler, "Temperature dependence of exciton peak energies in multiple quantum wells," *J. Appl. Phys.*, vol. 83, p. 3356, 1998.

[16] E. Peter, J. Hours, P. Senellart, A. Vasanelli, A. Cavanna, J. Bloch, and J. M. Gérard, "Phonon sidebands in exciton and biexciton emission from single GaAs quantum dots," *Phys. Rev. B*, vol. 69, p. 041307, 2004.

[17] P. Borri, W. Langbein, S. Schneider, U. Woggon, R. L. Sellin, D. Ouyang, and D. Bimberg, "Ultralong dephasing time in InGaAs quantum dots," *Phys. Rev. Lett.*, vol. 87, p. 157401, 2006.

[18] K. Matsuda, K. Ikeda, T. Saiki, H. Tsuchiya, H. Saito, and K. Nishi, "Homogeneous linewidth broadening in a $In_{0.5}Ga_{0.5}As$/GaAs single quantum dot at room temperature investigated using a highly sensitive near-field scanning optical microscope," *Phys. Rev. B*, vol. 63, p. 121304, 2001.

[19] C. Kammerer, G. Cassabois, C. Voisin, C. Delalande, P. Roussignol, A. Lemaitre, and J. M. Gérard, "Efficient acoustic phonon broadening in single self-assembled InAs/GaAs quantum dots," *Phys. Rev. B*, vol. 65, p. 033313, 2001.

[20] S. Sanguinetti, E. Poliani, M. Bonfanti, M. Guzzi, E. Grilli, M. Gurioli, and N. Koguchi, "Electron-phonon interaction in individual strain-free GaAs/$Al_{0.3}Ga_{0.7}As$ quantum dots," *Phys. Rev. B*, vol. 73, p. 125342, 2006.

[21] M. Bayer and A. Forchel, "Temperature dependence of the exciton homogeneous linewidth in $In_{0.60}Ga_{0.40}As$/GaAs self-assembled quantum dots," *Phys. Rev. B*, vol. 65, p. 041308, 2002.

[22] C. Kammerer, C. Voisin, G. Cassabois, C. Delalande, P. Roussignol, F. Klopf, J. P. Reithmaier, A. Forchel, and J. M. Gérard, "Line narrowing in single semiconductor quantum dots: Toward the control of environment effects," *Phys. Rev. B*, vol. 66, p. 041306, 2002.

Chapter 9

Multiexcitonic Emission Decay Times

Dans ce chapitre, nous présentons la méthode de spectroscopie, résolue en temps, appliquée à une boîte quantique unique. Le temps de relaxation de l'émission totale de boîtes quantiques sous excitation non résonante est très long, de l'ordre de quelques dizaines de microsecondes. Cette observation est en contradiction avec les temps typiquement mesurés sur d'autres systemes de boîtes quantiques, qui sont plutôt de l'ordre de la nanoseconde. Dans le cas d'une excitation résonante, nous observons aussi un temps de relaxation de l'ordre de la nanoseconde. Nous donnons une interprétation de cet effet comme résultant de l'interaction du système d'excitons indirect dans le double puits quantique présentant de très longs temps de relaxation, avec le système de boîtes quantiques. Dans ce cadre, la structure à double puits quantique agit comme un réservoir d'excitons pour les boîtes. Ce modèle permet d'évaluer certaines propriétés des excitons bidimensionnels indirects comme leur constante de diffusion et leur mobilité.

The time evolution of the photoluminescence spectra of a single quantum dot was observed.

The following chapter discusses how the excitation power and the temperature from 4K up to 60K influence the derived characteristic times.

In the first section the general excitation power and temperature effects on time-resolved spectra are discussed.

In the second section, a more detailed analysis of the observed decay times is given.

The experimental setup for time resolved experiments is described in 4.5.

9.1 Spectrally and temporally resolved emission from a single dot

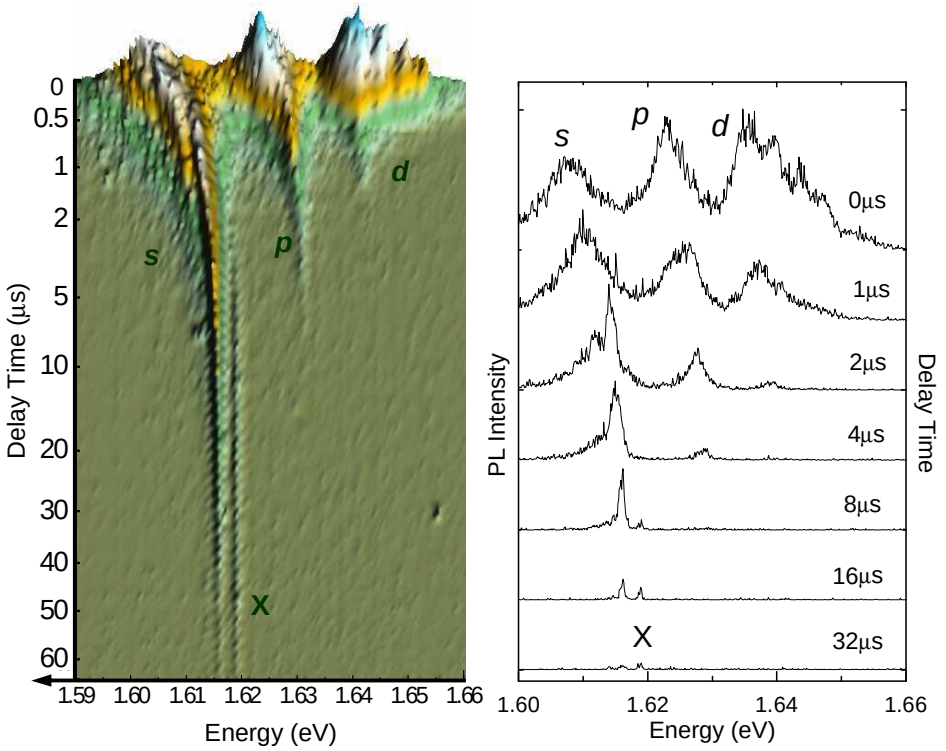

Figure 9.1: *Photoluminescence spectra of a single GaAs quantum dot recorded at different delays from the excitation pulse. The excitation pulse was high enough to achieve population of up to three excited shells. Left panel: PL intensity map. Right panel: several corresponding spectra.*

The concentration of carriers in a single quantum dot is controlled by a precise determination of the exciting laser power. As it was described in chapter 7.1, where the excitation power evolution of the single dot emission spectra was discussed, with increasing excitation power the subsequent occupation of first single exciton, trion and biexciton states (s-shell), then subsequently p, d, f, ... and higher states can be achieved.

Typical photoluminescence spectra taken under cw laser excitation represent the emission from the equilibrium state that is achieved in the dot when the processes of electron and hole capture and annihilation are occurring simultaneously. In a time-resolved experiment the process of emptying the dot states due to carrier radiative recombination can be traced in time. The photoluminescence spectra are therefore recorded at different delays from the end of the excitation pulse. Fig.9.1 illustrates temporally and spectrally resolved photoluminescence from a single quan-

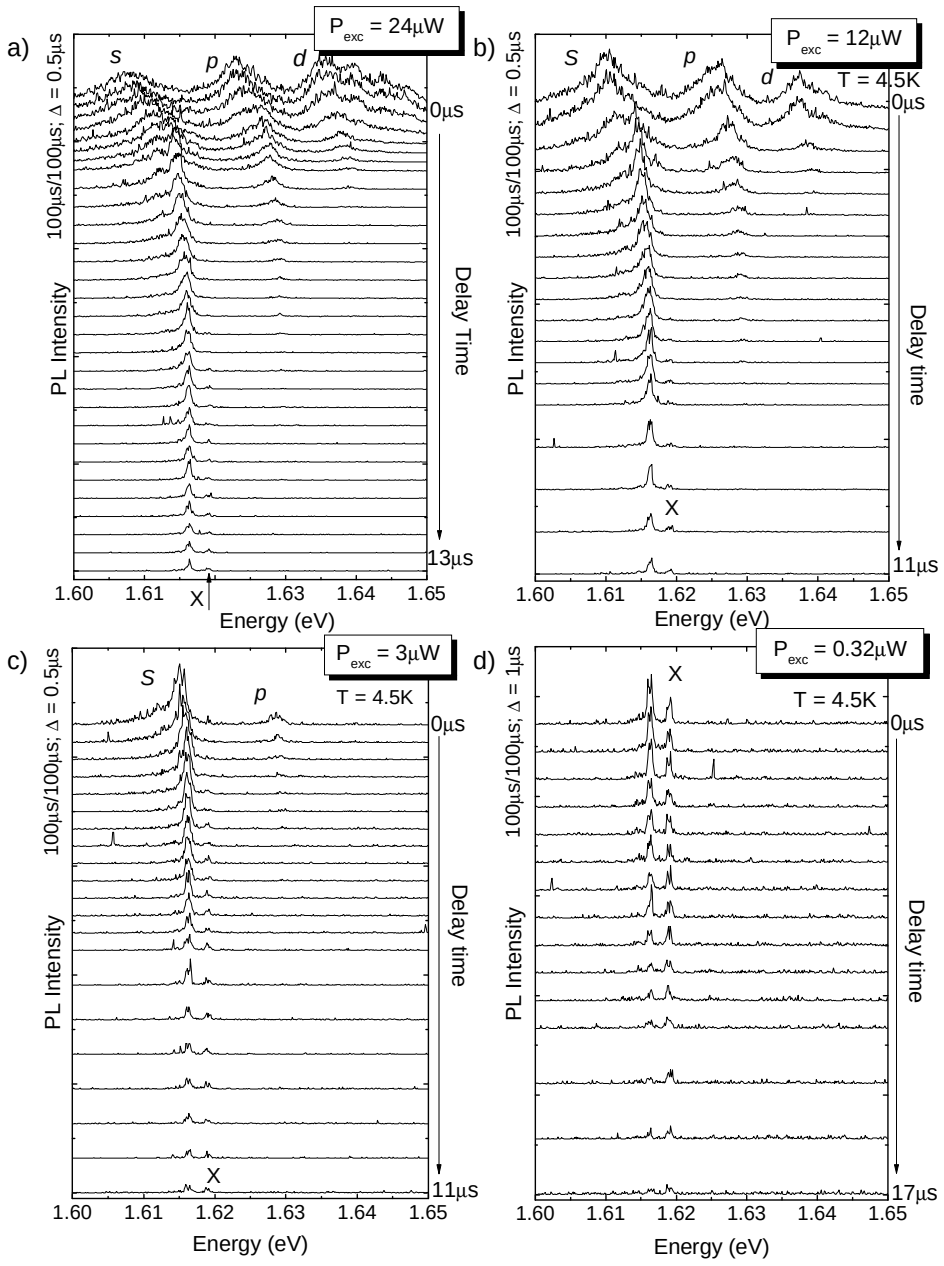

Figure 9.2: *Time resolved photoluminescence spectra of single GaAs quantum dot for different powers of the excitation pulse at 4.2K.*

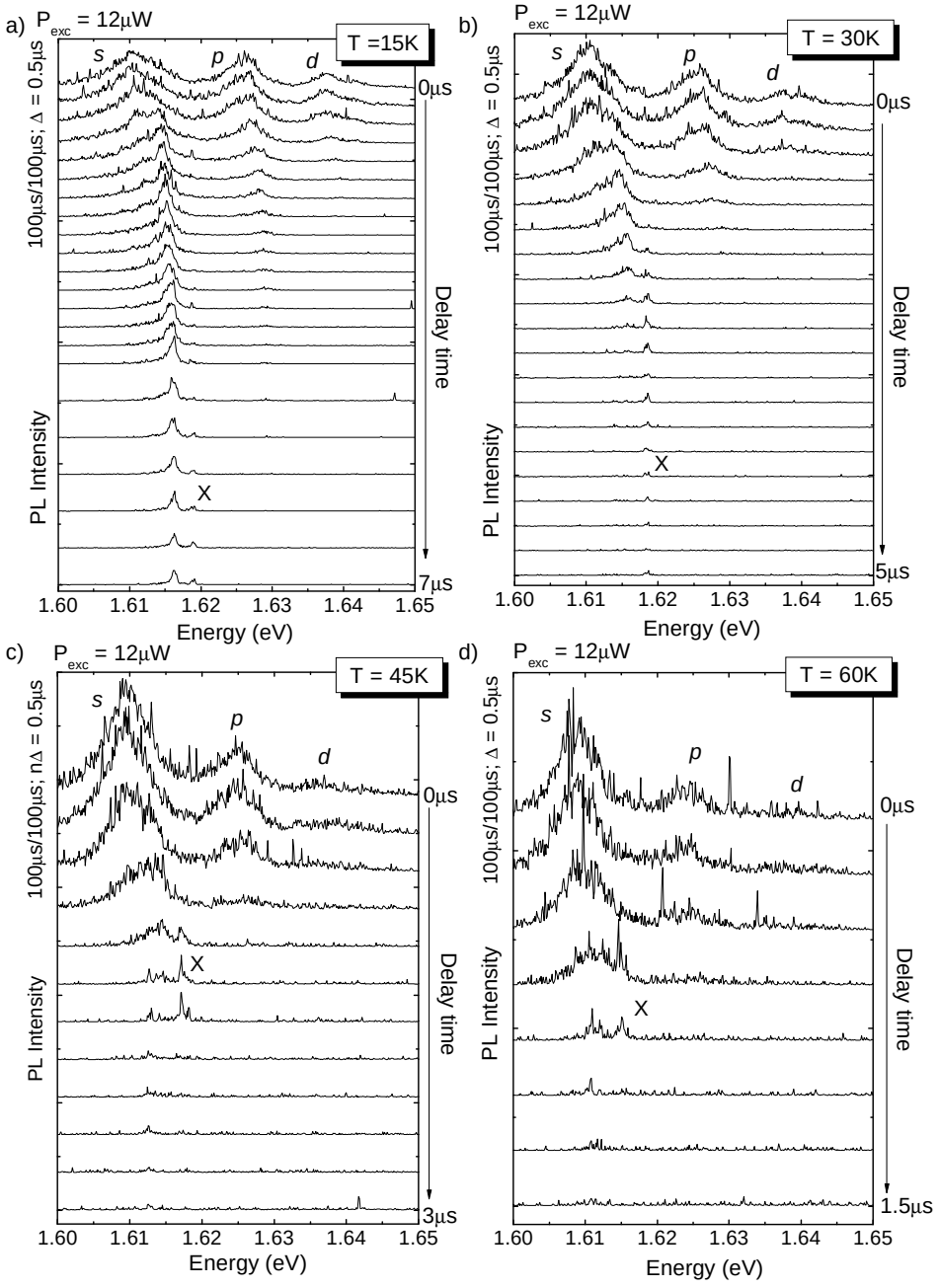

Figure 9.3: *Time resolved photoluminescence spectra of a single GaAs quantum dot for different temperatures and the same power of the excitation pulse.*

tum dot. The power of the excitation pulse was high enough to achieve population up to the third electronic level (s, p and d shells) at zero delay.

By tracing radiative recombination, the process of emptying the dot states is precisely monitored. It is observed that at certain delays the photoluminescence is similar to those observed under cw excitation, but taken with successively reduced excitation power (compare with Fig.7.1 and Fig.7.2). This effect is visible for all different excitation powers, as illustrated in Fig.9.2.

The fastest decay is observed for the excited p and d shells and their luminescence is observed to disappear quickly from the spectra (Fig.9.2a). The emission form most simplest excitonic complexes is observed for longer delays, very often even after 15μs. This is believed to be the effect of the very long lifetime of the carriers in the 2D system, which is constantly supplying the dot with carriers. The emission from quantum dot reflects the dynamics in the quantum well system dominated by (mostly) diffusion and (slightly) recombination processes. This is discussed in more details in the next section.

The effect of increasing temperature on the observed dynamics is illustrated in Fig.9.3. The excitation power in the laser pulse is constant for all measurements and the changes in time of the spectra are traced for different temperatures of the lattice. Similarly to the experiment performed for different excitation powers, a subsequent emptying of the dot states is observed. The time resolved spectra are very similar to those obtained in cw excitation but for various excitation laser powers (compare with Fig.8.2). The effect of the temperature increase is very visible, as for the longest delays at high temperatures it is not the single X line that remains in the spectra, but the low energy components that appear below the X* emission with increasing temperature (compare with Fig.8.1).

Interestingly, very long decay times $\sim 1\mu s$ are observed in all presented spectra. This is an unusual effect for direct type structures. In general the typical PL decay times observed in quantum dots are of the order of ns. The effects observed in this case are caused by special properties of the indirect surrounding system, as discussed in the next section.

The time evolution of photoluminescence spectra of a single quantum dot revealed very long decay times, of the order of tens of μs. Tracing the dot emission in time it is possible to observe the subsequent emptying of dot energy states. This is the same effect as observed when decreasing the excitation power in a cw photoluminescence experiment. The increase of temperature does not change the observed effects; however, the typical high temperature consequences are visible in the spectra (such as the change of the emission energy or temperature induced appearance of new emission lines).

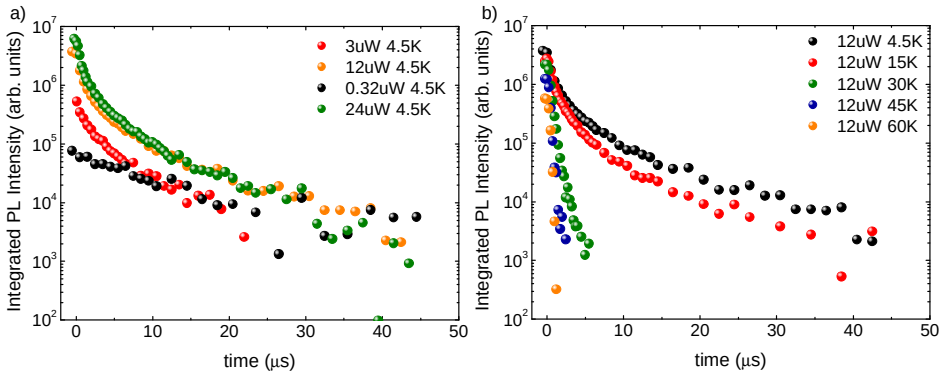

Figure 9.4: *The transients measured for a single quantum dot for different excitation powers in the laser pulse (left panel) and temperatures (right panel).*

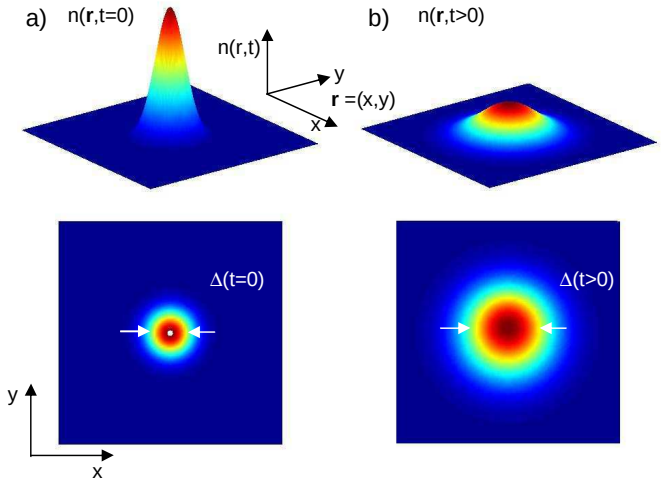

Figure 9.5: *The Gaussian function representing the carrier density in the quantum well plane, (x,y), created by the laser spot directly after the laser pulse at a) zero delay and b) after a certain time. The "top" view illustrates the increase with time of the width of the distribution. The presented picture is schematic.*

9.2 Diffusion of indirect excitons

As it was discussed already in chapter 5, the investigated quantum dots are formed in the indirect, type II GaAs/AlAs double quantum well structure. The barriers for the dots are composed of X_{XY}-type electrons and Γ-type holes. The optical transitions associated with these states are strongly forbidden in real and k-space. The photo-created 2D carriers confined in the quantum well have very long lifetimes, in the ms range, (as shown in chapter 5.3). When the number of carriers is sufficiently high, they diffuse at large distances in the quantum well plane, up to hundreds of μm. The diffusion process can be described by a characteristic time in the μs range (see 5.4). The quantum dots therefore, being of direct-type, serve as an efficient recombination channel and are the "probes" of diffusing carriers.

As shown in Fig.9.4, a non-exponential decay of the single quantum dot emission, with a characteristic μs time scale, is observed.

The luminescence dynamics observed in the quantum dot reproduces the carrier dynamics in the indirect, GaAs/AlAs double quantum well. When applying the excitation above the quantum dot barrier, the carriers are primary created in the 2D quantum well system and then they are trapped into the quantum dot. The carrier concentration n_{2D} in the 2D system, after the excitation laser is turned off, is determined by two factors: carrier decay and diffusion. Due to the long lifetimes of 2D carriers, the diffusion of carriers from the excitation spot is the major effect in the case of the investigated system.

In the first approximation it can be assumed that the 2D carriers, created by the laser spot, spread in the quantum well plane according to the diffusion equation:

$$\frac{\partial n(\mathbf{r},t)}{\partial t} = D\nabla^2 n(\mathbf{r},t) - \frac{n}{\tau} \tag{9.1}$$

where D is the diffusion coefficient and τ is the 2D carrier decay time.

Eq.9.1 has a simple solution in two-dimensions in the form:

$$n_{2D}(r,t) = \frac{M_d}{4\pi D\cdot(t+t_0)} e^{-\frac{r^2}{4D\cdot(t+t_0)}} e^{-t/\tau} \tag{9.2}$$

where the first therm illustrates the spreading of the 2D carriers in the quantum well plane according to broadening of the Gaussian function (what is schematically illustrated in Fig.9.5); the second term represents carrier decay. M_d is proportional to the laser power and t_0 is the constant reflecting the size of the laser spot at $t = 0$. The width of the Gaussian function $\sigma = 2\sqrt{D\cdot t_0}$ in the experiment can be set as $\sigma = 5\mu m$. The 2D X_{XY} carrier decay time τ at 4.2K is $\sim 20\mu s$ (see Ref.[1] and chapter 5.3).

The carrier density in the investigated quantum dot n_{QD} (located in the center of the excitation spot) is proportional to the number of carriers in the 2D system at $\mathbf{r}$=0: $n_{2D}(0,t)$. Therefore the emission intensity from the dot $I(t) \sim n_{2D}(0,t)$ can be expressed as:

$$I(t) = \frac{M_d}{4\pi D\cdot(t+t_0)} e^{-t/\tau} \tag{9.3}$$

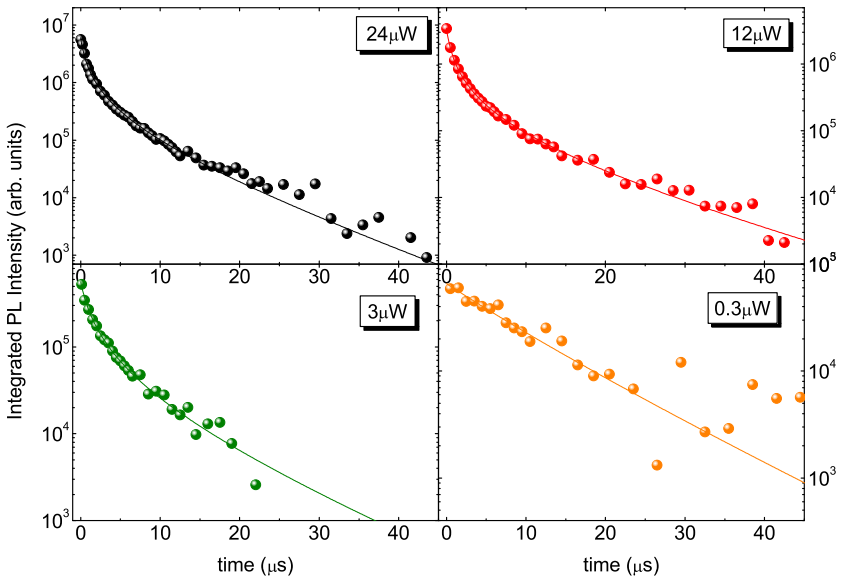

Figure 9.6: *Transients measured for the same quantum dot for different excitation powers (the same as illustrated in Fig.9.4a) fitted with eq.9.3, see text for details.*

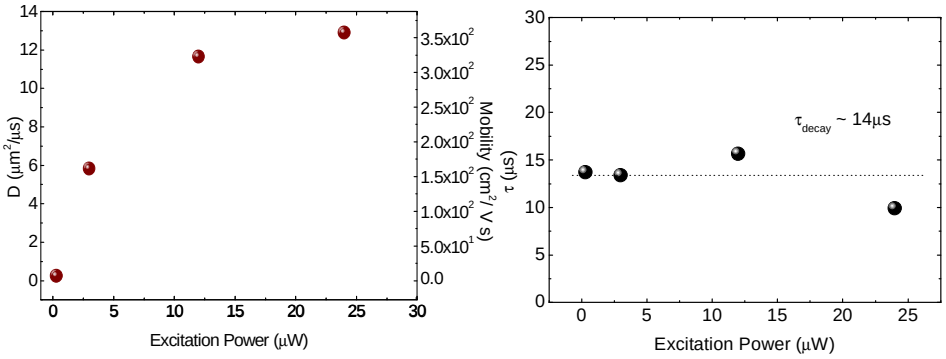

Figure 9.7: *The diffusion coefficient (left panel) and the decay time (right panel) obtained from experimental data illustrated in Fig.9.6 for different excitation powers. The mobility was evaluated according to eq.9.4.*

Fig.9.6 illustrates the results of the fit of eq.9.3 to the experimental data shown in Fig.9.4a).

The obtained values of diffusion coefficient D, and decay times τ for different excitation powers are illustrated in Fig.9.7. It is observed that D increases with increasing excitation power. The diffusion coefficient is directly related to the carrier mobility μ by:

$$D = \mu \cdot k_B T \tag{9.4}$$

The obtained values of 2D carrier mobilities are in the order of $200 cm^2/(V \cdot s)$, which is a reasonable value for the indirect excitons (compare with Ref.[2]).

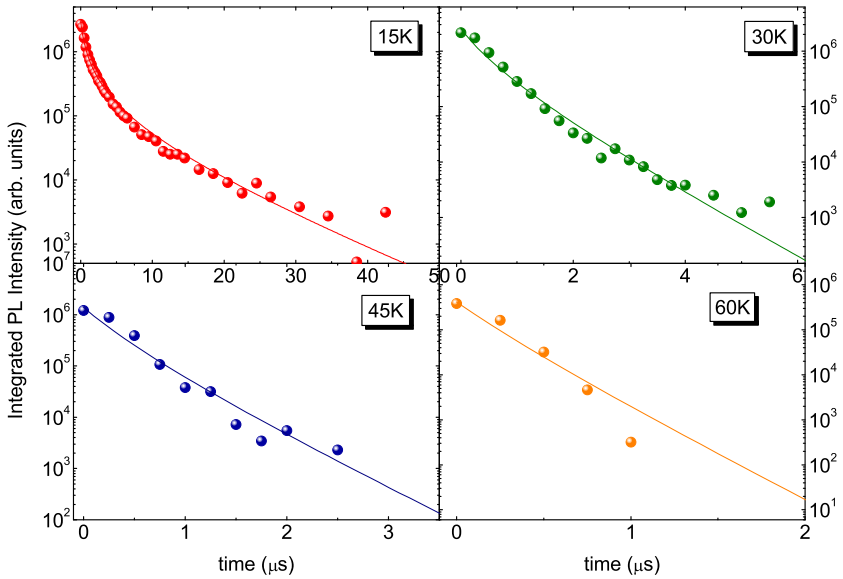

Figure 9.8: *Transients measured for the same quantum dot for different temperatures (the same as illustrated in Fig.9.4b) fitted with eq.9.3 (solid line) setting* $D = 12 \mu m^2/\mu s$*, see text for details.*

When temperature is increased above 4.2K the transients are observed to be much steeper. Fig.9.8 illustrates the results of fitting eq.9.3 to the data shown in Fig.9.4b).

It is observed that the PL decay obtained for 15K is still possible to fit with eq.9.3. However, for higher temperatures the PL decay is mostly determined by the exponential therm and the diffusion coefficient cannot be evaluated from the results. Therefore, when fitting eq.9.3 to the experimental data obtained for $T > 4.5K$, the value of D was taken from the results for 4.5K.

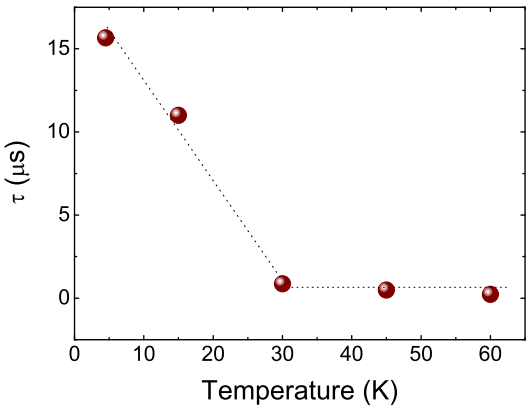

Figure 9.9: *The decay time of indirect excitons τ evaluated from experimental data illustrated in Fig.9.8 for different temperatures. Dotted line: schematically shown presumed dependence.*

Fig.9.9 illustrates the derived decay times in the 2D system with increasing temperature. It is observed that with the increase of temperature the 2D carrier decay time becomes shorter. The temperature of approx. 30K was evaluated as the temperature when the non-radiative processes are activated, as described in chapter 8. Therefore it is believed that the shortening of the carrier lifetime in a 2D system at high temperatures is caused by the non-radiative processes.

The temporal evolution of the emission from the quantum dot reflect the dynamics of carriers in the 2D quantum well system. Diffusion is found to play a major role in decreasing the density of 2D carriers which can be efficiently trapped in the quantum dot. The mobility of diffusing 2D carriers was found to be $200cm^2/(V \cdot s)$ with agreement to previous reports.
The important role of non-radiative processes in shortening the lifetime of 2D carriers has been observed at temperatures T>∼30K. This observation is in agreement with conclusions presented in chapter 8.3 which have been drown from different experimental results.

Bibliography

[1] A. Wysmolek, B. Chwalisz, M. Potemski, R. Stepniewski, A. Babinski, S. Raymond, and V. Thierry-Mieg, "Emission from mesoscopic-size islands formed in a GaAs/AlAs double layer structure," *Acta Physica Polonica A*, vol. 106, p. 367, 2004.

[2] M. Hagn, A. Zrenner, G. Böhm, and G. Weimann, "Electric-field-induced exciton transport in coupled quantum well structures," *Appl. Phys. Lett.*, vol. 67, p. 232, 1995.

Chapter 10

Multi-excitonic Emission : Photon Correlation Experiment

Une accumulation de porteurs dans une boîte quantique conduit à la formation de complexes multi-excitoniques. Une telle accumulation peut être obtenue dans le cas de boîtes quantiques fortement excitées ou les porteurs photo-créés occupent les états excités de la boîte. Dans ce cas, la luminescence se répartit en plusieurs raies provenant de la recombinaison sur l'état fondamental et de recombinaisons provenant des premiers états excités.
Nous présentons alors des études de corrélation de photons entre ces différentes raies d'émission qui permettent d'étudier la chronologie d'émission, la charge de l'état fondamental et la configuration des porteurs dans la boîte fortement dépendante du spin électronique.
Nous donnons ensuite les détails des variations de charges dans les boîtes quantiques sur la base des expériences de corrélation de photons sous excitation non-résonante ou quasi-résonante qui nous permettent de faire la distinction entre la capture de porteurs individuels ou d'excitons.
Nous pouvons observer le nombre de cascades entre les états neutres de la boîte et nous démontrons l'existence d'états triplets et singulés pour le biexciton.

At moderate excitation power, the emission from a single dot is composed of a number of sharp lines that are due to the recombination of a number of stable multiexcitonic complexes that include carriers confined on *s*- and *p*- shells. Emission lines from a single quantum dot may appear in cascades and the detailed investigation of the correlation of photons emitted from a quantum dot allowed to identify the origin of a number of lines.

In section 10.1 the differences in the emission spectra under resonant and non-resonant excitation are discussed.

In section 10.2 the details of photon correlation experiments and the measured second order correlation function are given. The most simple X - X histogram is

discussed in detail.

Then, in section 10.3, the cross - photon correlation histograms of X - X* obtained under resonant and non-resonant excitation are compared. This allowed a discussion about the single carrier capture and creation of carriers in pairs directly in the quantum dot.

Section 10.4 is devoted to the problem of charge state variation in the dot. The time scale of switching of the dots between neutral and charged states is discussed.

Section 10.5 illustrates that in the case of the investigated quantum dots only two groups of emission lines can be distinguished among the multiexcitonic states emissions : those due to the recombination of neutral and charged multiexcitonic complexes.

Section 10.6 discusses the charge state variation of the quantum dot observed in the timescale of the experiment, which is in the range of several seconds. This intriguing result is connected with the change of surroundings of the dot.

Section 10.7 demonstrates that there exists a direct relation between emission lines within "neutral" groups, which is exhibited in the number of cascades. The experimental evidence for biexciton triplet state observation is shown.

10.1 Excitonic states observed at quasi resonant excitation

As it was already discussed in previous chapters, many electron - hole pairs can be generated in a single quantum dot at moderate laser powers, which creates many multicarrier states, including charged and neutral ones, in the dot. This gives a large, though finite, number of possible recombinations. Thus, the resulting emission spectrum is composed of multiple sharp lines, each one corresponding to a single exciton annihilation at a given exact configuration of electrons and holes. Such single pair annihilation processes involve transitions from the ground state of N pairs to the ground or (slightly) excited state of N-1 pairs.

There have been many theoretical papers published with the results of calculations of the many electron - hole pair emission and/or absorption spectrum [1, 2, 3, 4, 5, 6]. The main goal is to include the many body effects, exchange and correlation, in the single particle problem of many excitons in a strongly confined system, with the specific shell degeneracy. Although different approaches have been used for differently modelled dots, sets of discrete lines have been obtained (compare with section 10.7.2).

A typical spectrum taken under `quasi-resonant excitation` for several excitation powers is illustrated in Fig.10.1. The most pronounced lines, relevant for further study in photon correlation experiments, are marked in the spectrum.

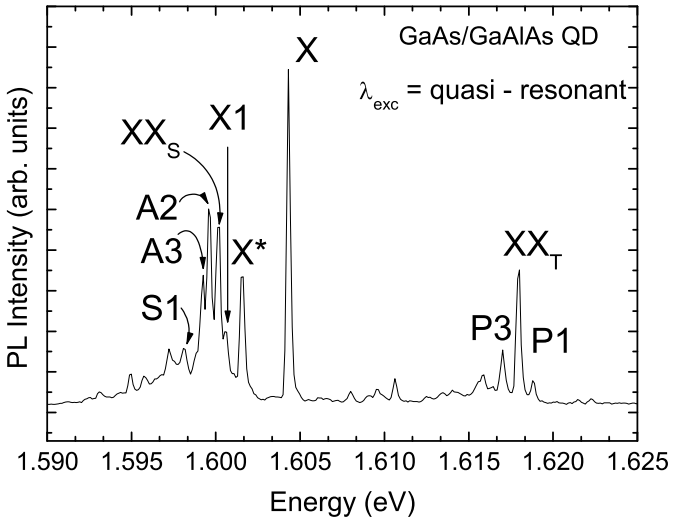

Figure 10.1: *Micro-PL spectrum of a single GaAs/AlAs quantum dot at moderate excitation power at resonant excitation. The most pronounced lines are marked in the picture.*

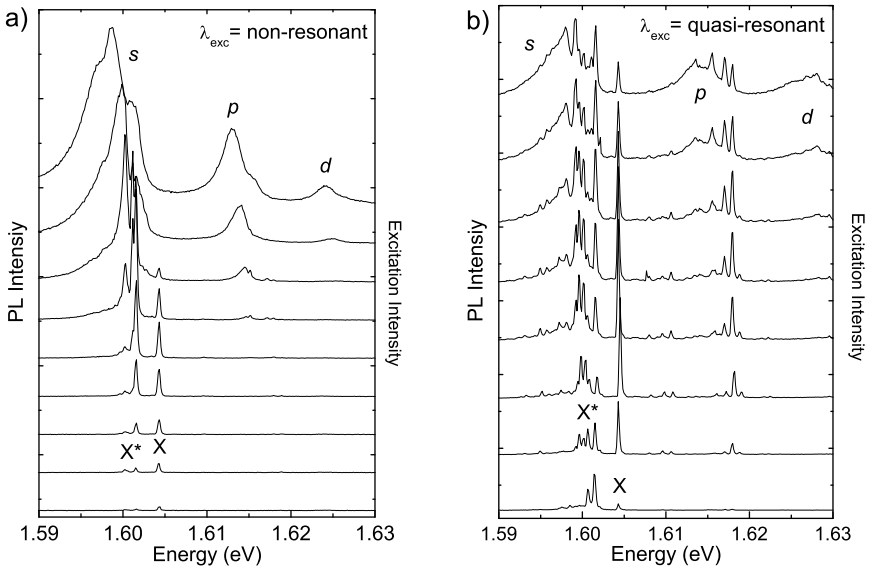

Figure 10.2: *Micro-PL spectra of the single GaAs/GaAlAs quantum dot at different excitation powers at a) non-resonant and b) quasi-resonant excitation.*

Quasi-resonant excitation, λ_{exc}= quasi-resonant, is excitation at an energy below quantum dot barriers, i.e. below the energy levels of the surrounding double quantum well system. Thus it is assumed that the excitation is performed in the excited states of a dot. The non-resonant excitation, λ_{exc}=non-resonant, was always performed with the energy of the laser higher than the energy levels of the double quantum well system.

One of the differences between the two excitation energies is the process of exciton formation. Whereas in one case it is due to single carrier capture in the dot (non-resonant excitation), in the second case the carriers are created preferentially in pairs in the dot. This effect is discussed in section 10.3.

The second difference is that under quasi-resonant excitation, the spectrum is composed of very well isolated lines, including the emission form carriers confined on the p shell. In the case of non-resonant excitation the spectra revealed only a few sharp lines (mostly X, X*, XX) in the s-shell emission regime. It is difficult to observe sharp emission lines related to the p-shell under non-resonant excitation.

Fig.10.2 illustrates the comparison of the excitation power evolution of the same quantum dot spectra under quasi-resonant and non-resonant excitation. The broadening of the emission lines under non-resonant excitation is clearly visible, especially in the s-shell recombination regime and under high excitation power. It is believed that this is due to the strong interaction of carriers with the local dot environment [7] (spectral diffusion [8, 9]), and disorder effects, which are significant

when the capture of carriers in the dot involves relaxation from higher energy levels, which is the case of non-resonant excitation.

The energy position of the emission lines stayed unchanged under the two excitation energies and no additional emission lines were observed in comparison to other reports [10].

The excitation power dependent emission spectra from a single quantum dot taken under quasi-resonant and non-resonant excitation revealed that in the case of quasi-resonant excitation the sharp line emission is much pronounced in a wide range of excitation powers. If the dot is excited above the band gap, a rapid appearance of broad bands is observed with increasing excitation power, which suggest stronger interactions of carriers with the dot environment, leading to emission line broadening.

10.2 General characteristics of the photon correlation experiment

The photon correlation experiment was performed under cw excitation in a Hanbury-Brown and Twiss setup [11], as illustrated and described in Fig.4.6 in chapter 4.6.

If not otherwise stated (only in section 10.3) the photon correlation experiment was performed under quasi-resonant excitation.

The general convention for all histograms presented in this work is that the first photon, due to a particular recombination as marked in the pictures, was set to "start" and the second to "stop" photodiodes (for positive delays).

10.2.1 Second order correlation function

The measured photon correlation distribution is equivalent to the second-order cross correlation function $g^{(2)}_{\alpha,\beta}(\tau)$ of electromagnetic field filtered at two frequencies α and β, and is expressed as:

$$g^{(2)}_{\alpha,\beta}(\tau) = \frac{< I_\alpha(t) I_\beta(t+\tau) >}{< I_\alpha(t) >< I_\beta(t+\tau) >} \tag{10.1}$$

where $I_i(t)$ is the intensity of the signal measured at frequency i.

In the weak laser excitation regime [12], the distribution can be described by a simple exponential law:

$$g^{(2)}(\tau) = 1 - exp(-(\Gamma + W_p)\tau) \tag{10.2}$$

where Γ is the electron - hole recombination rate and W_p is the effective pump rate. The parameter $\tau_d = 1/(\Gamma + W_p)$ illustrates the decay time in the investigated system.

In all experimental results presented below, the exponential law according to eq.10.2 was fitted to the exponential decays. The obtained values of decay time τ_d are marked directly in the pictures.

10.2.2 Exciton in a quantum dot as a single photon source

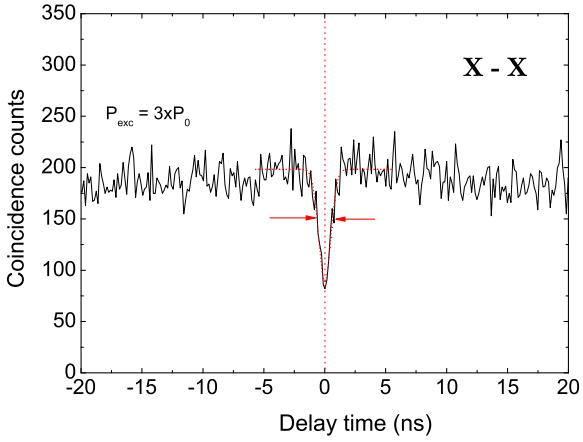

Figure 10.3: *Typical X-X auto-correlation histogram taken around small delay times and with the best possible time resolution.*

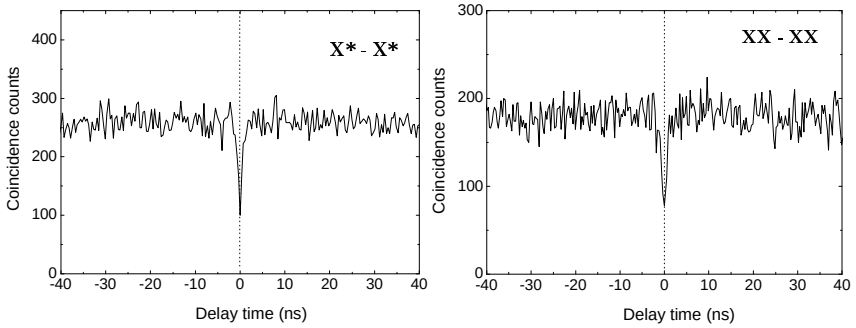

Figure 10.4: *X*-X* (left panel) and XX-XX (right panel) typical auto-correlation histograms.*

A typical X - X auto-correlation histogram taken under quasi-resonant excitation is illustrated in Fig.10.3. The picture is presented in a small time range, around zero delay time with the best resolution that is possible in the experimental

setup.

The sharp anti-bunching peak precisely at zero delay time is a typical feature of auto-correlation histograms. It is a signature that indeed the observed emission is from a single quantum dot and it exhibits the single photon character of excitonic emission. This reveals that there is no possibility of emitting two exciton photons at the same time from a single quantum dot. This feature well establishes quantum dots as the emitters of single photons [13, 14].

The width of the anti-bunching dip decreases as the excitation intensity is increased (compare with Fig.10.7). For a very high excitation intensity the width of the anti-bunching dip reflects directly the exciton lifetime, it is however limited by the experimental resolution and it can only be estimated to be below 1ns.

In comparison to previously reported data [15], the bunching effect at high excitation powers in the X - X auto correlation histograms at zero delay time even at high excitation powers was not observed.

The anti-bunching peak should be observed for all auto-correlation histograms. Two examples of X*-X* and XX-XX auto-correlation histograms are illustrated in Fig.10.4. For both the anti-bunching dip is observed at zero delay time.

The anti-bunching dips precisely at zero delay time in auto-correlation photon histograms reveal that at a given time, there exists only one configuration of carriers in the quantum dot. This constitutes the quantum dot as a single photon emitter.

10.3 Charge fluctuation in a quantum dot - single carrier capture or electron-hole pair creation

The charge fluctuation in a quantum dot is a particular effect, which leads to the change of the quantum dot state. It has already been studied and is very often reported as the "blinking" effect [12, 14]. It is assumed that the QD switches between the excluding configurations, or so called 'on' and 'off' states, of which one state can be dark. This can be due to single charge fluctuation, putting the dot in a neutral or charged configuration of carriers. If all states are bright, the recombination from each configuration results in the emission lines at different energies (for example X and X* as the simplest neutral and charged states of a quantum dot).

At moderate excitation power, at a given time, the state of the quantum dot is composed of a particular multiexcitonic complex that recombines through different possible channels. However, the last emitting state is a single exciton, either neutral or charged. If the charge state variation in the dot is for some reason forbidden, the recombination will always occur in the same ladder of states, thus no correlation between the two possible quantum dot states is expected. On the other hand, if the charge state variation is very effective, even cascaded emission between X and X* lines is expected.

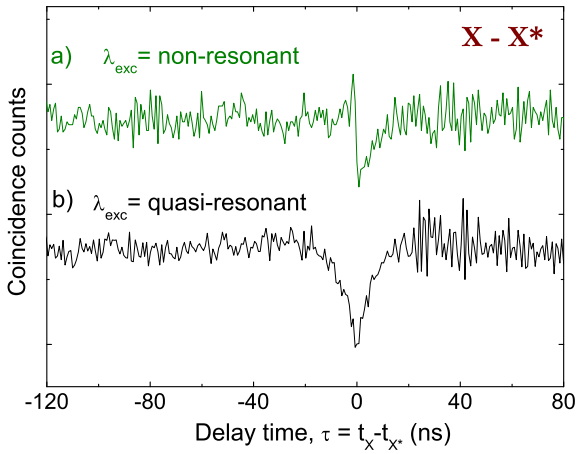

Figure 10.5: *X-X* cross-correlation histogram taken under a) non-resonant and b) quasi-resonant excitation.*

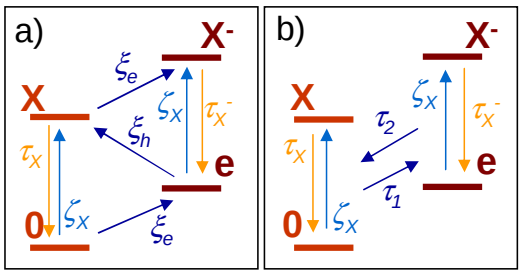

Figure 10.6: *The comparison of two different types of population dynamics in the case of non resonant (a) and resonant (b) excitation. ξ_e, ξ_h and ζ_X are time dependent capture rates of the electron, hole and exciton respectively; the constants τ_X, τ_X^- are decay times of respective states; τ_1 and τ_2 are switching times between neutral and charged configurations of carriers in the quantum dot.*

The X - X* cross correlation histograms taken at `non-resonant excitation` are illustrated in Fig.10.5a). This shape is now well established as the typical shape of a histogram of correlated photons due to neutral and charged state recombination [16, 17, 18, 19]. It shows the asymmetry around zero delay time: the positive correlation for τ <0 and negative correlation for τ >0. The bunching-type effect at negative delay times illustrates the increased probability of X detection after the X* photon has been emitted. In other words, the re-excitation of the quantum dot directly after charged exciton recombination requires a single carrier to be trapped, while three carriers are necessary for the opposite emission order, i.e. when the neutral exciton was emitted first. The strong bunching at τ <0 shows that the single carrier capture process is very effective and the shape of the histogram resembles those of cascade emissions (compare with Fig.10.12)

The process can be well described by the rate equations according to the population diagram illustrated in Fig.10.6a). It assumes that the switching of the quantum dot between the "neutral" ladder of states and the charged one is due to single carrier capture. Starting from the empty dot, the capture of single carriers (with a rate ξ_e) puts the dot in the charged state with one electron. Further single hole capture (described by ξ_h) is enough to form an exciton. An exciton can be also formed directly in a dot, and this occurs with the rate ζ_X. The X* formation from X involves only a single electron capture (rate ξ_e). The recombination occurs always in one ladder only, thus after X recombination (with τ_X decay time) the dot is empty, after X* recombination (with τ_X^- decay time) the dot is left with a single electron. The model including rate equations to fit the histogram illustrated in Fig.10.5a) is done in Ref.[19] and will not be repeated here.

As it is demonstrated below, this asymmetric type X - X* histogram is only possible when single charge injection is the main source of carriers in the quantum dot. If the process is suppressed, for example by the resonant excitation, significantly different effects are observed.

Fig.10.5b) illustrates the X - X* cross photon correlation histogram taken under `quasi - resonant excitation`. An ideally symmetric histogram around zero delay times is observed with characteristic long time, in the hundred of ns range, anti-correlation effect for both, negative and positive delays.

The symmetry around zero delay time of the cross charge-neutral photon correlation histogram is a unique observation. It illustrates that, in the case of resonant excitation, the single carrier capture is inefficient, resulting in the same probability of the detection of X* after X was detected and detection of X after X* was detected. In other words, the process of charge variation in the dot is independent of the particular configuration of carriers. This is in contrast to the non-resonant excitation case, when a single particle left in the dot after the charged exciton recombination gave the increased probability of binding the neutral exciton by simply trapping one additional carrier.

The same decay times on both negative and positive sides of the histogram in Fig.10.5b) may be described within the model of a two level system [10]. Fig.10.6b) illustrates the population dynamics scheme in the case of resonant excitation, which

is significantly different in comparison to non-resonant excitation illustrated in Fig.10.6a). In the case of quasi-resonant excitation the two stable states of the dot are the neutral state and the particular X*-type charged state. The quantum dot switches naturally between them within a time scale (τ_d), up to hundreds of ns. The fact that an additional ladder of charged states in cross-photon correlations is not observed confirms the population dynamics according to a two level model.

Histograms of different shapes, either symmetric or asymmetric with respect to zero delay time, are observed depending on whether the excitation energy is high above the dot barriers or below the barrier energy gap. A strong asymmetry of the X*-X cross-correlation histogram shows that at high excitation energies the dots are filled with individual photoexcited electrons and holes. The symmetric shape of the X*-X cross-correlation histogram under quasi-resonant excitation indicates that in this case the dot is predominantly filled with electron-hole pairs.

10.4 Charge fluctuation process under resonant excitation

The observed long time anti-correlation effect under quasi-resonant excitation in the X-X* histograms illustrates (see Fig.10.5b) that the time required to change the state of the quantum dot from charged to neutral (and the other way round) is very long, the order of hundreds of ns.

The decay time on both sides of the histogram around zero delay time describes the decreased probability of detecting the photon due to the charged state recombination after the photon from the neutral state recombination was detected. At infinitely long delay times the quantum dot reaches a steady state, which is a mixture of neutral and charged states.

A similar, long-time effect is observed in X-X auto correlation histograms for long delay times. Fig.10.7a) illustrates the X-X auto-correlation histograms taken for different excitation powers in a broad range of delay times. Strong positive correlation effects between two exciton photons are observed for τ >1ns, which means that after the emission of X there is a decreased probability of finding the dot still in the neutral state. The decay times fitted with eq.10.2 are marked in the picture for various excitation powers and are up to a hundred ns, similarly to those found in X-X* histograms.

It is observed that the time after which the dot is no longer found in the neutral state at very low excitation power can be as long as τ_d =400ns and significantly decreases with increasing excitation power, up to τ_d =15ns for the highest excitation power investigated. This suggests that the more carriers are created in the quantum dot, the smaller is the probability of capturing/removing a single carrier from the dot or of changing the dot surroundings to change the state from neutral to charged.

The excitation power also modifies the X-X* cross-correlation histograms, as the mechanism of the long-time effects in both cases is the same. Fig.10.7b) il-

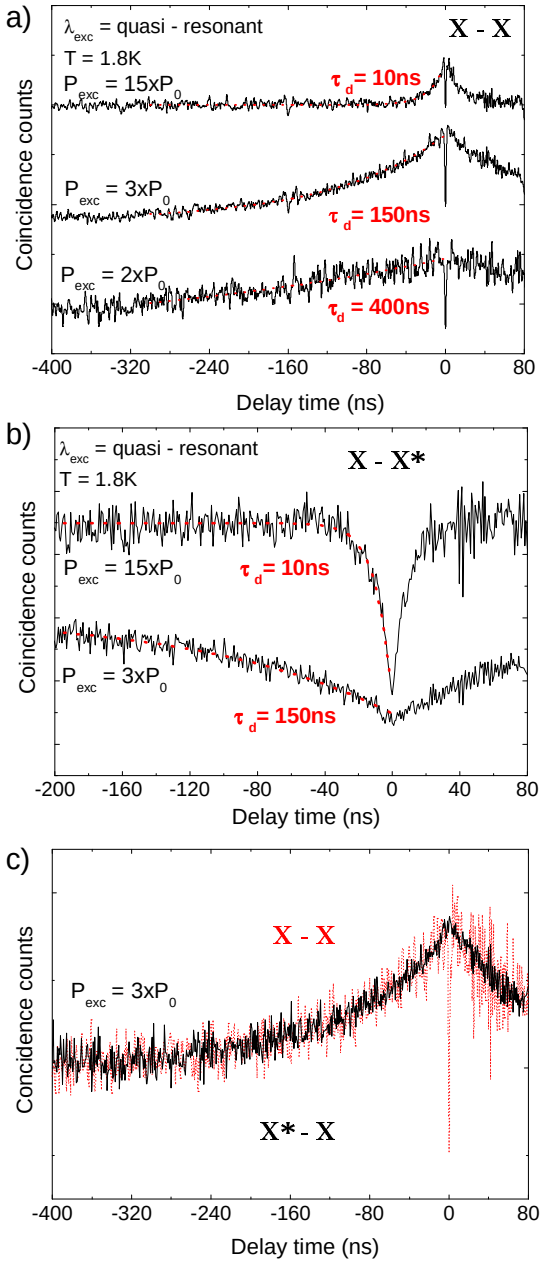

Figure 10.7: *a) X - X auto-correlation histograms and b) X - X* cross-correlation histograms for different excitation powers at quasi-resonant excitation, different for a) and b) (see text for details). The dashed lines represent the fit of the exponential law as described by eq.10.2. c) The comparison between the X - X (dotted line) and X - X* (solid line) correlation histograms taken under the same conditions of excitation power and excitation energy. The X - X* histogram was shifted in intensity and reversed to compare the long time decay tails on both histograms.*

lustrates the X-X* histograms taken for different excitation powers with the decay times marked in the picture. Similarly, the increase of the number of carriers in the dot significantly shortens the observed times.

A comparison of X-X auto-correlation and X-X* cross-correlation histograms taken for the same excitation power and excitation energy is illustrated in Fig.10.7c). In the picture the X-X* histogram is reversed and both are normalized to the same number of counts. The same decay time in both histograms is clearly visible. It confirms that the charge state variation in the dot occurs between the two possible (neutral and one type of charged) configurations of carriers.

The symmetric photon correlation histogram obtained under resonant excitation with long time effects was already observed for auto X - X emission [10] and interpreted as the blinking effect in a two level system.

A long time process, on the scale of 10ns-100ns, seen in photon correlation experiments, reflects switching of a dot between its neutral and charged state. The dynamics of this process is shown to be dependent on the excitation power. High excitation power quickens the process of charge fluctuation in the dot.

10.5 Neutral and charged families of quantum dot states

The X-X* histogram, with long-time anti correlation effects, is a typical histogram that is obtained under quasi-resonant excitation for the emission lines that are due to the recombination of differently charged states.

The photo correlation experiment performed within the same "family" of charged or neutral emission lines give different types of histograms, mainly with long time positive correlation effects and/or cascades. The histograms give additional information about the sequences in the emissions discussed in section 10.7.

Fig.10.8 illustrates various types of cross-photon correlation histograms obtained for emission lines shown in the spectrum in Fig.10.1. Only the photon-correlation histograms that give long-time anti correlation effects are shown. Other type histograms (cross-correlation histograms between the emission lines from the same "charged" family) are illustrated in section 10.7.

A histogram similar to that observed for X - X*, with a long time anti-correlation effect, is obtained for: X-X1, X*-XX_S, XX_T-X*, XX_T-X1, X*-A2, X1-A2, X-S1, X-P1, X-P3. This distinguishes between the emission due to recombination of the neutral (such as X) and charge (such as X*) states of a dot.

Thus, the emissions due to the neutral states recombination are:

X, XX_S, XX_T and A2

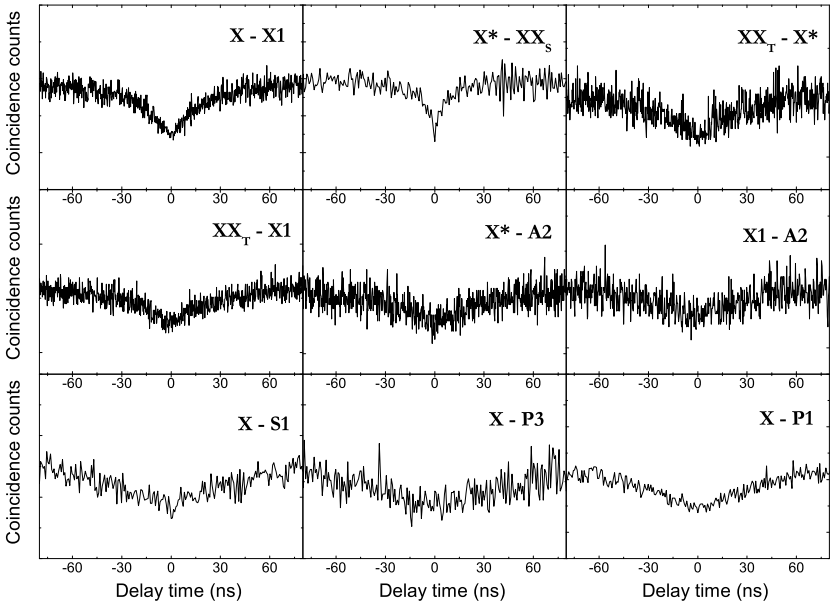

Figure 10.8: *The set of cross-photon histograms of correlated counts as a function of time interval $\tau = \tau_{STOP} - \tau_{START}$ between photon registration events in start and stop detectors, tuned to indicated transitions (start-stop order). Only the histograms that reveal long-time anti correlation effects are shown. The spectrum where the emission lines are marked is presented in Fig.10.1.*

and due to the charged states:

X*, X1, P3, P1, S1 and A3.

No other additional family of charged states was found that in experiment should give long time anti-correlation effects with both X and X* emissions. Thus it can be concluded that, in the case of the quantum dot studied, only one type of charged states is observed. This statement is confirmed by the shape of the histograms that can be described by a two-level model, as discussed in section 10.3.

The charge of X* is probably negative due to the particular shape of the quantum dot confining potential, with a significantly deeper trap for electrons than for holes (compare with Fig.2.4).

A multi-line emission spectrum of a single dot has been found to display two and only two, [X] and [X*], sets of lines. These two sets regroup the emission lines characteristic of a dot in a neutral state and a dot that is charged with one carrier (probably an electron). Clear anti-bunching effects are seen in cross-correlation histograms of photons associated with emission lines from different groups.

10.6 Charge variation on the "macro" time scale

Apart from the natural blinking of the quantum dot, it was observed that the process of charge variation can be visible even on the time scale of a few seconds. If series of μ-PL spectra of the same dot are recorded sequentially with an integration time of 1s, it is possible to observe that the intensity of particular emission lines significantly changes from one spectrum to another.

Fig.10.9 illustrates two μ-PL spectra of the quantum dot taken at the same excitation conditions at two limits: when the X emission intensity is weakest and strongest in the whole series of measurements. It is observed that the emission lines gained in intensity in the same spectrum belong to the same "family" of neutral or charged excitonic configuration recombination, as it was deduced from the photon correlation experiment (compare with discussion in previous section).

This process occurs, however, on a "macro" time scale range in comparison to the one in the hundreds of ns range that was observed in the photon correlation experiment.

Fig.10.10 shows the calculated classical intensity cross-correlation coefficient for the emission lines at different energies α and β:

$$\Gamma = \frac{\sum_i (I_i^\alpha - \overline{I}^\alpha)(I_i^\beta - \overline{I}^\beta)}{\sqrt{\sum_i (I_i^\alpha - \overline{I}^\alpha)^2 \sum_i (I_i^\beta - \overline{I}^\beta)^2}} \tag{10.3}$$

where I_i^α, I_i^α are the intensity of the signal in the following spectra i measured at energy α and β, respectively; $\overline{I}^\alpha$ and $\overline{I}^\beta$ are the average intensities over all spectra at energies α and β, respectively. Γ=1, denoted in the plot by a red colour, represents

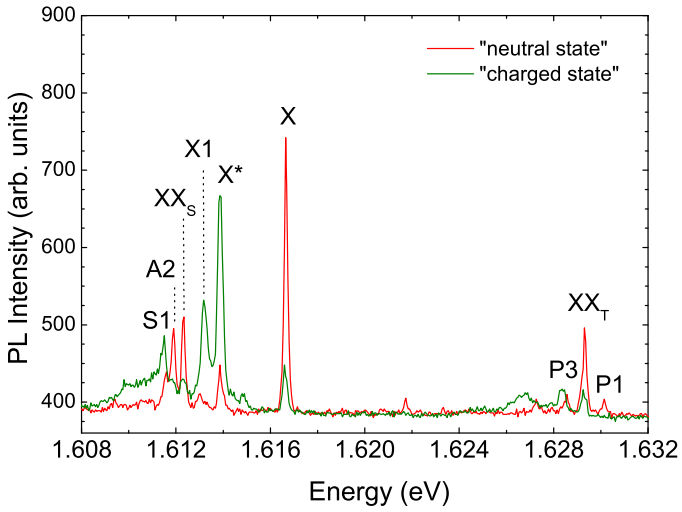

Figure 10.9: *The very long time blinking effect visible in the micro-PL spectrum of the single GaAs/AlAs quantum dot (different dot than the one whose emission spectrum is illustrated in Fig.10.1) at moderate excitation power and quasi-resonant excitation. The red curve illustrates the emission spectrum from the quantum dot mainly due to neutral states recombination and the green curve that due to charged states recombination. The most pronounced lines are marked in the picture.*

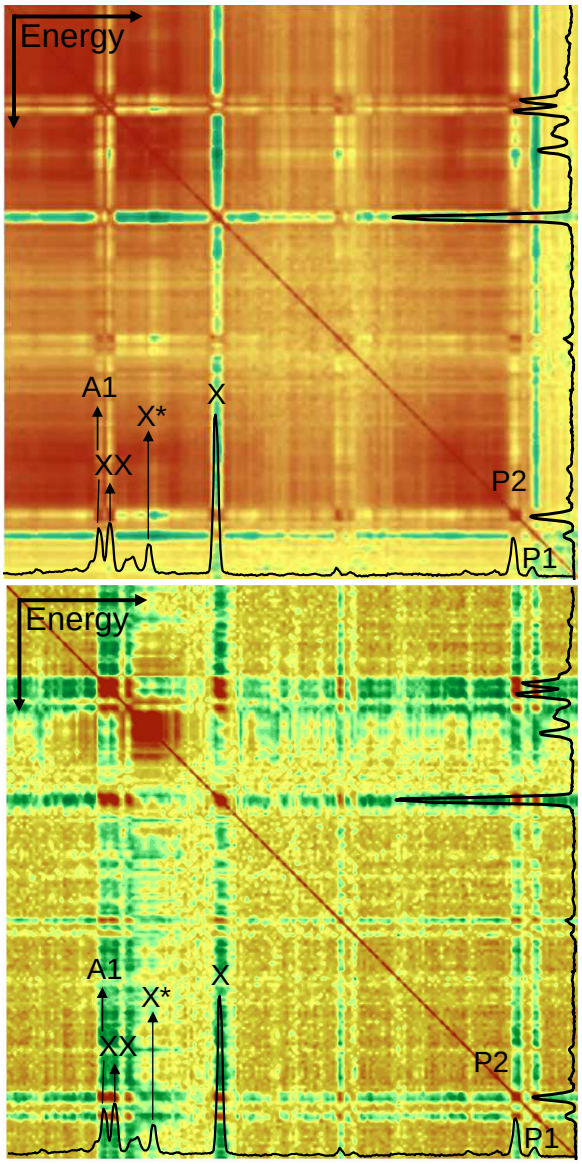

Figure 10.10: *The map illustrates the matrix of the* Γ *correlation coefficient according to eq.10.3 for a number of micro-PL spectra of a single quantum dot. Red and green colour at the cross points illustrates positive and negative correlations, respectively, between emission lines that correspond to the spectrum marked at the bottom and on the right hand side of the map. The spectrum is the average of all recorded spectra. The maps illustrated in the top and bottom panels represent the data recorded with slight variations of the exciting laser spot position and with a slight change of the excitation power, respectively.*

the positively correlated signals and Γ=-1, denoted in the plot by a green colour, the anti-correlated signals. The diagonal in the map illustrates the auto-correlation of the same emission line. Thus at the diagonal Γ=1. The cross-correlations between different emission line intensities are found at respective coordinates. The map is thus symmetric with respect to the diagonal. For example, the red spot is found at the x-coordinate corresponding to X emission and y-coordinate corresponding to XX emission. This illustrates the positive correlation between X and XX emission lines.

Both maps illustrated in Fig.10.10 are represented in the same colour scale. The experimental conditions differ slightly in both cases. In the case of the top plot the spectra were recorded while the position of laser spot on the sample was slightly changed. In the case of the bottom plot, the excitation intensity was varied to a very small degree. Therefore both maps reveal slightly different features. In the first one the positive correlations are better seen, in the latter the negative correlations are more pronounced.

The obtained results of positive and negative correlations are similar to those from the photon correlation experiment discussed in the previous section. The positive correlations are found in two groups of lines:

X, XX_S, XX_T, A2 and
X*, P1, X1, P3, S1, A3.

The negative correlations are found between emission lines belonging to different groups. Additionally, the correlations of some less pronounced lines are visible, suggesting their charged or neutral origin.

The blinking effect has already been reported [10, 12, 14, 16, 20, 21, 22]. It was discussed mainly in terms of Auger type processes [12], the vicinity of the impurities and/or defects [16, 21] and/or generally, the interactions with the surroundings of the quantum dot. In the present experiment, by slightly scanning the dot with the laser beam or by small variations of the excitation power under the quasi-resonant excitation it was possible to change between the two spectra illustrated in Fig.10.9. Thus it was possible to switch between more charged and neutral configurations of carriers in the dot. Most probably, this effect is caused by locally heating the surrounding matrix of the dot (possibly an impurity) and therefore enhancing the charge transfer. It is believed, however, that this long time effect is different in nature than the natural charge variation that was observed on the *ns* time scale.

The charge variation in quantum dots is visible in the "macro" time scale, up to several seconds. This extremely long time is assigned to the change of the surroundings of the quantum dot, which can supply the quantum dot with free charges.

10.7 Cascaded multiexcitonic emission

When investigating the cross-correlations between emission lines within the family of the same charge state, mainly positive correlations are found. This is because

different emissions are strictly connected. For example: after the biexciton recombination the quantum dot is left with a single electron-hole pair, from which the neutral exciton is formed and can recombine radiatively shortly afterwards. The most straightforward demonstration of the sequence in the recombination process is the cascaded emission.

In the following section (10.7.1) the cascaded emission within the "neutral" family of states is discussed. The presented results allow to demonstrate (10.7.2) that triplet biexciton states can be detected in a photon-correlation experiment.

Several cascades within the "charged" family of states were also observed in the experiment. However, the interpretation of the obtained results is complicated and involves more advanced theoretical calculations to provide a better understanding of the observed effects. Therefore, the cascades within the "charged" family of states will not be discussed in this work.

10.7.1 Neutral cascades

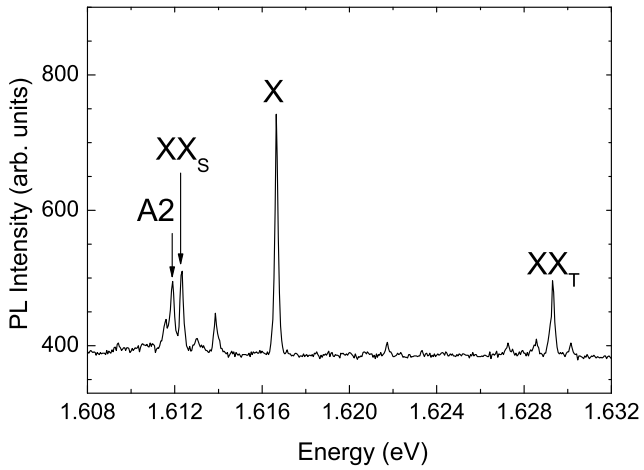

Figure 10.11: *Micro-PL spectra of the single GaAs/AlAs quantum dot taken at quasi resonant excitation at relatively small excitation power. The illustrated spectrum is mainly due to the recombination of the neutral configuration of carriers in the dot. The most important lines with the origin in neutral states are marked in the picture.*

The spectrum of the quantum dot taken at relatively low excitation power for the most "neutral" configuration of carriers in the average time of spectrum accumulation is illustrated in Fig.10.11. The single exciton X, biexciton singlet XX_S and biexciton triplet XX_T emission lines are marked in the picture.

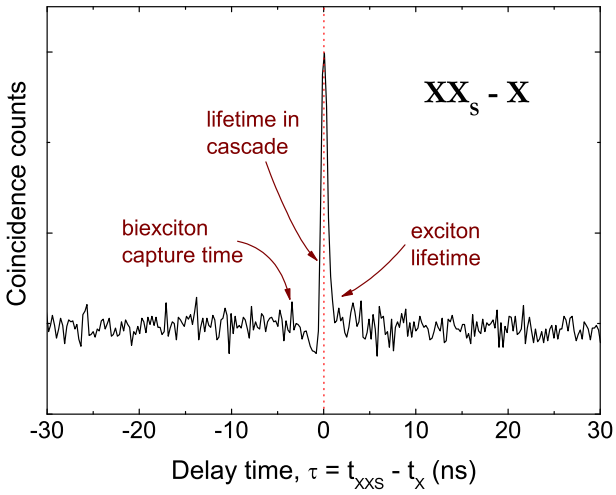

Figure 10.12: *X-XX cross-correlation histogram illustrating that the two states are connected into a cascade with XX being the initial state.*

The typical fingerprint of the cascaded emission [15, 23] from the quantum dot is the shape of the histogram that is observed for exciton (X) and biexciton singlet (XX_S) states. This is illustrated in Fig.10.12. The pronounced bunching close to zero delay time means that shortly after the XX_S recombination, the X recombination is observed, before the dot reaches its ground state. The particular asymmetry around zero delay time means that the XX_S photon is emitted first and then the X photon can be detected. Thus the XX_S recombination supplies the X state.

The decay of the bunching peak at the negative delay time in the picture represents the lifetime of the excitons, approx. $0.3ns$ ($\pm 0.02ns$) and the rise of the signal at positive time illustrates the time required for the quantum dot to capture two electrons and two holes to form an XX state. This recovery time is estimated to be approx. $1.3ns$. Very short time of the rise of the signal at zero delay time represents the lifetime in the cascade, it is however impossible to estimate due to insufficient resolution of the detection system.

The same experiment performed in the linear polarization revealed that the investigated quantum dots are anisotropic. Fig.10.13 illustrates that if XX_S and X are detected in the same polarization, the cascaded emission is observed, while with cross-polarization the anti-bunching dip is observed, according to the scheme illustrated in the right panel in Fig.10.13. This demonstrates that the recombination of XX_S in a particular linear polarization implies the linear polarization of X. This is only possible if the X state is split due to quantum dot anisotropy.

This particular effect observed in the linear polarization demonstrates that in

the case of the investigated quantum dot, photon entanglement can not be achieved.

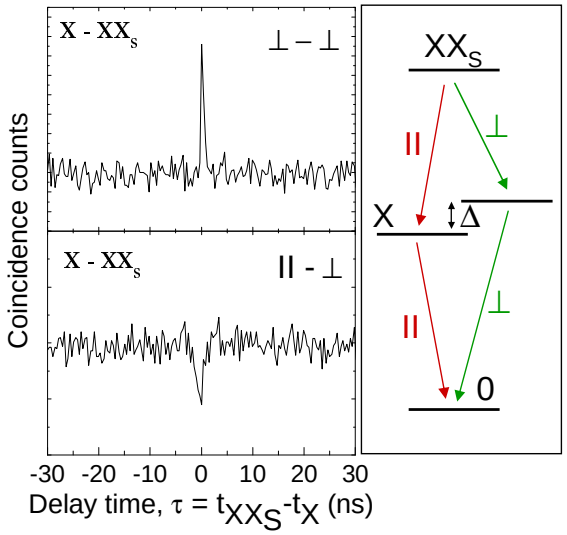

Figure 10.13: *Left panel: linear polarization resolved X - XX_S cross-correlation histograms. Right panel: the selection rules for recombination in linear polarization for an anisotropic quantum dot. Δ is a measure of the X state anisotropy.*

Typical cascaded emission is observed between X and XX_S states. This particular cascade observed in linear polarization of emitted light showed the sequential emission only in the same polarization of both emission lines, which means that the quantum dots are anisotropic.

10.7.2 Biexciton triplet state

The cascade type histogram is also observed for the biexciton triplet XX_T - X correlation histogram, what is illustrated in Fig.10.14. The small bunching at negative delays and anti-bunching at positive delays around zero delay suggests that the two states are connected in cascade, with the XX_T emission being initial. However it is more complicated in structure than a simple X - XX_S cascade. In particular the anti-bunching dip is much more pronounced than those in the X-XX_S cascade, indicating that the recovery time after X emission is much longer.

The long time positive correlation effect indicates again that the two correlated emissions are due to the recombination of two states of the same charge configuration of carriers in the dot.

The lack of XX_T - XX_S cascades, as illustrated in Fig.10.14, indicates that the XX_T emission cannot be due to triexciton recombination. The observed anti-bunching for zero delays for the XX_T - XX_S correlation suggests that XX_T and XX_S are two mutually excluding states. The origin of both lines must be due to biexciton recombination. This implies that the triplet and the singlet state of XX

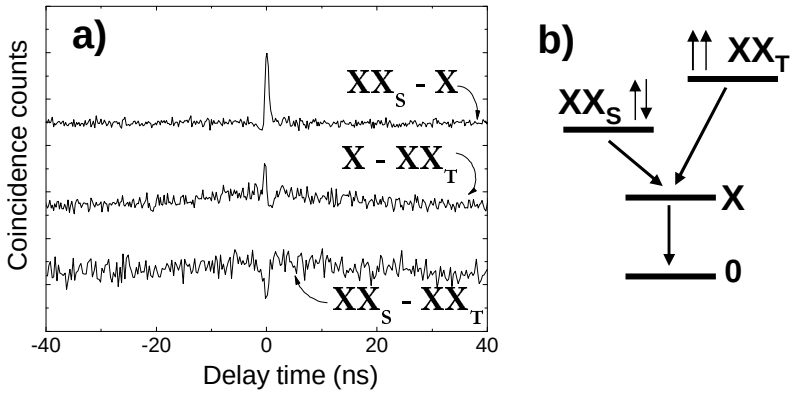

Figure 10.14: *a): XX_S - X; X - XX_T and XX_S - XX_T cross-photon correlation histograms. b): proposed recombination diagram with schematic electron configuration of XX_S and XX_T states.*

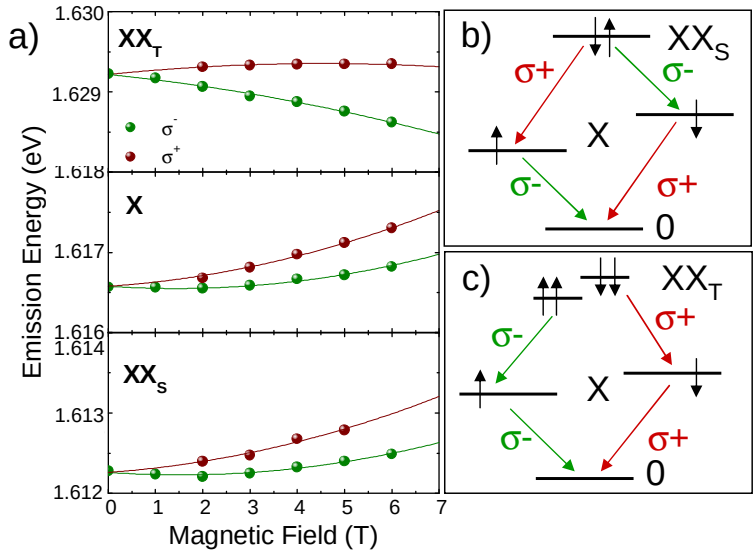

Figure 10.15: *a) The energy shift of X, XX_S and XX_T emissions in magnetic field up to 6T. The red and green points illustrate the σ^+ and σ^- polarizations, respectively. The solid lines are the fitted diamagnetic shifts with Zeeman-split components. b) and c) schematic diagrams of the polarization rules for the X - XX_S and X - XX_T cascades, respectively.*

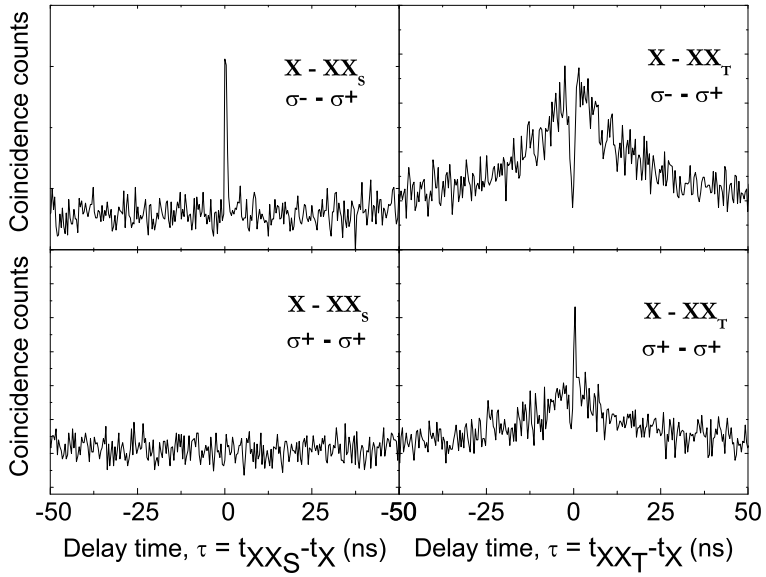

Figure 10.16: *Circular polarization resolved photon correlation experiment for X - XX_S and X - XX_T emission lines in a small magnetic field of 0.5T.*

are observed.

The recombination diagram between XX_T, XX_S and X states is illustrated in Fig.10.14b). The scheme of the electron configuration is marked for singlet and triplet states. Both XX recombinations supply the X state while no correlation is expected between them.

The evolution of the emission line when a magnetic field is applied justifies this statement. In the XX_S the carriers with opposite spin occupy the ground, *s*-type shell, energy level. Thus the energy shift in magnetic field is similar to that observed for the X emission line, as illustrated in Fig.10.15a). However, due to the particular degeneracy of the s-shell, in the triplet state one of the carriers with the same spin has to be put on the excited, p-type shell. Consequently, a red shift of the XX_T emission line is observed.

The evidence for the observation of XX singlet and triplet states comes from the photon correlation polarization resolved experiment.

In the experiment a small magnetic field of 0.5T was applied to better resolve the polarization of the emission lines. It was small enough not to cause an observable spin-splitting of the emission lines.

The polarization rules for the sequential emission for XX_S and the X states are illustrated in Fig.10.15b). Consequently, the cascade between the XX_S and X states is observed in the crossed circular polarization ($\sigma+/\sigma-$ or $\sigma-/\sigma+$), what is illustrated in Fig.10.16. In contrary, in co-polarizations ($\sigma+/\sigma+$ and $\sigma-/\sigma-$) no sequence in the XX_S and X emission is expected. And indeed, the bunching peak in this case is not observed (see Fig.10.16).*

In the case the the sequential emission for XX_T and the X states (the polarization rules are illustrated in Fig.10.15c) the cascade between the XX_T and X states is observed in co-polarizations ($\sigma+/\sigma+$ and $\sigma-/\sigma-$). In the crossed circular polarization ($\sigma+/\sigma-$ or $\sigma-/\sigma+$) the observed anti-bunching dip at zero delay time confirms that no sequence is expected between these states in different polarizations of emitted light.

The theoretical calculations of the possible emission energies of XX_S and XX_T states were done by P. Hawrylak and M. Korkusiński from the *Institute for Microstructural Sciences*, NRC in Ottawa, in Canada.

The modelled GaAs quantum dot was a lens shape disk with the characteristic electron and hole energies $\hbar\omega_e$=10meV and $\hbar\omega_h$=3meV, respectively, and an effective Rydberg of $Ry*$=4.78meV. The emission spectra of X, XX_S and XX_T were

*Also in this case the anti-bunching peak is not very well pronounced. However, the anti-bunching peak at the negative delay time is very small in all X - XX_S correlations histograms. Thus it is possible that the histogram of X($\sigma+$) - XX_S($\sigma+$) in Fig.10.16 is flat. This anti-bunching dip is somehow hidden. This can be due to the large background in the experiments. In general, the depth of the anti-bunching dip does not depend on the polarization of the emitted light.

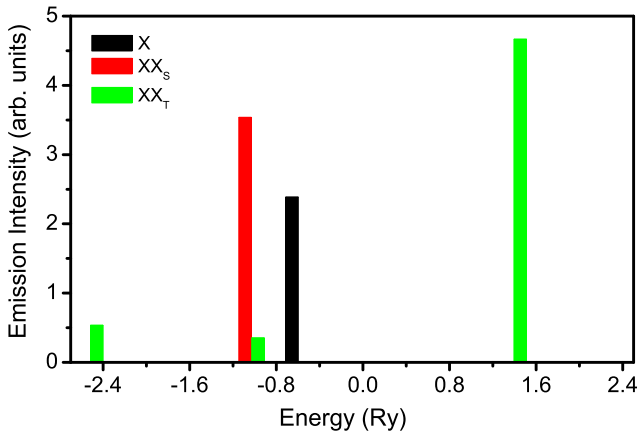

Figure 10.17: *Calculated emission spectra of the exciton (black), the singlet biexciton (red) and the triplet biexciton (green). The hight of the lines is proportional to the calculated emission intensity. P.Hawrylak and M. Korkusiǹski.*

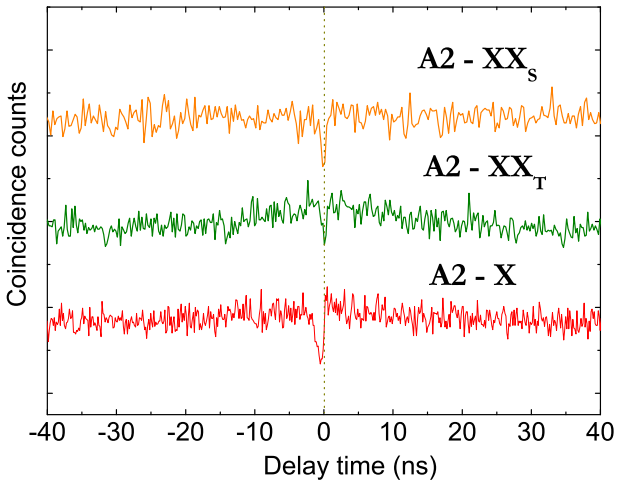

Figure 10.18: *A2 - XX_S, A2 - XX_T and A2 - X photon correlation histograms.*

calculated in a model that includes scattering of the carriers to higher, empty shells (up to the d shell). The electrons and holes exchange and interact. The active state for a certain configuration of particles is composed of a mixture of all possible bright states. The method is described in Ref.[1, 6].

A calculated spectrum is illustrated in Fig.10.17. It is composed of a single exciton line (black), a single biexciton singlet line (red) and three lines related to biexciton triplet emission (green). The theoretically obtained spectrum is very similar to those observed in the experiment, as illustrated in Fig.10.11. The relative intensities agre well. The small discrepancies in the emission energy are probably caused by the difference in shape between a real quantum dot and an assumed one. Also the composition of dot material (and barriers) can vary slightly while in the theoretical model pure GaAs dot was used.

The theoretical model gives an indication of the position of the two additional emission lines that is expected due to XX_T state recombination. They should be observed in the low energy region, one close to the XX_S line, the second much below. The very low energy line is not well observed, it is probably the small feature at 1.6093eV in Fig.10.11 (compare with Fig.10.10), however its intensity is too small for the photon-correlation experiment.

The A2 emission is most probably the best candidate as being due to XX_T state recombination. Its energy is very close to XX_S recombination. Fig.10.18 illustrates the photon correlations between A2 and other "neutral": emission lines: XX_S, XX_T and X. The anti-bunching dips, precisely at zero delay times, are observed for A2-XX_S and A2-XX_T histograms. It means that A2 with XX_S and XX_T states are due to the same one-state recombination, thus their mutual existence in the dot is excluded. This is a very strong indication that A2 is also due to biexciton state recombination. In that case, it should give cascaded emission with single exciton. And this is seen in the A2-X histogram in Fig.10.18. The dip at $\tau < 0$ is much more pronounced than the bunching at $\tau > 0$. It is probably due to the complicity of the initial XX_T state. However, the shift of the anti-bunching dip from zero delay time is well seen and a cascade between the two states is observed.

Clear evidence of biexciton singlet and biexciton triplet states observation is given by the polarization resolved photon correlation experiment. As theoretically predicted, the emission from the biexciton triplet state results in three spectral lines, two of which were possible to identify in the experiment.

Bibliography

[1] P. Hawrylak, "Excitonic artificial atoms: Engineering optical properties of quantum dots," *Phys. Rev. B*, vol. 60, p. 5597, 1999.

[2] A. Wojs, P. Hawrylak, S. Fafard, and L. Jacak, "Theory of the luminescence from highly excited self-assembled quantum dots," *Physica E*, vol. 2, p. 603, 1998.

[3] S. V. Nair and Y. Masumoto, "Multi-exciton states and many-body correlations in quantum dots," *phys. stat. sol. b*, vol. 224, p. 739, 2001.

[4] E. Dekel, D. Gershoni, E. Ehrenfreund, D. Spektor, J. M. Garcia, and P. M. Petroff, "Multiexciton spectroscopy of a single self-assembled quantum dot," *Phys. Rev. Lett.*, vol. 80, p. 4991, 1998.

[5] A. Barenco and M. A. Dupertuis, "Quantum many-body states of excitons in a small quantum dot," *Phys. Rev. B*, vol. 52, p. 2766, 1995.

[6] P. Hawrylak and M. Korkusiński, "Electronic and optical properties of self-assembled quantum dots" in "Single quantum dots: Fundamentals, applications, and new concepts.," *P.Michler, Editor, Topics in Applied Physics, Springer-Verlag*, vol. 90, p. 25, 2003.

[7] C. Kammerer, C. Voisin, G. Cassabois, C. Delalande, P. Roussignol, F. Klopf, J. P. Reithmaier, A. Forchel, and J. M. Gérard, "Line narrowing in single semiconductor quantum dots: Toward the control of environment effects," *Phys. Rev. B*, vol. 66, p. 041306, 2002.

[8] H. D. Robinson and B. B. Goldberg, "Light-induced spectral diffusion in single self-assembled quantum dots," *Phys. Rev. B*, vol. 61, 2000.

[9] V. Türck, S. Rodt, O. Stier, R. Heitz, R. Engelhardt, U. W. Pohl, D. Bimberg, and R. Steingrüber, "Effect of random field fluctuations on excitonic transitions of individual CdSe quantum dots," *Phys. Rev. B*, vol. 61, p. 9944, 2000.

[10] C. Santori, D. Fattal, J. Vučković, G. S. Solomon, E. Waks, and Y. Yamamoto, "Submicrosecond correlations in photoluminescence from InAs quantum dots," *Phys. Rev. B*, vol. 69, p. 205324, 2004.

[11] R. Hanbury-Brown and R. Q. Twiss, "The question of correlation between photons in coherent light rays.," *Nature (London)*, vol. 178, p. 1447, 1956.

[12] P. Michler, A. Imamoğlu, M. D. Mason, P. J. Carson, G. F. Strouse, and S. K. Buratto, "Quantum correlation among photons from a single quantum dot at room temperature," *Nature (London)*, vol. 406, p. 968, 2000.

[13] P. Michler, A. Kiraz, C. Becher, W. V. Schoenfeld, P. M. Petroff, L. Zhang, E. Hu, and A. Imamoğlu, "A quantum dot single-photon turnstile device," *Science*, vol. 290, p. 2282, 2000.

[14] C. Santori, M. Pelton, G. Solomon, Y. Dale, and Y. Yamamoto, "Triggered single photons from a quantum dot," *Phys. Rev. Lett.*, vol. 86, p. 1502, 2001.

[15] D. V. Regelman, U. Mizrahi, D. Gershoni, E. Ehrenfreund, W. V. Schoenfeld, and P. M. Petroff, "Semiconductor quantum dot: A quantum light source of multicolor photons with tunable statistics," *Phys. Rev. Lett.*, vol. 87, p. 257401, 2001.

[16] A. Kiraz, S. Fälth, C. Becher, B. Gayral, W. V. Schoenfeld, P. M. Petroff, L. Zhang, E. Hu, and A. Imamoğlu, "Photon correlation spectroscopy of a single quantum dot," *Phys. Rev. B*, vol. 65, p. 161303, 2002.

[17] A. Malko, M. Baier, E. Pelucchi, D. C. al kar, D. Oberli, and E. Kapon, "Correlated photon emission from semiconductor quantum dots grown in inverted pyramids," *Physica E*, vol. 26, p. 194, 2005.

[18] M. H. Baier, A. Malko, E. Pelucchi, D. Y. Oberli, and E. Kapon, "Quantum-dot exciton dynamics probed by photon-correlation spectroscopy.," *Phys. Rev. B*, vol. 73, p. 205321, 2006.

[19] J. Suffczyński, T. Kazimierczuk, M. Goryca, B. Piechal, A. Trajnerowicz, K. Kowalik, P. Kossacki, A. Golnik, K. Korona, M. Nawrocki, and J. A. Gaj, "Excitation mechanisms of individual CdTe/ZnTe quantum dots studied by photon correlation spectroscopy.," *Phys. Rev. B*, vol. 74, p. 085319, 2006.

[20] D. Bertram, M. C. Hanna, and A. J. Noizk, "Two color blinking of single strain-induced GaAs quantum dots," *Appl. Phys. Lett.*, vol. 74, p. 2666, 1999.

[21] M.-E. Pistol, P. Castrillo, D. Hessman, J. A. Prieto, and L. Samuelson, "Random telegraph noise in photoluminescence from individual self-assembled quantum dots," *Phys. Rev. B*, vol. 59, p. 10725, 1999.

[22] H. Robinson and B. B. Goldberg, "Light-induced spectral diffusion in single self-assembled quantum dots," *Phys. Rev. B*, vol. 61, 2000.

[23] E. Moreau, I. Robert, L. Manin, V. Thierry-Mieg, J. M. Gérard, and I. Abram, "Quantum cascade of photons in semiconductor quantum dots," *Phys. Rev. Lett*, vol. 87, p. 183601, 2001.

Chapter 11

Conclusions

Nous présentons dans ce chapitre les conclusions de cette étude et nous récapitulons les principaux résultats obtenus.

The presented work uncovered the existence of a particular system of quantum dots, with an extremely low surface density of $10^6 \mathrm{cm}^{-2}$ and very deep potential traps, where stable multiexciton complexes can be formed. The spectroscopic studies allowed a detailed investigation of the properties of the multi-carrier systems confined in the quantum dot potential. The most important results obtained in the work are:

- The typical emission of a single exciton, charged exciton and biexciton at low dot populations allowed us to formulate a general description of these simple exciton complexes:
  - The binding energy of an exciton in a quantum dot could be evaluated to be about 10meV.
  - The trion binding energy was observed to be approx. 2.7meV. The values were similar for different quantum dots (of different size and alloy composition).
  - The value of the diamagnetic coefficient, $10\mu\mathrm{eV/T}^2$, allowed to determine the size of the $1s$ exciton wave function approx. 5nm, in agreement with the estimated size of the first electronic level in a harmonic confining potential in the investigated dots.
  - The effective g-factor of an exciton in the investigated quantum dots varies from dot to dot from 0.8 to 2.2. An increase of the g* factor was found for excitons emitting at higher energies.
  - The thermal broadening of the exciton emission line was not observed, what was interpreted as being due due to the weak interaction of electrons with acoustic phonons.
- Multiexciton complex formation was observed at high carrier populations. Electrons and holes occupy a number of excited "atomic-like" shells, which is a typically zero-dimensional effect with strong 3D confinement.

- A strong effect of intra-shell interactions was observed for closed shells. The particles in open shell seem not to interact, which was explained by hidden symmetry property of the investigated system. Inter-shell interactions between particles from different energy shells were visible for very high carrier concentrations.
- The effects of band-gap renormalisation were observed with an increasing number of carriers in the quantum dot, as the emission energy shifted towards lower energies. This tendency was especially well visible for the ground state emission and could be very well approximated assuming a continuous change of carrier density in the dot, populating energy shells of bigger dimensions. Therefore the model usually applied to describe band gap renormalisation in bulk materials was successfully applied to a quantum dot.
- The application of a magnetic field revealed that the effects of strong intra-shell carrier interactions are observed on excited states for completely populated, closed shells. Almost perfect agreement with the Fock - Darwin model was found for the valence shells, confirming the very weak interactions between carriers confined in open shells.
- The quenching of the total emission intensity from quantum dots with increasing temperature was observed to be due to the important role of non-radiative processes that are activated at temperatures above $\sim$30K.
- Temporally and spectrally resolved emission from a single quantum dot was reported, what is a unique observation. The results revealed that the dot emission reproduces the dynamics in the 2D, type II, quantum well system. Diffusion was found to be the major mechanism of carrier spreading from the excitation spot. For the quantum dot this results in a decreased carrier density that supplies the dot. The mobility of indirect excitons was found to be in the order of $200cm^2/(V \cdot s)$.
- The multi-line emission spectrum of a single dot was found to display two and only two, [X] and [X*], sets of lines. These two sets regrouped the emission lines characteristic of a dot in a neutral state and a dot that is charged with one carrier (probably an electron). This indicates that in the vicinity of the quantum dot a source of charge fluctuation was present, and single carriers could be captured form the surroundings of the dot material. This process was observed on a long time scale of 10-100nsec.
- It was directly demonstrated that, at above band gap excitation, the dots are filled with individual photoexcited electrons and holes, while under quasi-resonant excitation, the dots are predominantly filled with electron-hole pairs. This effect, observed in photon-correlation experiment, is a particular result.
- The charge variation in the quantum dots was visible also on the "macro" time scale, up to several seconds. This extremely long time was assigned to the change of the surroundings of the quantum dot.
- The sequential emission between different multiexciton-complex states was demonstrated to be due to independent neutral and charged cascades in the photon correlation experiment.
- The first clear evidence of the observation of biexciton singlet and triplet states was given in the polarization resolved photon correlation experiment.

Chapter 12

Appendix

Nous présentons dans cet appendice les résultats obtenus sur les fortes oscillations de l'intensité d'émission d'une boîte quantique unique sous champ magnétique intense. Ces oscillations apparaissent comme étant périodiques en fonction du champ magnétique appliqué. Cette dépendance en champ magnétique est intrigante. Après avoir démontré que ces oscillations ne sont pas un artefact de mesure, nous discutons les différentes interprétations possibles : en terme d'effet Aharonov-Bohm ou en terme de modification par le champ magnétique des propriétés des excitons indirects qui constituent un réservoir de porteurs pour les boîtes quantiques.

The pronounced field-induced changes in the intensity of the dots' emission are characteristic effect which is often observed in the μ-magneto-PL spectra in the investigated quantum dots.

This can be clearly seen in the spectra shown in the a) and b) panel of Fig.6.12 and Fig.12.3 in the case of low excitation power, or in Fig.12.1 and Fig.12.2 in the case of high excitation power.

The experimental result is that the oscillations of the total emission intensity are caused by the change of the quantum dot population. The spectrum at minimum intensity is similar to that obtained by reducing the excitation power. This is well seen in Fig.12.1 a) and b) when magnetic field and excitation power evolutions are compared for the same quantum dot. The excitation power used in this experiment was very high and in this case the shape of the spectra changes significantly.

The experimental results that strongly suggest that the observed oscillations are not caused by the excitation power variation during the measurements are:

- the spectra are stable and very well reproducible at a given magnetic field
- the magnetic field of the observed maxima and minima versus integer number were found to be a linear function *, what is illustrated in Fig.12.2 c).

*The linearity of the oscillations maxima is an intriguing effect. It is in contrast to Shubnikov de Haas oscillations of the Fermi energy (the linearity has been shown in the inverse value of magnetic field). A physical effect that gives the oscillatory behavior (of energy, intensity, phase) with a linear dependence of the observed maxima in magnetic field

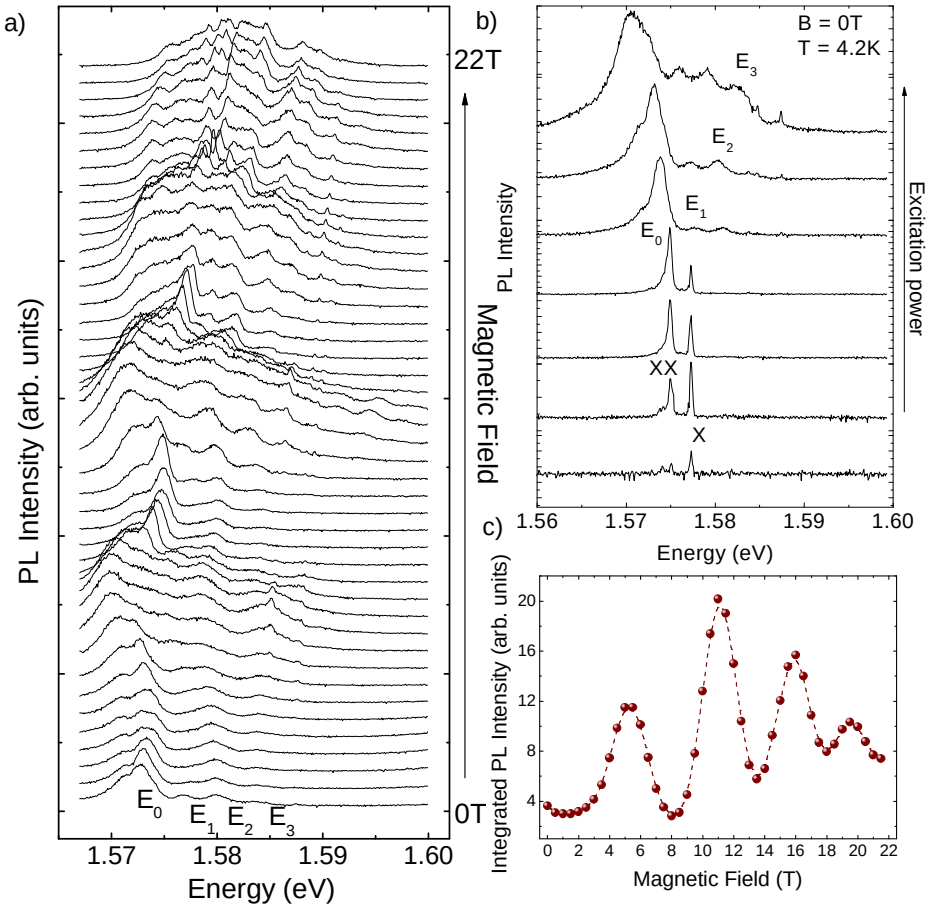

Figure 12.1: *a) Magnetic field evolution of the emission lines from a large (the distance between the excited shells is small, approx. 3meV), single quantum dot excited with very high excitation power. b)The excitation power evolution of the emission from the quantum dot. c) Integrated PL intensity oscillations in magnetic field.*

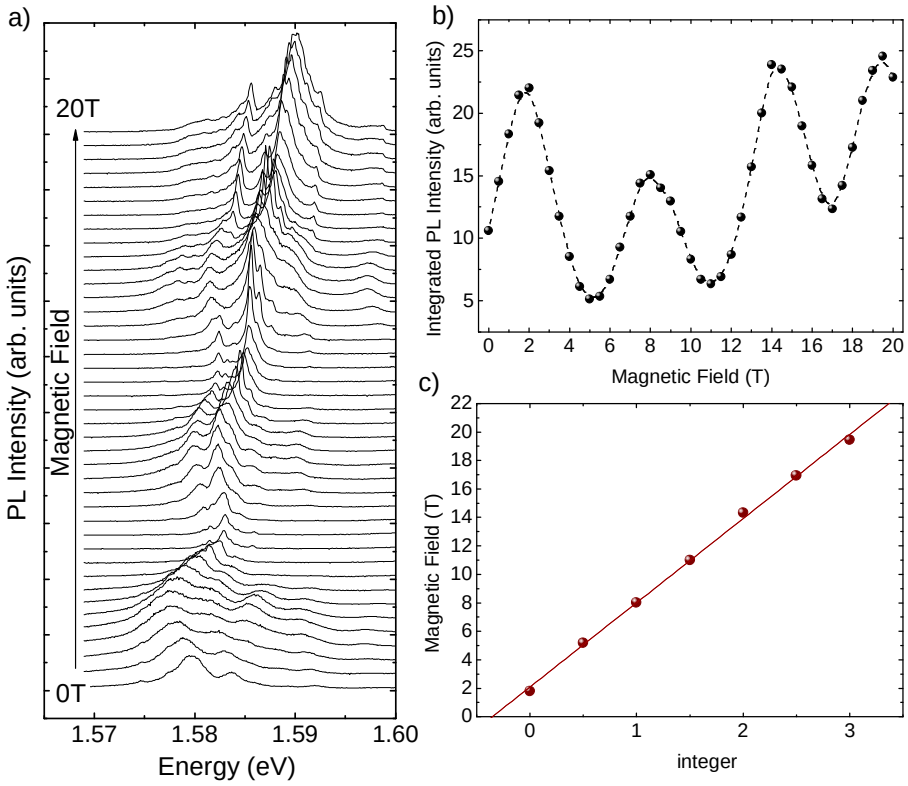

Figure 12.2: *a) Magnetic field evolution of the emission lines from a single quantum dot excited with high excitation power. b) Integrated PL intensity oscillations in magnetic field. c) The magnetic field corresponding to observed maxima of the oscillations versus integer number.*

Fig.12.3 illustrates the situation when three quantum dots, A, B and C are located very close one to another in geometry illustrated in Fig.12.4a) . All spectra were measured simultaneously in the same spectral window. At a magnetic field where the suppression of the A and C dot emission is observed, the emission intensity from the B dot is enhanced. This effect is marked by a vertical arrow in the picture. Similarly, when the emission from the B dot decreases, the emission from the A and C dots gains in intensity (Fig.12.4b).

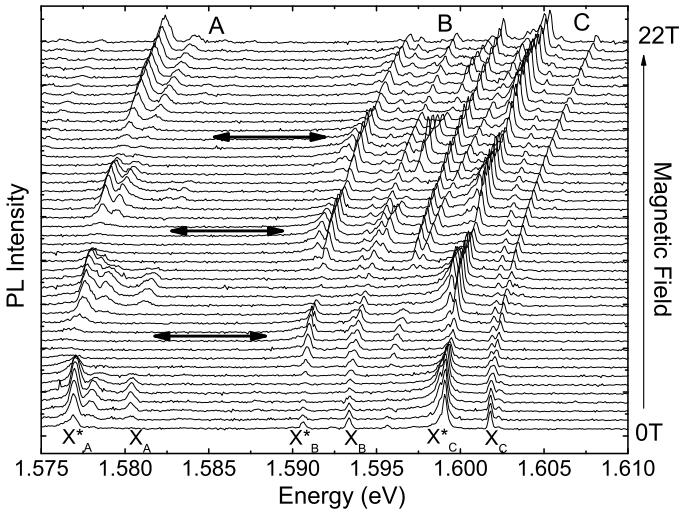

Figure 12.3: *Magnetic field evolution of the emission lines from three quantum dots (A, B and C) measured at low excitation power. The excitation spot was located close to the B dot, as illustrated in Fig.12.4a) in point -7- .*

In general, the origin of the observed effect is not completely clear. It is speculated, however, that the magnetic field may either modify the carrier diffusion process (compare with section 5.4, Fig.5.4) or influence the process of carrier capture into the dot. The intensity oscillations are enhanced in photoluminescence experiments in which the laser spot is well laterally separated from the dot location and this points to the "diffusion scenario". Nevertheless, the oscillations are also well visible if the laser spot coincides with the dot location. This, on the other hand, indicates that the carrier capture might also be modified by magnetic field, for example, via a field-induced rearrangement of energy levels in the dot with respect to the 2D levels of the surrounding material (in which the carriers are initially located in the "non-resonant excitation" experiments).

is the Aharonov - Bohm effect. However, in this case, the spatial separation of electron and hole is required, which is difficult to realize in the investigated quantum dot system. Therefore the cause of the linearity of the observed effect remains an open question.

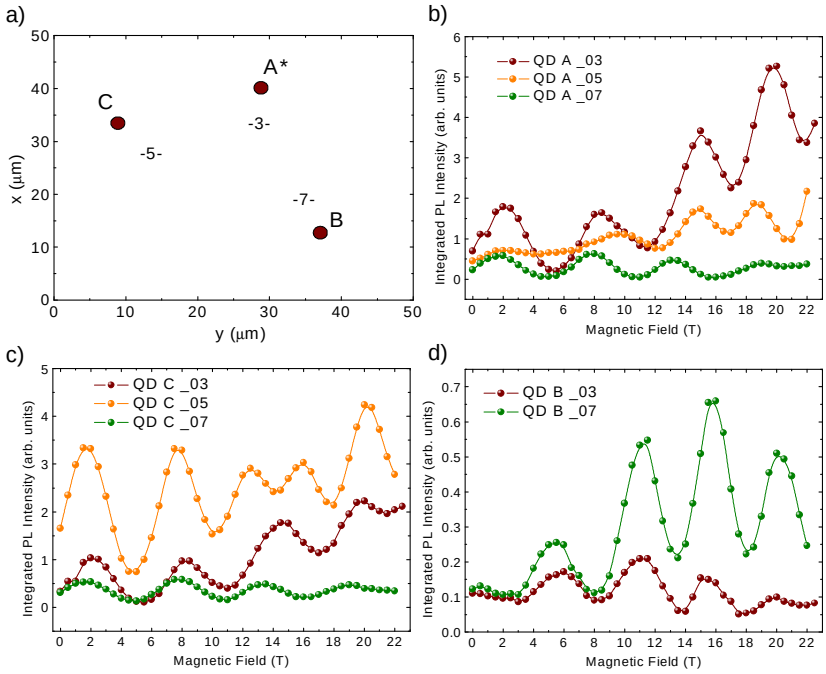

Figure 12.4: *a) Geometry of the experiment. A, B, C - respective positions of the dots; -3-, -5- -7- - three different configuration of the laser spot. b), c), d) The intensity oscillations of A, B and C dots emission for the laser spot position at points -3-, -5- and -7-, respectively.*